UCRL-16753

University of California

Ernest O. Lawrence Radiation Laboratory

TWO-WEEK LOAN COPY

This is a Library Circulating Copy
which may be borrowed for two weeks.
For a personal retention copy, call
Tech. Info. Division, Ext. 5545

INVESTIGATION OF LATTICE VACANCIES IN COPPER
UNDER NONEQUILIBRIUM CONDITIONS

Berkeley, California

DISCLAIMER

This document was prepared as an account of work sponsored by the United States Government. While this document is believed to contain correct information, neither the United States Government nor any agency thereof, nor the Regents of the University of California, nor any of their employees, makes any warranty, express or implied, or assumes any legal responsibility for the accuracy, completeness, or usefulness of any information, apparatus, product, or process disclosed, or represents that its use would not infringe privately owned rights. Reference herein to any specific commercial product, process, or service by its trade name, trademark, manufacturer, or otherwise, does not necessarily constitute or imply its endorsement, recommendation, or favoring by the United States Government or any agency thereof, or the Regents of the University of California. The views and opinions of authors expressed herein do not necessarily state or reflect those of the United States Government or any agency thereof or the Regents of the University of California.

Special thesis

UCRL-16753

UNIVERSITY OF CALIFORNIA

Lawrence Radiation Laboratory
Berkeley, California

AEC Contract No. W-7405-eng-48

INVESTIGATION OF LATTICE VACANCIES IN COPPER UNDER NONEQUILIBRIUM CONDITIONS

Dennis Martin Maher

(Ph. D. Thesis)

May 1966

TABLE OF CONTENTS

ABSTRACT

I. INTRODUCTION 1

A. Vacancy Abundance 2

B. Thermal Equilibrium Measurements 4

C. Self-Diffusion Experiments 6

D. Nonequilibrium Experiments 7

E. Present Investigation 20

II. EXPERIMENTAL PROCEDURE 22

A. Electrical Resistance Experiments 22

B. Electron Microscopy Experiments 43

III. EXPERIMENTAL RESULTS 56

A. Formation Enthalpy Data 56

B. Isochronal Annealing Data 67

C. Experimental Accuracy 68

D. Defect Aggregates 74

IV. DISCUSSION 86

A. Monovacancy Formation Enthalpy 87

B. Monovacancy Resistivity and Formation Entropy 96

C. Monovacancy Migration Enthalpy 97

D. Comparison with Theory 100

E. Isochronal Annealing and Vacancy Aggregation 102

V. CONCLUSIONS 113

ACKNOWLEDGEMENTS 115

APPENDICES

I. Purification of Helium Gas 116

II. Temperature Dependence of the Resistance 119

TABLE OF CONTENTS (Continued)

III. Formation of Divacancies During an Exponential Quench .. 123

REFERENCES 127

FIGURE CAPTIONS 134

INVESTIGATION OF LATTICE VACANCIES IN COPPER UNDER NONEQUILIBRIUM CONDITIONS

Dennis Martin Maher

Inorganic Materials Research Division, Lawrence Radiation Laboratory,
Department of Mineral Technology, College of Engineering,
University of California, Berkeley, California

ABSTRACT

May 1966

High purity copper wires were quenched to -196°C from temperatures greater than 450°C and less than 800°C in a static atmosphere of purified helium gas. The change in residual resistance, measured at liquid helium temperature, was used to detect retained defects and quenched induced damage. Considerable care was taken to ensure reproducibility of the well-annealed state, and the quenched-in increment characteristic of any particular temperature. The temperature dependence of quench induced resistivity is interpreted as indicating that the monovacancy formation enthalpy in nominally 99.999% pure copper is (1.09±0.04)eV. If the activation enthalpy for self-diffusion is taken as (2.10±0.02)eV then the monovacancy migration enthalpy is (1.01±0.06)eV. When the present resistivity data are combined with the equilibrium measurements of R. O. Simmons and R. W. Balluffi, the resistivity per atomic percent vacancies and monovacancy formation entropy are estimated to be (0.75±0.4)μohm-cm and (0.8±0.5)k, respectively.

Isochronal recovery of copper quenched from ≈ 700°C exhibits three annealing stages. Maximum annealing rates occur at about -40°,

+200°, and +400°C. Numerous possible processes are suggested to explain the observed recovery spectrum. Detailed kinetic studies under carefully controlled conditions are necessary to completely clarify the reported behavior.

When copper single crystals are gas quenched from vacuum and subsequently annealed under quite restrictive conditions, planar vacancy aggregates are observed by transmission electron microscopy. The aggregates are identified as both perfect and imperfect dislocation loops. The presence of vacancy loops which are large enough to be directly observed, is shown to be a sensitive function of the nucleation processes and the availability of mobile defects in a sufficiently high concentration to support growth processes at higher annealing temperatures.

It is felt that the reported results are representative of vacancy behavior in nominally 99.999% pure copper and that the difficulties arising from the numerous possible complicating features reported previously in the literature have, for the most part, been minimized.

I. INTRODUCTION

A quantitative description and understanding of the properties of vacancy defects has now been obtained for a number of pure face-centered cubic metals. This is mainly a consequence of: 1) direct measurement of defect concentrations at elevated temperatures by a technique involving the simultaneous determination of the relative linear expansion, $\Delta L/L_o$, and the relative x-ray lattice parameter expansion, $\Delta a/a_o$, during equilibrium heating, 2) accurate determination of the temperature dependence of the self-diffusion coefficient, D^{sd}, by radio-tracer sectioning techniques, 3) nonequilibrium experiments in which the high temperature state is "frozen-in" by rapid cooling and the defects are then studied at lower temperatures.[1] The information obtained by these experiments has definitely aided the interpretation of more complicated phenomena such as radiation damage[2] and cold work.[3]

The results of equilibrium measurements,[4,5,6] self-diffusion studies,[7,8] and numerous quenching experiments[9,10] carried out with aluminum, silver, and gold are in reasonable agreement although many of the details are still being debated.[9] Experimentally, this is not the case for copper. For instance, the monovacancy formation enthalpy, ΔH^f_{1v}, as estimated from high temperature equilibrium measurements by Simmons and Balluffi[11] has been disputed.[12,13] As a consequence of this situation and because the accepted value of the activation enthalpy, $Q^{sd} = -\frac{d(\ln D^{sd})}{d(1/kT)}$, for self-diffusion in copper appears to be in question,[14] the corresponding monovacancy migration enthalpy, as calculated from $Q^{sd} - \Delta H^f_{1v} = \Delta H^m_{1v}$, is certainly not well defined. When the present work was initiated, no unambiguous quenching experiments had yet been conducted with copper.

In contrast, theoretical estimates of vacancy properties, primarily calculated for the copper lattice, have played an important role in the interpretation of numerous point defect phenomena.[1]

In the following, a few basic relationships are presented which allow one to describe the equilibrium vacancy population as a function of temperature. In addition, certain pertinent experimental results regarding vacancy behavior in copper are described and discussed. These introductory remarks do not represent a complete discussion of the general problem of vacancies in copper, but are meant to serve as a framework for the presentation and evaluation of the present quenching investigation.

A. Vacancy Abundance

The point defect structure present in thermal equilibrium in copper is thought to be relatively simple. Theoretical calculations predict that the formation enthalpy of a vacancy should be much smaller than that for an interstitial.[3] This conclusion is supported by stored energy measurements on irradiated copper[15] which have been interpreted as indicating that $\Delta H^f_{1i} \cong 2.5\Delta H^f_{1v}$. In addition, equilibrium concentration measurements and quenching experiments are consistent with the belief that interstitial defects are unimportant in thermal equilibrium.[3] Therefore, assuming that only vacancy type defects need be considered, the total concentration of vacant sites in copper at a particular temperature is given by

$$\left(\frac{\Delta N}{N}\right)_T = C_{1v}(T) + 2C_{2v}(T) + 3C_{3v}C(T) + \ldots \qquad (1)$$

where the fractional concentration of the jth vacancy cluster is, according to equilibrium statistical mechanics,

$$C_{jv} = g_j \exp[-\Delta G^f_{jv}/kT] = g_j \exp[\Delta S^f_{jv}/k] \exp[-\Delta H^f_{jv}/kT] \ . \quad (2)$$

Here ΔG^f_{jv}, ΔS^f_{jv}, and ΔH^f_{jv} are, respectively, the changes in Gibbs free energy, vibrational entropy, and enthalpy associated with the formation of the jth type defect, and g_j is the number of independent orientations of the jth cluster in the lattice. T is the temperature in degrees Kelvin and k is the Boltzmann constant.

The concentration of a particular vacancy cluster is generally considered in terms of a so-called binding energy. If ΔG^b_{jv} is defined as the negative change in the Gibbs free energy associated with the formation of a jth type cluster from j isolated vacancies (e.g., $\Delta G^b_{2v} = -(\Delta G^f_{2v} - 2\Delta G^f_{1v})$), then from Eq. (2) the fractional concentrations of mono-, di-, and trivacancies are given by,

$$C_{1v}(T) = \exp[-\Delta G^f_{1v}/kT] = \exp[\Delta S^f_{1v}/k] \exp[-\Delta H^f_{1v}/kT] \quad (3)$$

$$C_{2v}(T) = 6C_{1v}{}^2 \exp[\Delta G^b_{2v}/kT] = 6C_{1v}{}^2 \exp[-\Delta S^b_{2v}/k] \exp[B_{2v}/kT] \quad (4)$$

$$C_{3v}(T) = 2C_{1v}{}^3 \exp[\Delta G^b_{3v}/kT] = 2C_{1v}{}^3 \exp[-\Delta S^b_{3v}/k] \exp[B_{3v}/kT] \quad (5)$$

where ΔS^b_{2v}, ΔS^b_{3v} and B_{2v}, B_{3v} are the entropies and binding energies, respectively. It was assumed that a divacancy consists of a pair of nearest neighbor vacancies and that the trivacancy has tetrahedral symmetry with an atom in the center (after Damask, et al.[16]).

It is apparent from these relationships that the fractional concentration of divacancies and trivacancies rises with increasing temperature and increasing binding energy. On the other hand, for a constant total defect population the abundance of clusters increases at the expense of monovacancies with decreasing temperature. This situation

could possibly exist when a highly perfect crystal is rapidly quenched from an elevated temperature.

B. Thermal Equilibrium Measurements

The accurate determination of the temperature dependence of any physical property of copper which is markedly influenced by the presence of vacancies during equilibrium heating, would in principle allow an estimate of $(\Delta N/N)_T$ or a quantity proportional to it and therefore under certain limiting conditions an estimate of ΔH^f_{1v}. The electrical resistance of copper has been measured during equilibrium heating by Meechan and Eggleston[17] and Gertsriken and Slynar.[18] The results in both cases were described by an equation of the form

$$R(T) = a + bT + cT^2 + d \exp(-\Delta H^f/kT), \qquad (6)$$

and interpreted as indicating that $\Delta H^f_{1v} = 0.9 \pm 0.05$ eV and 0.6 eV, respectively. In the case of gold, the discrepancy between the formation enthalpy obtained by this technique[17,19] and that obtained by, say, quenching experiments[10] is about 0.2 - 0.3 eV. In determining these energies it is necessary to know or estimate the temperature dependence of the resistance of the perfect crystal. The extrapolation of the low temperature behavior (i.e., $a + bT + cT^2$) to higher temperatures is suspect because of poor theoretical knowledge of the contribution of anharmonic effects at these higher temperatures.[20] Because of this difficulty these values are generally considered to be unacceptably low.[1]

The most direct method of determining $(\Delta N/N)_T$ involves the simultaneous measurement of the change in the x-ray lattice parameter, a, and the macroscopic change in length, L, of a crystal at elevated temperatures. The complications just outlined are avoided in such experiments.

These changes are related to the fractional concentration of vacancies by the equation[1]

$$(\Delta N/N)_T = 3\left[\Delta L(T)/L_o - \Delta a(T)/a_o\right] . \qquad (7)$$

It has been shown that the lattice relaxation around the defect and lattice thermal expansion contribute equally to $\Delta L/L_o$ and $\Delta a/a_o$.[21,22]

Measurements of this type were made by Simmons and Balluffi[11] on copper. From a knowledge of $\Delta N/N$ at the melting point, the fractional concentrations C_{1v}, C_{2v}, and C_{3v} were calculated employing Eqs. (1), (3), (4), and (5) and assuming values of B_{2v} and B_{3v}. For $B_{2v} < 0.5$ eV and $B_{3v} < 1.5$ eV, it was found that more than 90% of all vacant sites in copper are present as monovacancies.

Since these binding energies are reasonable estimates (possibly even upper limits), it was concluded that the monovacancy is the predominant equilibrium defect, i.e., $(\Delta N/N)_T \cong C_{1v}(T)$. The formation enthalpy, ΔH^f_{1v}, was then calculated from Eq. (3) by assuming a value for the formation entropy, ΔS^f_{1v}, and selecting a temperature at which $(\Delta N/N)_T$ is known most accurately. Therefore at 1075°C, $\Delta N/N = (1.9\pm0.5)\times10^{-4}$, and assuming $\Delta S^f_{1v} = (1.5\pm0.5)k$, Simmons and Balluffi[11] obtained $\Delta H^f_{1v} = 1.17\pm0.11$ eV. The formation enthalpy was not estimated from the temperature dependence of $(\Delta N/N)_T$ because these values were small and the data limited. The assumption $\Delta S = (1.5\pm0.5)k$ was considered well justified in view of previous experiments on other fcc metals and by theory.[6]

Ramsteiner et al.[13] object to this selection of ΔS^f_{1v}, and favor a lower value of ΔH^f_{1v}. At 1083°C, $\Delta N/N = (2.0\pm0.5)\times10^{-4}$, and using the theoretical value $\Delta S^f_{1v} = (0.5\pm0.2)k$ calculated by Schottky et al.,[23]

these authors obtained $\Delta H^f_{1v} = 1.05 \pm 0.06$ eV. They also considered the problem in terms of

$$(\Delta N/N)_T = C_{1v}(T) + 2C_{2v}(T) = C_{1v} + 12C_{1v}^2 \exp(-\Delta S^b_{2v}/k) \exp(B_{2v}/kT). \quad (8)$$

Again taking $(\Delta N/N)_{1083°C} = (2.0 \pm 0.5) \times 10^{-4}$, using the theoretical values $\Delta S^f_{1v} = (0.5 \pm 0.2)k$ and $-\Delta S^b_{2v} = (1.8 \pm 0.2)k$,[21] and the experimentally determined binding energy $B_{2v} = 0.13 \pm 0.04$ eV,[24] they obtained $\Delta H^f_{1v} = 1.06 \pm 0.06$ eV. Therefore the uncertainties in the values of the binding energy and binding entropy of divacancies, in contrast to the formation entropy of monovacancies, effectively have no influence on the calculated value of the monovacancy formation enthalpy in copper.

C. Self-Diffusion Experiments

The temperature dependence of the self-diffusion coefficient of copper has been studied by a number of investigators.[23-25] The results are summarized in Table I.

Table I. Temperature Dependence of Self-Diffusion of Copper

Temperature Range (°C)	$D^{sd} = D_o \exp(Q^{sd} = kT)$	
	Q^{sd}(eV)	D_o(cm^2/sec)
840 - 970	2.12±0.02 [a]	0.6
800 - 980	1.96± ? [b]	0.1
850 - 1064	2.15±0.01 [c]	0.62
685 - 1062	2.05±0.02 [d]	0.47

[a] Ref. 25 - Single Crystals
[b] Ref. 25 - Poly Crystals
[c] Ref. 26
[d] Ref. 27 - Single Crystals

It has recently been pointed out by Slifkin[14] that for low values of D^{sd} (i.e., $D^{sd} < 10^{-11}$ cm^2/sec), diffusion along dislocations can contribute significantly to mass transport. Therefore in a $\ln D^{sd}$ versus 1/T plot, the low temperature values tend to be relatively larger. Because of this, LeClair[8b] has re-analyzed the accurate data of Kuper et al.[25] using only their high temperature results and obtained a value for Q^{sd} of 2.10±0.02 eV and D_o = 0.33 cm^2/sec.

If it is assumed that self-diffusion at high temperatures in copper is controlled by the motion of monovacancies, then the migration enthalpy ΔH^m_{1v} can be calculated directly from the relation $\Delta H^m_{1v} = Q^{sd} - \Delta H^f_{1v}$. Ramsteiner et al.[13] favor a value of 2.12±0.02 eV for Q^{sd} and therefore set ΔH^m_{1v} = 1.06±0.08 eV consistent with ΔH^f_{1v} = 1.06±0.06 eV. On the other hand, Simmons and Balluffi[11] have repeatedly favored Q^{sd} = 2.05±0.02 eV and thus set ΔH^m_{1v} = 0.88±0.13 eV consistent with ΔH^f_{1v} = 1.17±0.11 eV. The limit of error is obtained by summation of the stated uncertainties in the individual values.

D. Nonequilibrium Experiments

In order to investigate many of the properties of point defects, it is often desirable to produce and retain them under nonequilibrium conditions. Three important techniques have been utilized in introducing point defects under this condition, namely, quenching, plastic deformation, and high energy radiation. The present discussion will be limited to quenching.*

---

* After quenching only vacancies will exist, whereas high energy radiation and plastic deformation produce vacancies, interstitials, and complex aggregates.

If a crystal is rapidly cooled from an elevated temperature, the equilibrium concentration of vacancies characteristic of that temperature can, in principle, be "frozen-in" and subsequently detected at low temperatures. Any physical property that depends sensitively and proportionally on the concentration of defects may be used to measure the quench induced vacancy concentrations. The residual resistance is very sensitive to the presence of imperfections because any disturbance of the ideally periodic lattice results in scattering of the conduction electrons and hence produces an increase in the electrical resistance. The accurate determination of changes in the electrical resistance at 4.2°K has proven to be an extremely valuable parameter for the investigation of point defects in general, and vacancies in particular. Therefore, from the variation of quenched-in resistance with the quenching temperature the enthalpy of formation can be estimated directly. Such experiments, however, are complicated by:

1. Small concentrations of metallic impurities present in so-called high purity material,[1]

2. Gaseous contamination of the specimen from the atmosphere or quenching medium prior to and during the quench or retained during preparation,[11,13,28-36]

3. Thermal and mechanical strains accompanying rapid quenching techniques,[37-42]

4. Concentrations of multi-vacancy complexes present in thermal equilibrium at T_q,

5. Loss of vacancies during the quench to permanent sinks (i.e., free dislocations, subgrain and grain boundaries, and free surfaces),[28,29,42-46]

6. Formation of vacancies clusters (e.g. di- and trivacancies) at the expense of monovacancies during the quench.[47-52,75]

Experimental data[28,29,42,44-46] indicate that the perturbations caused by these factors increase with increasing quench temperature and in general result in the estimated value of the monovacancy formation enthalpy being somewhat lower than the "true" value. These effects can, in part, be minimized by careful selection and control of the experimental conditions.

Assuming for just this reason, that complications 1-3 have a negligible effect on the quenched-in vacancy concentration, the expected change in the electrical resistance of a "well annealed" crystal immediately after quenching from T_q can be represented by

$$\left[\Delta R(T_q)\right]_{4.2°K} = 100\ g\left[\Delta\rho_{1v}\ C_{1v}(T^*) + \Delta\rho_{2v}\ C_{2v}(T^*) + \ldots\right] \quad (9)$$

where

g = geometric factor of dimension cm^{-1},

$\Delta\rho_{jv}$ = resistivity per atomic percent of the jth type defect

$C_{jv}(T^*)$ = fractional concentration of the jth type defect characteristic of some temperature T^* and a total vacancy concentration of $f(T_q)[\Delta N/N]_{T_q}$. Here $f(T_q)$ is the fraction of the equilibrium concentration, $(\Delta N/N)_{T_q}$, retained. The temperature T^* is defined as that temperature, above which the concentration of the jth type defect is equal to its equilibrium value corresponding to the instantaneous temperature and below which the equilibrium concentration characteristic of T^* is frozen-in.

Under the limiting conditions

$$f(T_q) \cong \text{constant}, \tag{10}$$

$$(\Delta N/N)_{T_q} \cong C_{1v}(T_q), \tag{11}$$

$$\Delta\rho_{1v} \cong 1/2\ \Delta\rho_{2v} \cong 1/3\ \Delta\rho_{3v} \cong \ldots \tag{12}$$

it follows that

$$[\Delta R(T_q)]_{4.2°K} \cong A \exp(-\Delta H^f_{1v}/kT_q) \quad . \tag{13}$$

Here $A = 100 \cdot g \cdot f \cdot \Delta\rho_{1v} \exp(\Delta S^f_{1v}/k)$, where ΔS^f_{1v} is the monovacancy formation enthalpy. Low quenching temperatures and cluster binding energies favor conditions (10) and (11), and the linear approximation, i.e., $\Delta\rho_{jv} = j\Delta\rho_{1v}$ where $j \leq 3$,* is expected to be true within about 10%.[53,54] Experimental results for aluminum,[55] gold,[56] silver,[28,29] and platinum[42] indicate that there is a limited temperature range over which the above conditions are approximately satisfied, thus allowing a determination of ΔH^f_{1v} to be made from the temperature dependence of $\Delta R(T_q)$.

The existing data from quenching experiments on pure copper are, in many cases, inconclusive. The temperature dependence of the quenched-in resistance has apparently been investigated in a number of laboratories, however, some of these results have gone unpublished.[11] In at least one case, anomalously large and erratic resistance increments precluded any analysis.[65]

Airoldi, et al.[66] quenched 0.04 mm diam. wires of nominally 99.999% pure copper in gaseous argon at an initial rate of 5×10^3 deg/sec. Over

---

* It is presently thought that in the noble metals most of the vacant lattice sites present immediately after a quench exist either as isolated vacancies or in clusters of order $j \leq 3$, if the temperature to which the specimen is quenched is sufficiently low.

a temperature range from 600 to 800°C, the increase in resistivity could be described by

$$\Delta\rho(T_q) = [(11\pm3)\times10^{-4} \text{ ohm-cm}] \exp(-1.0\pm0.1 \text{ eV}/kT_q) . \quad (14)$$

This corresponds to about 0.2μ ohm-cm at the melting point, 1083°C. If it is assumed that the data are representative of the equilibrium concentration of defects at the quench temperature, then by combining this increment with the directly measured concentration given by Simmons and Balluffi,[11] namely $(\Delta N/N)_{1083°C} = 2.0\times10^{-4}$, one obtains $\Delta\rho_{1_v} \approx 10\mu$ ohm-cm per atomic percent vacancies. This estimate is about six times the upper limit expected from theory.[67]

Martin[68] has quenched 0.1 mm diam. wires (99.999% pure copper) from temperatures up to 800°C into methyl alcohol at -78°C at an estimated quenching speed of $\approx 5\times10^3$ deg/sec. The specimen was heated in vacuum prior to the quench. The quenched-in resistivity increments never exceeded about 2×10^{-10} ohm-cm. This change is more than two orders of magnitude smaller than that obtained by Airoldi et al.[66] at comparable temperatures even though the reported quenching rates are similar.

Budin et al.[32,33] have reported on 0.1 mm diam. copper wires (99.999%) quenched from a hydrogen atmosphere at 25×10^3 deg/sec. The resistance increments were complicated by a reasonably large contribution from dissolved hydrogen. The increment of resistance proportional to the retained vacancy concentration was obtained from the difference between the total change in resistance and that due to dissolved hydrogen. An explicit relationship between T_q and C_{1v} was <u>not</u> given. The data are interpreted in terms of $\Delta H^f_{1v} = 1.17\pm0.06$ eV and $\Delta\rho_{1v} = 1.1\mu$ ohm-cm per atomic percent vacancies. The authors commented on the good agree-

ment between their estimate of the formation enthalpy and that found by Simmons and Balluffi.[11]

The migration characteristics of vacancies can be investigated from a detailed analysis of the kinetics associated with the disappearance (i.e., to permanent sinks and by aggregation) of quench induced defects. This is usually accomplished by determination of changes in the electrical resistance as a function of time and temperature. The principle objectives are (1) a characterization of the main annealing stages during isochronal recovery processes, (2) identification of the migrating defect, estimation of its migration enthalpy, and, in the case of multivacancies, an estimation of its characteristic binding energy, and (3) the identification of the operative vacancy sinks. The experimental situation is complicated:

1. Because the observed recovery processes are extremely sensitive to the total thermal history of the crystal,[1,57-59]

2. Because of interactions between quenched-in vacancies and impurity atoms, pre-existing dislocation, and dislocation damage resulting from quenching stresses,[1,34-36,42,57-60,75]

3. Because of complicated interactions between the various types of vacancy defects both during the quench[47-52,75] and during low temperature annealing.[1,59]

Unequivocal identification and quantitative assignment has been agreed upon in very few cases.

For copper there is disagreement concerning the main annealing stages. The results and some of the pertinent experimental conditions associated with the work (which the writer is aware of) are summarized in Table II.

The data of Airoldi et al.[66] indicate that rapid isothermal annealing

is observed only at temperatures above 350°C. Analysis of the annealing kinetics gave activation energies of 1.3 eV and higher. Martin[68] found that 50% of the quenched-in resistance annealed out after 15 min. at room temperature and reported, the seldom mentioned information, that all the increment could be annealed out. Budin and co-workers,[32,33] quenching from a hydrogen atmosphere, found a two stage recovery spectrum, -180 to -100°C and 0 to 100°C. These authors concluded that the low temperature activity was due to hydrogen, $\Delta H_h^m = 0.4$ eV and the higher temperature stage was attributed to monovacancies, $\Delta H_{1v}^m = 0.80$ eV. From results obtained from resistivity measurements and small-angle scattering of x-rays, Galligan and Washburn[64] detected considerable amount of point defect activity around room temperature subsequent to quenches from ~1070°C. Clarebrough et al.[35] studied, in some detail, the effects of neutral and reducing atmospheres on the isochronal annealing behavior of copper. For specimens quenched from a carbon monoxide atmosphere the resistivity decreases in two distinct stages of approximately equal magnitude. The low temperature stage (-50° to 100°C) was attributed to divacancy annealing by analogy with results from silver. The higher temperature stage (200° to 450°C) was attributed to the annealing out of submicroscopic vacancy clusters or dislocation loops. A more complicated annealing behavior was observed when specimens were quenched from an argon atmosphere (see Table II). This complication appears to be due to oxygen contamination resulting in the formation of stress induced dislocation loops during the quench (see Table III).

The most complete kinetic data for quenched copper has been reported in a series of papers by Seeger and co-workers.[13,24,69,70,71] Small-angle scattering of x-rays and electrical resistance results (-20° to

Table II. Recovery Processes Associated with Quench Induced Vacancies in Copper

Investigator et al.	Composition	Atmosphere	T_q (°C)	T_o (°C)	Quenching Medium	Property Measured	Observations (i.e., annealing stages, migration enthalpy, and binding energy)
Airoldi[a]	99.999%	Argon	~ 930	~ 20	Argon	$[\Delta R]_{300°K}$	Ann. stage: 350° to 470°C $\Delta H^f_{lv} \approx 1.3$ eV
Martin[b]	99.999%	Vacuum	< 800	-78 → -196	Methyl alcohol	$[\Delta R]_{4.2°K}$	Isothermal anneal: ≈50% annealed out after 15 min. at room temp.
Budin[c]	99.999%	Hydrogen	< 750	-196	Hydrogen gas	$[\Delta R]_{77°K}$	Ann. stage: -180° to -100°C $\Delta H^m_n \approx 0.4$ eV Ann. stage: 0° to 100°C
Galligan[d]	99.999%	Helium	1070	-20	Iced brine	$[\Delta R]_{77°}$ and [x-rays]$_{77°K}$	Isothermal annealing: considerable activity at room temperature
Clarebrough[e]	99.999%	Flowing carbon monoxide	Local melting	0 → -196	Distilled H_2O	$[\Delta R]_{77°K}$	Ann. stage: -50° to 100°C Ann. stage: 200° to 400°C

Table II (continued)

Investigator et al.	Composition	Atmosphere	T_q (°C)	T_o (°C)	Quenching Medium	Property Measured	Observations (i.e., annealing stages, migration enthalpy, and binding energy)
Clarebrough[e]	99.999%	Flowing argon	Local melting	0 → -196	Distilled H_2O	$[\Delta R]_{77°K}$	Ann. stage: -100° to -75°C Ann. stage: - 50° to 0°C Ann. stage: 0° to 120°C Continuous annealing 120° to 500°C
Seeger[f]	99.999%	Forming gas 92% N_2 + 8% H_2	Local melting	16 → -100	H_2O	[X-rays] 110°K	Ann. stage: 20° to 100°C ΔH^m_{2v} = 0.62+0.03 -0.07 eV B_{2v} = 0.13+0.03 -0.06
Ramsteiner[g]	99.999 or 99.99%	Vacuum → argon	900 830	0 → -183	H_2O	[ΔR] 90°K	Ann. stage: -20° to 50°C 100° to 250°C
	99.999 or 99.99%	Vacuum → argon	1000 900 800	20 → -183	H_2O	[ΔR] 90°K	Ann. stage: 100° to 250°C ΔH^m_{1v} = 1.08±0.03 eV
	99.999 or 99.99%	Argon or argon and alcohol vapor, or forming gas	1000	0 → -50	H_2O or H_2O with oil on top	$[\Delta R]_{77°K}$	Ann. stage: -50° to -75°C ΔH^m_{2v} = 0.64±0.05 eV B_{2v} = 0.12±0.05 eV Ann. stage: ≈100° to 200°C ΔH^m_{1v} = 1.1±0.1 eV

a. See reference 66; b. see reference 68; c. see references 32 and 33; d. see reference 64; e. see reference 35; f. see reference 24; g. see reference 13. T_q = Quenching temperature; T_o = Temperature to which the specimen is cooled.

250°C) indicate the existence of two main annealing stages, i.e., -20° to 100°C and 100°C to 200°C. The upper stage has been explained by the migration of a single vacancy, $\Delta H^m_{1v} = 1.08$ eV. The lower stage has been interpreted in terms of the annealing of divacancies which are in local thermal equilibrium with single vacancies. The migration enthalpy and binding energy of a divacancy are believed to be $\Delta H^m_{2v} = 0.67$ eV and $B_{2v} = 0.12$ eV. These results have recently been summarized and discussed.[12]

If the available annealing data are considered as a whole, they appear to indicate the existence of three annealing stages, i.e., $-80°C < T_1 < 100°C$, $100°C < T_2 < 250°C$, and $350°C < T_3 < 450°C$. The low temperature activity is quite sensitive to T_o and the intermediate stage has been observed in only one laboratory. The complications arising from gaseous contamination are quite marked and well documented in at least four different investigations.[13,32,33,35] In at least two cases, non-reproducible quenched-in increments for approximately the same T_q have been reported.[13,35]

In the majority of quenching experiments, the recovery processes are accompanied by the formation of vacancy aggregates.[9,61] Their detection and identification are of considerable importance in the understanding and theoretical interpretation of recovery processes.[57-59,62] Transmission electron microscopy of thin foils has proved to be a powerful technique in the investigation of defect clusters of diameter greater than about 40 Å.[61,63] In addition, small-angle scattering of x-rays can, under certain conditions,[24,64] be a revealing technique in studying the initial stages of vacancy precipitation. Cluster diameters in the range ≈10 to 60Å can be detected by this method.

Copper is unique in that the initial stages of vacancy aggregation

have been investigated by x-ray techniques. Analysis of small angle scattering measurements made on quenched copper annealed at, or slightly above, room temperature suggest that vacancy clusters have spherical shapes[64] or perhaps are oblate ellipsoids.[24] Clusters were first detected after about 30 min. annealing at 25°C and reached a maximum size of ≈ 30Å after 2 hrs.[64]

Transmission electron microscopy observations on quenched and isothermally annealed copper are far from satisfactory but in some respects quite revealing. These results are summarized in Table III. The only resolvable defects, appearing in a reasonable density, are loops which lie in rows along ⟨110⟩ directions. Smallman and co-workers[74] concluded from their observations that these loops were of the Jones-Mitchell type[76] and were formed as a result of large stresses around precipitates. The stresses develop during the quench because of differential thermal contraction. The fact that the loops were associated with particles was subsequently verified by Barnes and Mazey.[34] These authors also showed that the observed geometry of the rows was consistent with that predicted by theory[76] and that the loops were therefore produced by prismatic punching. It has also been suggested that the punched loops in copper are of interstitial character, and it is generally assumed that the precipitate particles responsible for the punching arise from the internal oxidation of trace impurities during pre-quench thermal treatments.[34,35] Both copper and its oxide can dissolve oxygen.[77] The absence of prismatic punching in crystals quenched from vacuum[34] and carbon monoxide[35] supports this argument.

The generation of such defects can, in part, account for non-reproducible and erratically large quenched-in increments that have been reported,

Table III. Transmission Electron Microscopy Investigations of Defect Aggregates in Quenched Copper

Investigator et al.	Composition	Atmosphere	T_q (°C)	T_o (°C)	Quenching medium	Annealing treatment	Observations
Hirsch[a]	-	-	-	-	-	-	Rows of loops lying along ⟨110⟩ directions.
Smallman[b]	OFHC Cu (>99.99%)	Purified argon	1050	-45 to +18	H_2O and iced brines	1 hr at 120°C	Prismatic loops (~200 A diam.); rows of loops lying along ⟨110⟩ directions; complex dislocation networks.
Smallman[c]	OFHC Cu (>99.99%)	Purified argon	1050	-20	Iced brine	30 min at 100°C	Prismatic loops; helical dislocations; deformation twins; complex dislocation networks; rows of loops lying along ⟨110⟩ directions.
Chik[d]	99.999%	Forming gas	Local melting	+16	H_2O	2 hrs at 80°C	Black spots; double arc loops; some loops ~200Å diam; denuded regions near grain boundaries.
Galligan[e]	99.999%	Vaccum	1070	-20	Iced brine	2 yrs at room temp.	Black spots; no resolvable dislocation loops.
Barnes[f]	99.999%	Argon	1055	20	H_2O	Room temp.	High density of precipitates; rows of prismatic loops lying along ⟨110⟩ directions.

Table III (continued)

Investigator et al.	Composition	Atmosphere	T_q (°C)	T_o (°C)	Quenching medium	Annealing treatment	Observations
Barnes[f]	99.999%	Vacuum	1055		Silicon oil	Room temp.	No precipitates and no rows of loops.
Clarebrough[g]	99.999%	Flowing argon	Local melting	-11	Iced brine	Room temp. 100°C 200°C	High concentration of loops lying in rows along ⟨110⟩ directions.
Clarebrough[g]	99.999%	Flowing CO	Local melting	-11	Iced brine	Room temp 100°C 200°C	No evidence for any type of defect cluster.
Cotterill[h]	Not reported	Nitrogen	1020	0	H_2O	100°C	Precipitates; rows of loops; black spot defects.
		Argon and 1% hydrogen	1030	0	H_2O	100°C	Rows of loops lying along ⟨110⟩ directions; black spot defects; tetrahedra (?).
Bell[i]	99.999%	Vacuum	Local melting	~0	Sprayed helium gas	15 min at 0°C → 60 min at 100°C	Perfect and imperfect prismatic loops.

a. See reference 72; b. see reference 73; c. see reference 74; d. see reference 70; e. see reference 64; f. see reference 34; g. see reference 35; h. see reference 75; i. see reference 78.

as well as, the more complicated annealing behavior reported by Clarebrough et al.[35] for specimens quenched into water from an argon atmosphere.

The first observable defect which is thought to be characteristic of the "pure" metal is the so-called black spot in bright field images. Prior to the contrast study of Bell et al.,[78] the results of which will constitute a part of the present report, little was really known about the nature of black spot defects or about their relationship to the vacancy recovery spectrum. It had been suggested that the smallest black spots might be voids consistent with the small angle x-ray scattering data and the larger ones dislocation loops,[70] or that they might actually be unresolved stacking fault tetrahedra consistent with energy considerations.[75]

E. Present Investigation

The present experimental investigation on copper was undertaken in an attempt to: 1. estimate the monovacancy formation enthalpy, ΔH^f_{1v}, under nonequilibrium conditions for comparison with equilibrium experiments and theory; 2. obtain an estimate of the monovacancy migration enthalpy from the relation $Q^{sd} - \Delta H^f_{1v} = \Delta H^m_{1v}$, where Q^{sd} is the experimentally determined self-diffusion activation enthalpy; 3. obtain data from which the resistivity per atomic percent vacancies, $\Delta\rho_{1v}$, can be evaluated in combination with equilibrium measurements and compared with theory; 4. investigate the isochronal annealing behavior of quenched-in vacancies over a sufficiently wide range of temperature so as to provide qualitative information about defect mobility and vacancy clustering phenomena; 5. determine conditions favorable for detailed observation of vacancy aggregates (e.g., voids, black spots, or resolvable loops) and

thereby investigate their nature and assess their relative importance in recovery processes; 6. establish a basis for future detailed investigations of vacancy annealing kinetics and nucleation and growth of vacancy aggregates in quenched copper; and 7. provide information useful in the atomic interpretation of the annealing of irradiated and cold-worked copper.

For these purposes, the temperature dependence of quench induced resistance was determined at 4.2°K. Changes in this quantity were measured as a function of time and temperature, and transmission electron microscopy observations were made on quenched and isothermally annealed foils. The experimental conditions were designed so as to overcome formidable difficulties previously encountered. Because of this, significant limitations were imposed on the techniques and thus precluded conducting the two types of measurements on the same specimen. It is felt that the present results are representative of vacancy behavior in nominally 99.999% pure copper and that difficulties from the numerous complicating features previously cited have, for the most part, been minimized.

II. EXPERIMENTAL PROCEDURE

A. Electrical Resistance Experiments

High purity copper wires were quenched in a static atmosphere of helium gas from temperatures greater than 450°C and less than 800°C. Specimens were d.c. resistance heated in a positive pressure of purified helium exchange gas while the experimental chamber was embedded in liquid nitrogen. The temperature of the specimen was determined from the known temperature dependence of the resistance. Quenching was accomplished by switching off ≈99% of the input power. Quenching profiles were recorded oscillographically under constant current conditions. The residual resistance, measured at liquid helium temperature by precision potentiometric techniques, was used to detect the quench induced damage. Pre-quench annealing was carried out in vacuum. Considerable care was taken to ensure reproducibility of the well annealed state. Isochronal annealing studies were conducted subsequent to quenches from ≈700°C. Specimens were resistance heated by electronically controlling the current passing through them. The annealing progress from -200° to +500°C was followed by measuring the change in electrical resistance of the specimens at 4.2°K.

1. Material

The copper specimens were 0.005 cm diameter hard drawn wires supplied by Sigmund Cohn Corporation. The wire was prepared from grade A-58 copper of nominal 99.999+% purity obtained from the American Smelting and Refining Company. According to the supplier, no impurities are detectable by spectrographic analysis with the following known limits of sensitivity (in parts per million by weight): Si < 0.1, Cr < 0.5, Fe < 0.7, Ni < 1,

As < 2, Ag < 0.3, Sn < 1, Sb < 1, Te < 2, Pb < 1, and Bi < 0.1 Chemical analysis showed that the copper contained Se < 1 and S < 1 parts per million. Spectrographic analysis* after drawing showed that the wire contained 1 to 2 parts per million of iron and silver. No other metallic impurities were detected. The limits of sensitivity were identical to those originally employed by the American Smelting and Refining Company. Mounted and annealed specimens had ratios of resistance at 273°K to that at liquid helium temperature from 450 to 650.

2. Experimental System

In view of the difficulties encountered during previous experimental investigations of quenched copper and as a result of experience gained during the early stages of the present work, the quenching and annealing environments were designed so as to minimize gaseous contamination and mechanical deformation. To this end, a system (see Figs. 1 and 2) was established which would permit work to be carried out in a dynamic vacuum or a controlled helium atmosphere with the experimental chamber at temperatures between 4.2°K and 673°K without necessitating moving the specimen.

The system was constructed from 304 stainless steel and Corning 7740 glass. Joints were heli-arc welded, copper gaskets were used wherever possible and parts were electropolished or chemically polished before assembly. For these reasons the experimental chamber and gas manifold were bakable to 400°C.

The glass construction of the double dewar cryogenic system and experimental chamber permitted visual observations of the copper wire

---

* Lucius Pitkin, Inc., New York, New York

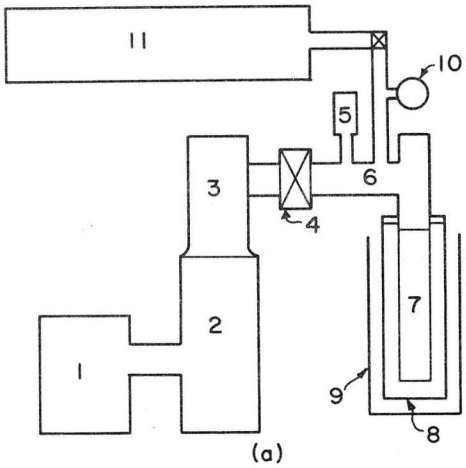

1. Mechanical pump
2. Oil-diffusion pump
3. Liquid nitrogen cold trap
4. High-vacuum valve
5. Bakeable high-vacuum gauge
6. Stainless steel manifold
7. Glass-specimen chamber
8. Glass liquid-helium dewar
9. Glass liquid-nitrogen dewar
10. Pressure gauge
11. Stainless steel gas-storage tank

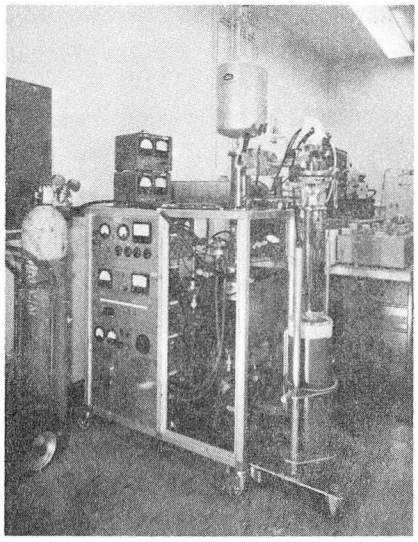

(b)

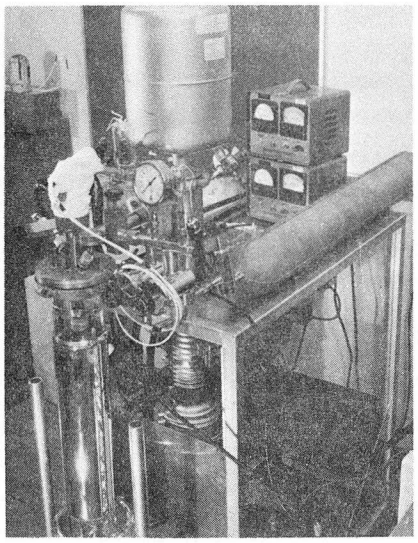

(c)

ZN-5626

Fig. 1 Experimental system: a. schematic of system; b. side view photo; c. front view photo.

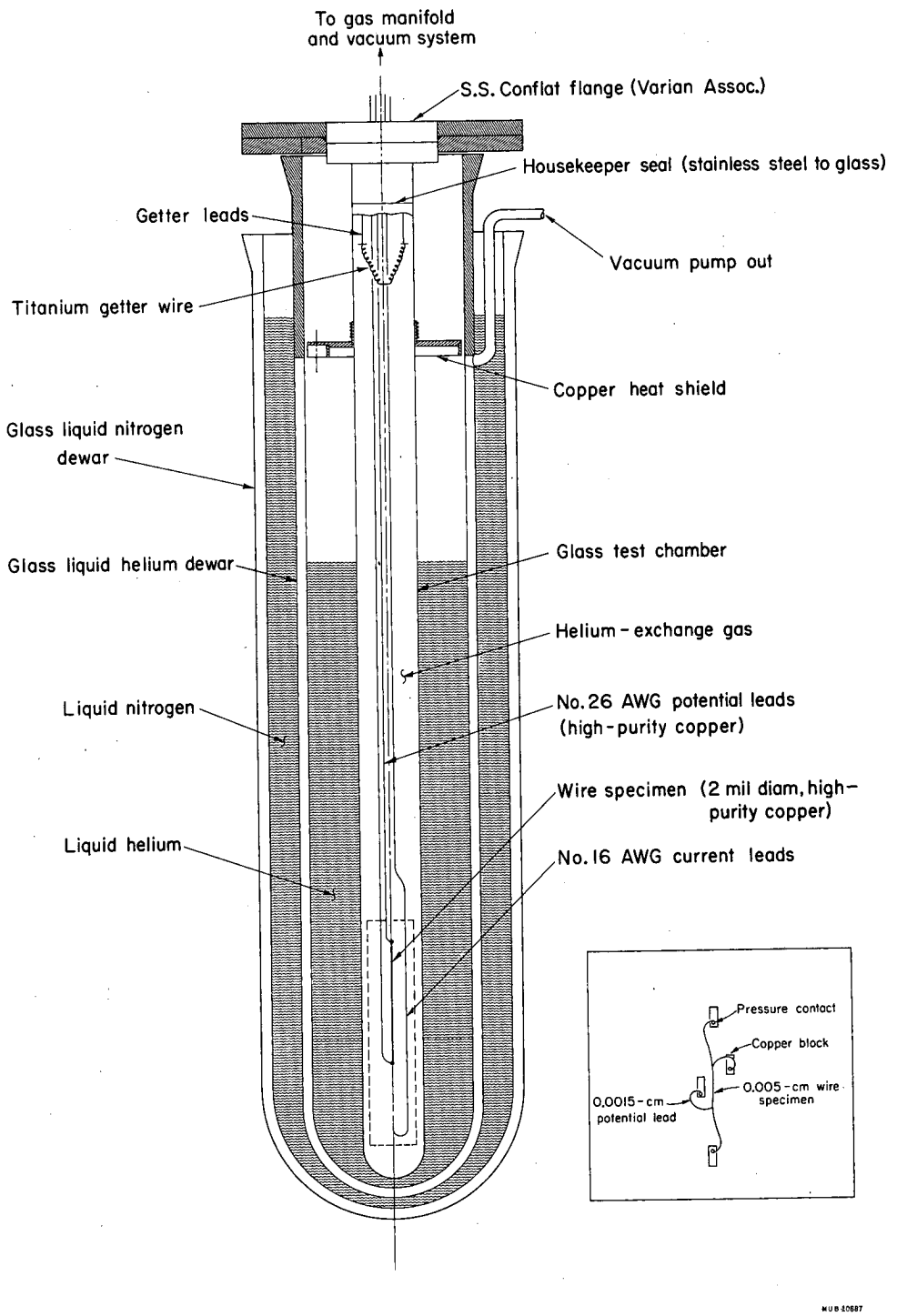

Fig. 2 Details of experimental chamber and double dewar cryogenic facilities. Inset is a schematic of wire specimen and potential leads.

to be made under all experimental conditions. This was a very desirable feature, inasmuch as temperature inhomogeneities during heating experiments could be detected visually.

Copper current and potential leads were brought out of the chamber through vacuum tight feed-throughs. Purified helium gas was stored in pre-baked stainless steel tanks and introduced into the system through an all metal valve. The gas pressure was monitored either on a Hasting (Model DV-17) bakable thermocouple sensing element in the range 0-1000μ Hg or on a USGA (Type C15-25) stainless steel compound gauge (30"-0-15#).

3. Specimen Preparation and Mounting

A 0.005 cm diameter wire specimen approximately 10 cm long was carefully chosen and inspected in order to detect any shape inhomogeneities which might have resulted from drawing and subsequent handling. A satisfactory wire was then cleaned in acetone and rinsed in ethyl alcohol. The top (≈ 1 cm long) and bottom (≈ 2.5 cm long) of the wire were chemically polished in a solution of 50% nitric acid, 25% glacial acetic acid, and 25% phosphoric acid and carefully rinsed. The cross sectional area at the ends was reduced by about 20% as a result of this operation, thus helping to promote a uniform temperature distribution along the gauge length.

The specimen was fixed inside the pyrex chamber as shown in Fig. 2 (see insert). Each specimen consisted of a straight gauge length bounded by two curved end sections which minimized restraints and also helped to establish a uniform temperature distribution. The gauge length was determined by two 0.0015 cm diameter wires, of the same material and nominal purity as the specimen, spot welded about 5 cm apart. Gauge

lengths were reproduced within ±0.2 cm so as to minimize effects resulting from differences in specimen geometry.

4. Pre-Quench Annealing Treatments

Prior to the introduction of a new specimen the chamber and manifold were baked at a temperature of 400°C for about 5 hours. After the speciment was mounted and system evacuated for 8 to 10 hours ($\approx 1\times10^{-7}$ torr), the chamber was again baked to a maximum temperature of 300°C over roughly a 6 hour period. The pressure never exceeded 5×10^{-7} torr during this interval and the maximum specimen temperature reached was estimated to be 200°C.

After bake-out the chamber was cooled to liquid helium temperature. Vacuum annealing was accomplished under this condition by d.c. resistance heating using the known temperature variation of the resistance to determine the specimen temperature. Vacuum conditions in the region of the specimen were estimated to be $< 2\times10^{-8}$ torr.

Hard drawn wires were given an initial high temperature anneal in order to promote grain growth and reduce the free dislocation density and thereby stabilize the specimen substructure. For this purpose the wires were annealed at ~400°C for 1 to 2 hours, 700 to 800°C for 30 minutes, ≈600°C for 1 hours, ≈500°C for 2 hours, and ≈400°C for 8-10 hours. While annealing at the higher temperatures, wires were examined for temperature inhomogeneities and only those having a uniform temperature distribution were retained for further use.

Before each quench cycle, wires were given an additional vacuum anneal of 15 min. at 500°C, 5 min. at 400°C, and 30 min. at 300°C. This procedure was required to ensure satisfactory reproducibility of the well annealed state (i.e. effectively vacancy free, impurity and

dislocation concentrations constant) as inferred from the residual resistance at liquid helium temperature.

The importance of such a reference base has been demonstrated by recent quenching work on gold.[56] The recipe presented here allowed a base to be obtained which was sufficiently reproducible to allow analysis of quenches from above about 460°C if considerable care and patience was taken in its execution.

5. Quenching Procedure

Both cryogenic dewars (see Fig. 2) were initially filled with liquid nitrogen. The residual helium gas from the previous quench-anneal cycle was evacuated (≈1 hr; ≈ 1×10^{-7} torr). A titanium getter wire, located in the upper part of the chamber, was outgassed (T ≈ 1500°C) by resistance heating for about 1 hr. The chamber and gas manifold were then isolated from the pumping station by way of a high vacuum valve. Previously purified helium gas (see Appendix I for purification details) was simultaneously leaked into the system. The gas pressure was slowly increased to 2 psi and the titanium getter wire maintained at a temperature of about 1200°C for 30 min in order to minimize the residual gases, other than helium, in the system resulting from the isolation step.

Specimens were d.c. resistance heated under constant voltage conditions.* Load regulation was better than 0.02%. The temperature of a test wire was determined from the experimentally measured temperature variation of the resistance. These data were normalized to a value of the resistance at 0°C, thus the ratio of the resistance at the quench

---

* Maximum power required was about 30 watts, i.e., 2.75 amps at 11 volts.

temperature (T_q) to that at 0°C could be compared to the known ratios in order to establish T_q. The data of Meechan and Eggleston[17] and of Leeds and Northrup[79] were used as standards. The nominal purity of the copper in both these cases was identical to that employed in the present work. For additional details refer to Appendix II.

The resistance at the quench temperature was determined from simultaneous measurements of the voltage drop across the specimen gauge length and across a 0.01Ω standard resistor connected in series with the specimen. In general it took about 3 min to bring the specimen to the desired temperature and it was equilibrated at the temperature for an additional 3 to 4 min.

Quenching was accomplished by switching off ≈99% of the input power. Quenching profiles were obtained from the change in specimen resistance during a quench by oscillographically recording the voltage drop across the gauge length under constant current conditions. For this purpose a silicon controlled rectifier switching unit was placed in series with the power supply (see Fig. 3). The heating power was switched off and in 1msec a 100 ma constant current was established. Figure 4 shows voltage time traces characteristic of this switching sequence for a fixed load. The importance feature is that at no time is additional energy brought to the sample. Mechanical switching techniques failed to display this property with any degree of reliability. The oscilloscope was triggered with an external pulse which was electronically coupled with the constant voltage → constant current operation and dealyed 1.1 msec so as to ensure that a quenching curve was characteristic of the constant current state. The switching, constant current power supply, and scope synchronization circuitry is shown in Fig. 5.

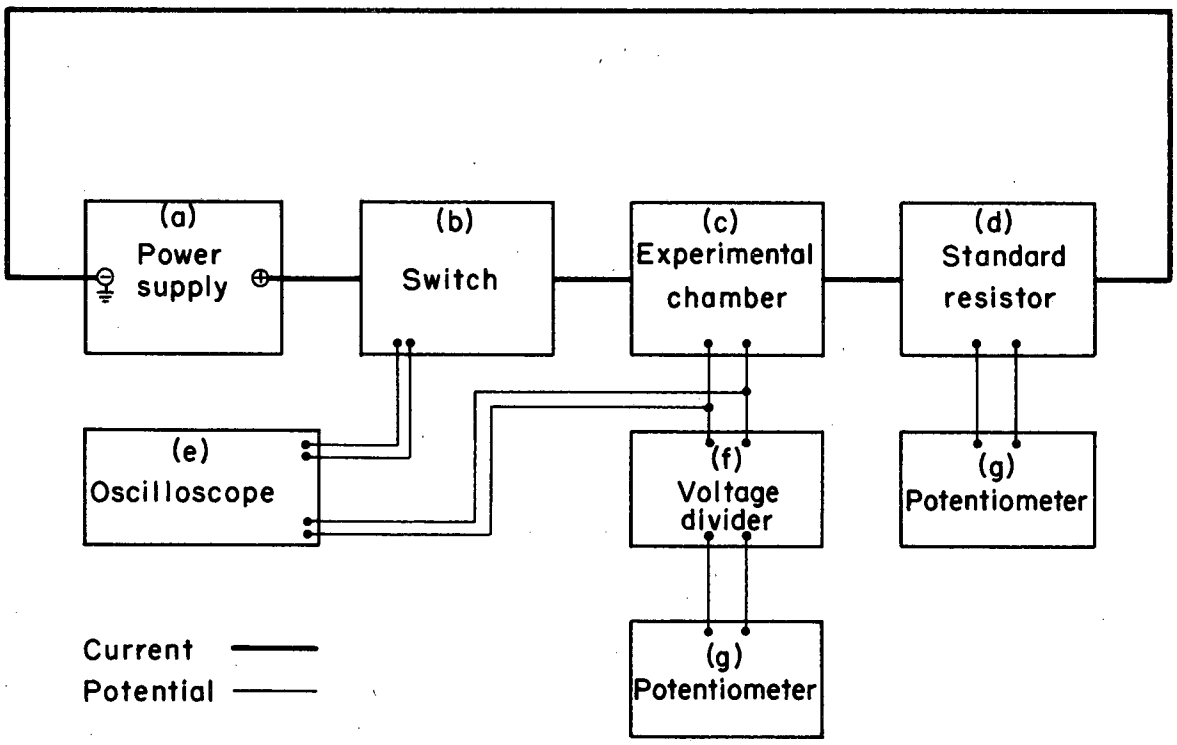

Fig. 3 Block diagram of components used for wire quenching cycles: a. constant voltage power supply (Lambda Electronic Corp., Model LE-103FM); b. silicon controlled rectifier switching unit, i.e., constant voltage to constant current and coupled oscilloscope synchronization pulse; c. experimental chamber; d. constant temperature oil bath containing precision 0.01Ω standard resistor (Leeds and Northrup No. 4222-B); e. oscilloscope (Tektronix Inc. dual-beam scope Type 502); f. precision voltage divider (×10); g. potentiometer (Leeds and Northrup, Model 8691).

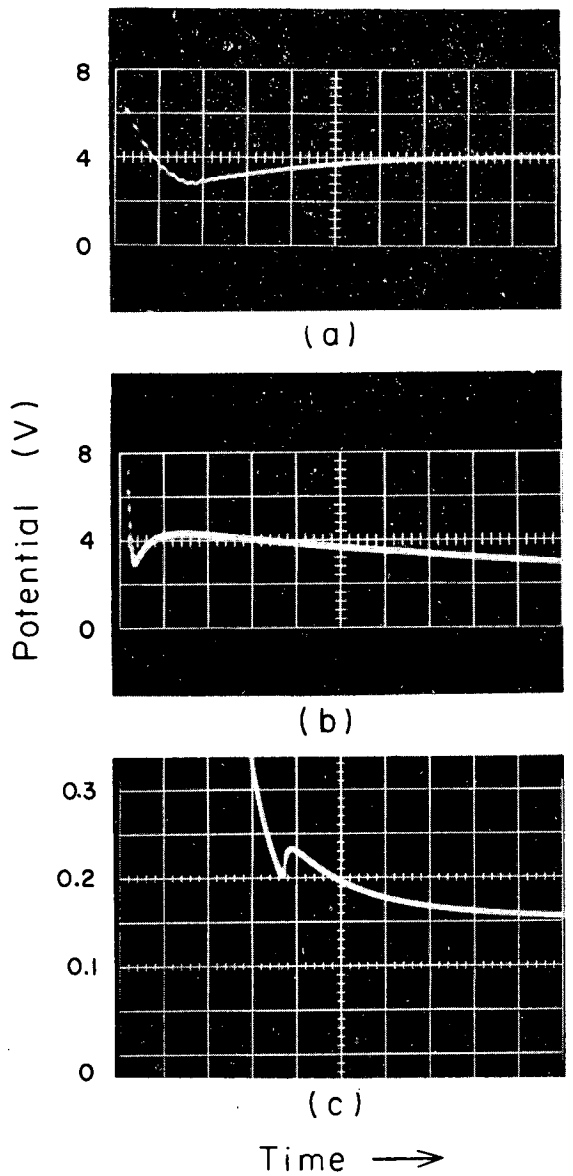

ZN5627

Fig. 4 Oscillographic traces of constant voltage (≈ 7.2 volts) → constant current (≈ 100 ma) switching sequence for a fixed load: a. 1μsec per division (≈1.8Ω load); b. 10μsec per division (≈1.8Ω load); c. 0.1msec per division (≈1.5Ω load).

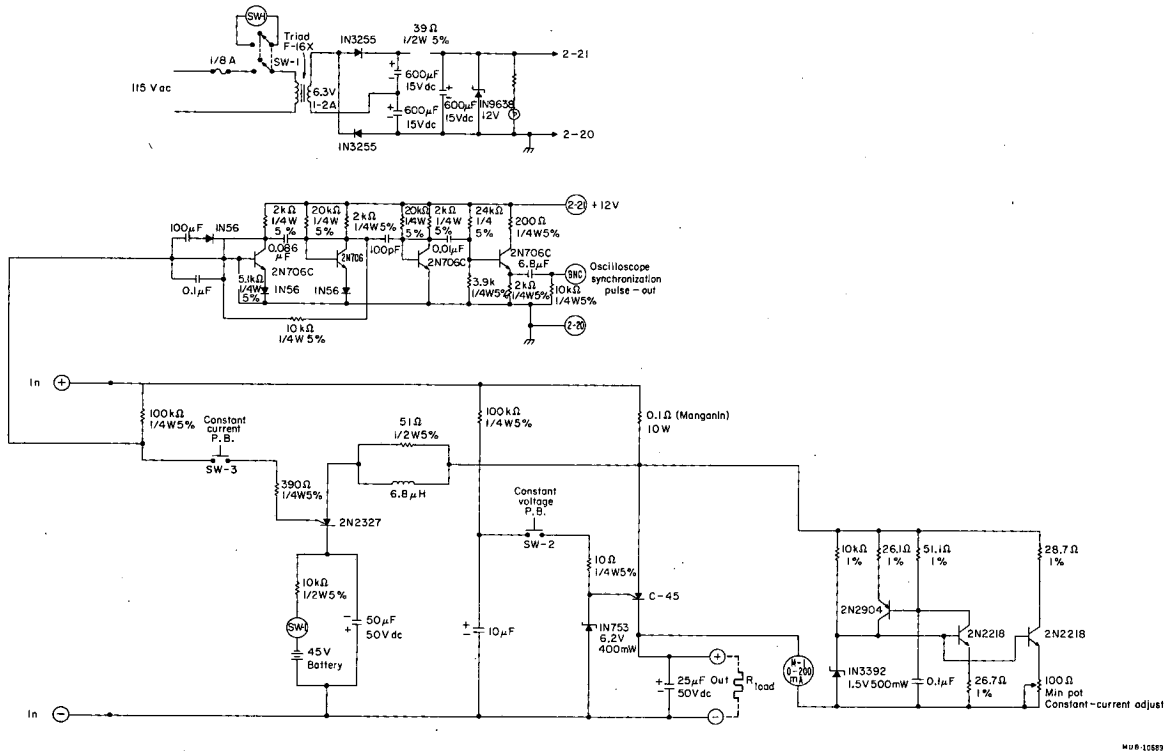

Fig. 5 Circuit diagram of constant voltage → constant current switching unit.

Quenching curves could be approximated by an exponential cooling law of the form

$$T(t) = T_o + \Delta T \exp(-\alpha t) \tag{15}$$

where $T_o = 77°K$ and $\Delta T = T_q - T_o$, α is the rate constant, and t the time in seconds. Initial quenching rates of about 25×10^3 deg/sec were obtained (i.e., $\alpha = 28 \pm 3$ sec^{-1}). The time required for the specimen to drop halfway to liquid nitrogen temperature was between 20 and 25 msec and to R(273°K) was between 50 and 60 msec. Typical quenching profiles for $T_q \approx 610°C$ are shown in Fig. 6.

Following a quench the helium gas pressure in the chamber was reduced to a value corresponding to about 500μ of Hg at 4.2°K. The liquid nitrogen in contact with the experimental chamber was removed by pressurizing the dewar with helium gas and blowing the nitrogen out through a small tube which extended to the bottom of the dewar. The resistance of the specimen remained approximately constant and characteristic of R(77°K) during this step. Standard techniques were then employed in transferring the liquid helium.

6. Resistance Measurements

All measurements of the residual resistance were made at liquid helium temperature in order to minimize the temperature dependent contribution to the resistance. This was essential in the present work since the quenched induced resistance was quite small.

The voltage across the specimen and across a 0.1Ω standard resistor connected in series with the specimen were measured simultaneously (see Fig. 7). To this end, two Rubicon 6-dial microvolt potentiometers (Model 2768) were employed. The galvanometer used for the current determination

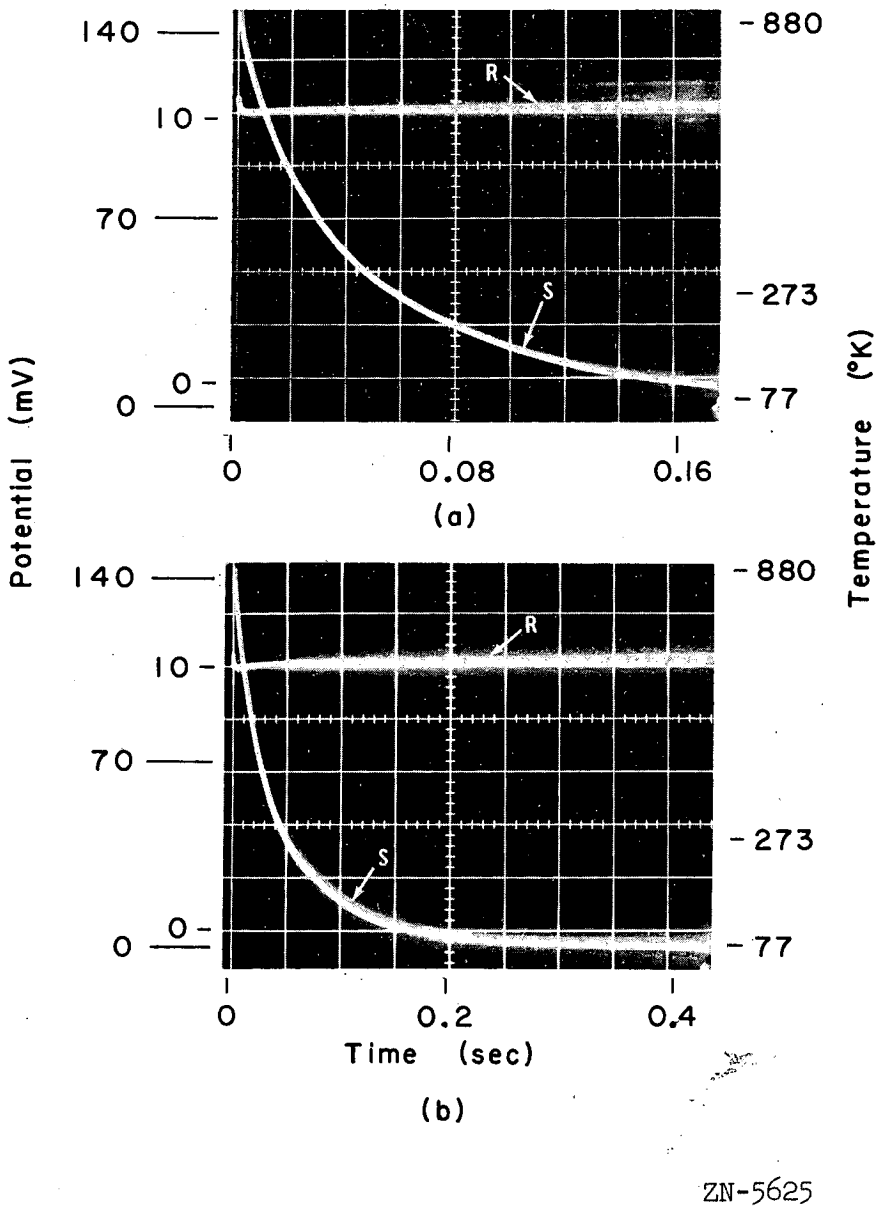

Fig. 6 Typical time-temperature characteristics during a gas quench. Here $T_q \approx 610°C$, R is the potential drop across a 0.1Ω standard resistor (0-10 mV) and S is the potential drop across the specimen (0-140 mV). (a) 20 msec per division; (b) 50 msec per division.

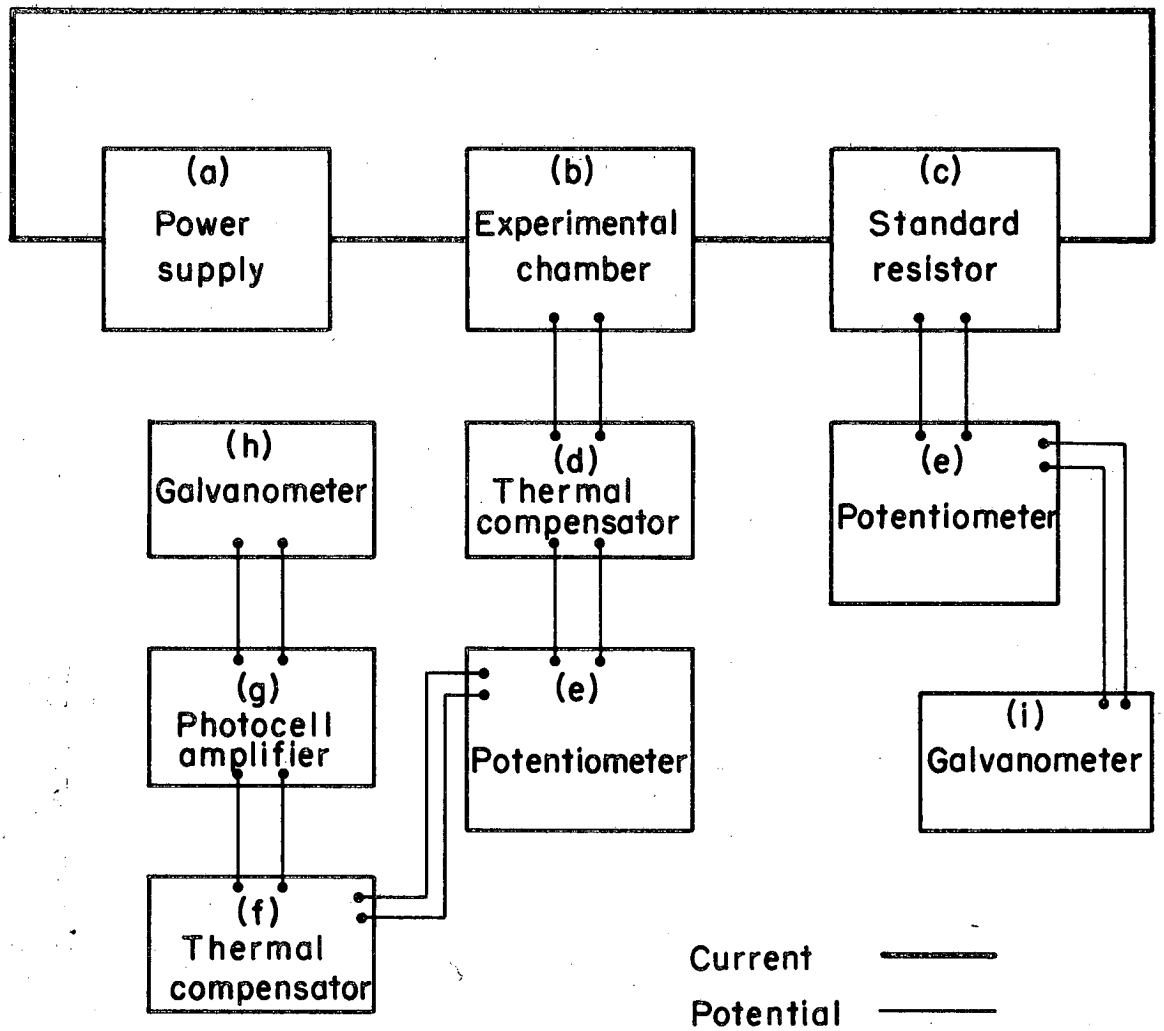

MUB-10690

Fig. 7 Block diagram of components used in making a resistance measurement: a. precision d.c. regulated power supply; b. experimental chamber; c. constant temperature oil bath containing 0.1Ω standard resistor (Leeds and Northrup No. 4221-B); d. thermal compensator; e. Rubicon 6-dial microvolt potentiometer (Model 2768); f. Guildline thermal compensator (Model 5214A); g. Guildline photocell amplifier (Model 5214/9460); h. Guildline secondary galvanometer (Model SR21/9461); i. Rubicon coil suspension galvanometer (Type 113493).

was a Rubicon coil suspension type (Model 113493) with a sensitivity of 1μ V/cm. In determining specimen voltages, a Guildline photocell amplifier (Model 5214/9460) and secondary galvanometer (Model SR21/9461) with a combined maximum sensitivity of 0.01μ V/cm were used. Due to the very high sensitivity of the amplifier, small thermal emfs produce very large signals. In view of this a Guildline thermal compensator (Model 5214A) was connected in series with the input to the amplifier. Therefore a small emf could be introduced in the circuit to balance out parasitic voltages and thereby bring the electrical zero and mechanical zero of the galvanometer system into coincidence.

The d.c. measuring current was maintained at 0.20000A and controlled to ±2 parts in 10^6 by a solid state regulator whose circuit is shown in Fig. 8. The peak-to-peak ripple was about 0.01%. A frequency response test showed that the specimen did not respond to the 60 period. No measurable self heating of copper wires was observed with this magnitude of current.

A Thompson emf, resulting from the fact that the specimen was at 4.2°K and the measuring equipment at room temperature, was found to be constant over periods of time considerably longer than necessary for making a measurement. This emf did vary in magnitude (0.1μV- 0.4μV) depending on the liquid helium level and exchange gas pressure in the experimental chamber. The effect of this latter variable was minimized by always making measurements at a gas pressure of 500μ Hg. Because of its stability with time, the Thompson emf was most easily accounted for by placing a precision thermal compensator (see Fig. 9) in the specimen potential loop and thereby balancing the emf out.

The background noise level in the measuring circuit was at most

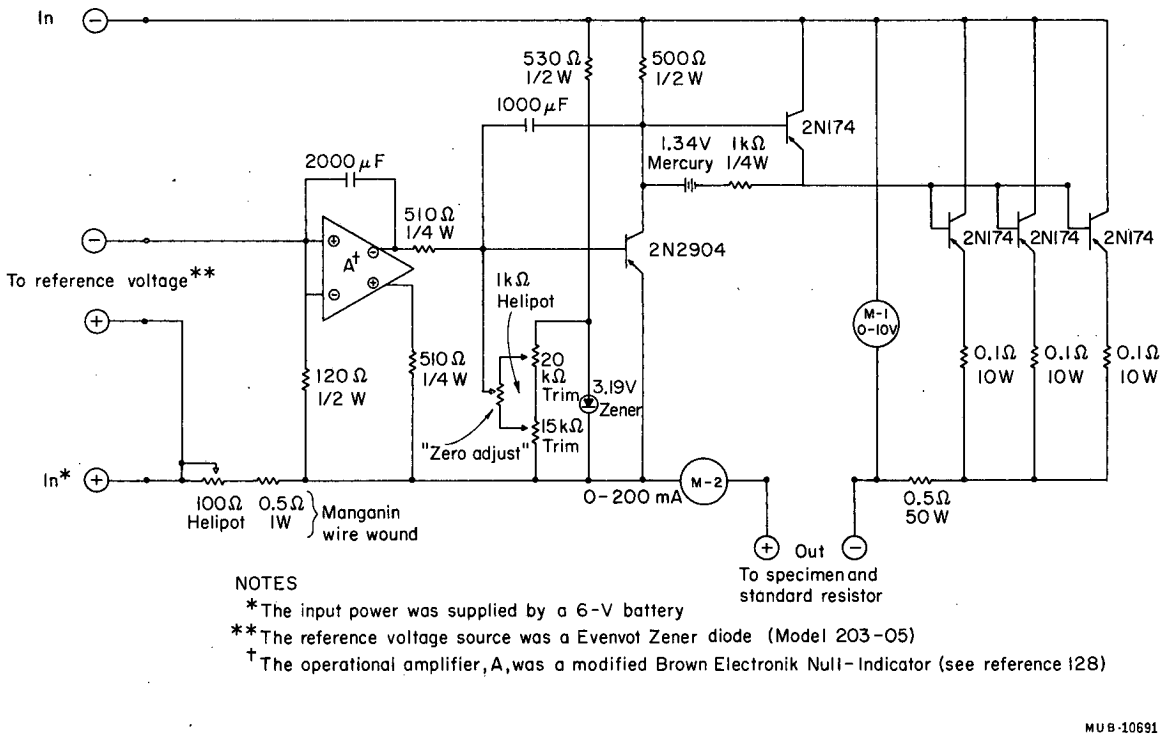

Fig. 8 Circuit diagram of precision direct current source.

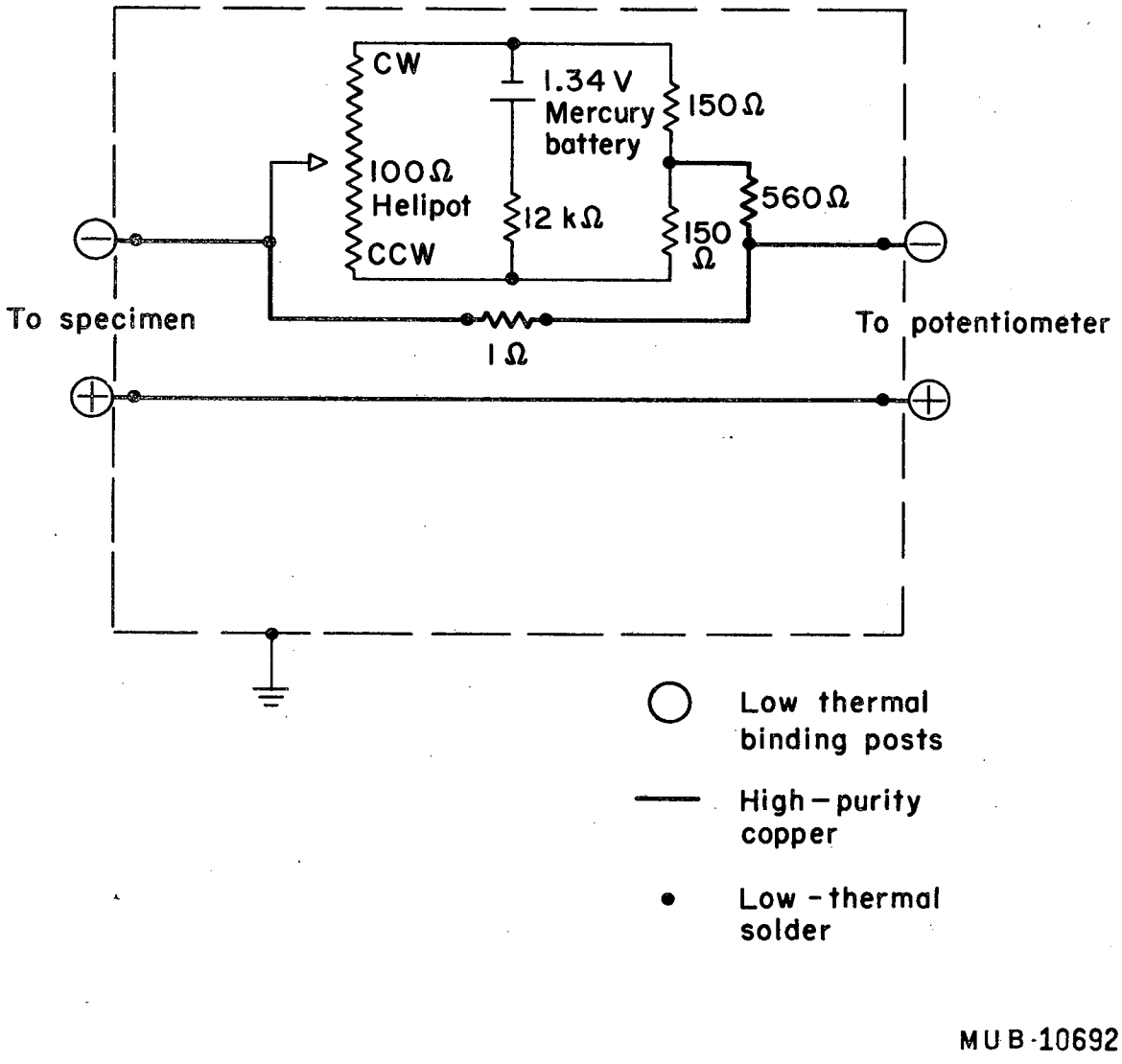

Fig. 9 Circuit diagram of precision thermal compensator (±6μV).

±0.002μ V and rapid fluctuations of thermal emfs were completely absent. It was estimated that the uncertainty in a potential reading, resulting from the noncoincidence of the electrical zero and mechanical zero (when referred to the galvanometer) due to background noise and uncompensated thermal fluctuations in the specimen and galvanometer pontential loops, was consistantly $\leq$ 0.005μ V and corresponded to about 0.004% for typical values of the specimen resistance. This was attributed in part to the following favorable conditions. The temperature of the room was thermostatically controlled to within ±2°C. Changes in room temperature which might effect equipment performance were quite minimal. Standard resistors, low thermal selector switch, and standard cell were housed in a large oil bath whose temperature remained constant to within ±0.02°C over periods of 8 to 10 hours. High purity copper wire (99.999+%) was used throughout the potential circuitry. Extreme care was taken in making potential lead contacts, in thermal and electrical shielding, and in the selection of grounding points.

It was possible for a single measurement of the residual resistance to be made with an uncertainty of about $\pm 5\times10^{-8}$ Ω (i.e., $\leq$ 0.01%) as determined from the previously quoted uncertainties in the measuring current and specimen voltage,* and a statistical uncertainty of about $\pm 1\times10^{-7}$Ω.

---

* This uncertainty is not meant to imply that the absolute value of the resistance is known to better than 0.01% since application of the manufacturer's specifications for all components would place an uncertainty of 0.02% on a measured value of the resistance for the calibrated accuracy and 0.04% for the limit of error case.

7. Isochronal Annealing

Subsequent to quenches from $T_q \approx 700°C$, a limited number of annealing experiments were conducted. Isochronal annealing consisted of heating the specimen for a fixed time (e.g. $\Delta t = 5$ min) at a series of increasing temperatures, selected so that $\Delta T/\Delta t$ remained constant.

Specimens were resistance heated in 500μ Hg of helium gas while the experimental chamber remained embedded in liquid helium. For this purpose the specimen was introduced as the "unknown" resistance in a Honeywell Kelvin double bridge (Model 1622). The bridge was operated in series with an external dc power supply (see Fig. 10). The resistance of the specimen was brought into coincidence with the present bridge resistance standard by controlling the current through the bridge. This was accomplished by taking the error signal from the bridge, amplifying it, and using the amplified signal to drive the series power supply. The temperature of the specimen was again determined from the known temperature dependence of the resistance.

Because of the rapid response time of the control system, a copper wire could be pulsed directly to a desired temperature from the liquid helium state. Care was taken to avoid overshoot by selection of appropriate amplifier gain conditions. Temperature-rise time of the specimen was of the order of 30 msec. Figure 11 shows an oscillographic trace of the bridge error signal for a pulse from 4.2° to 273°K. The approach to the null position clearly demonstrates the absence of overshoot.

Deviations from the balance position during an anneal were monitored on a Brown electronic null detector (Model 104W1-G) having a maximum sensitivity of 5μV/cm. From the observed fluctuations from null it was

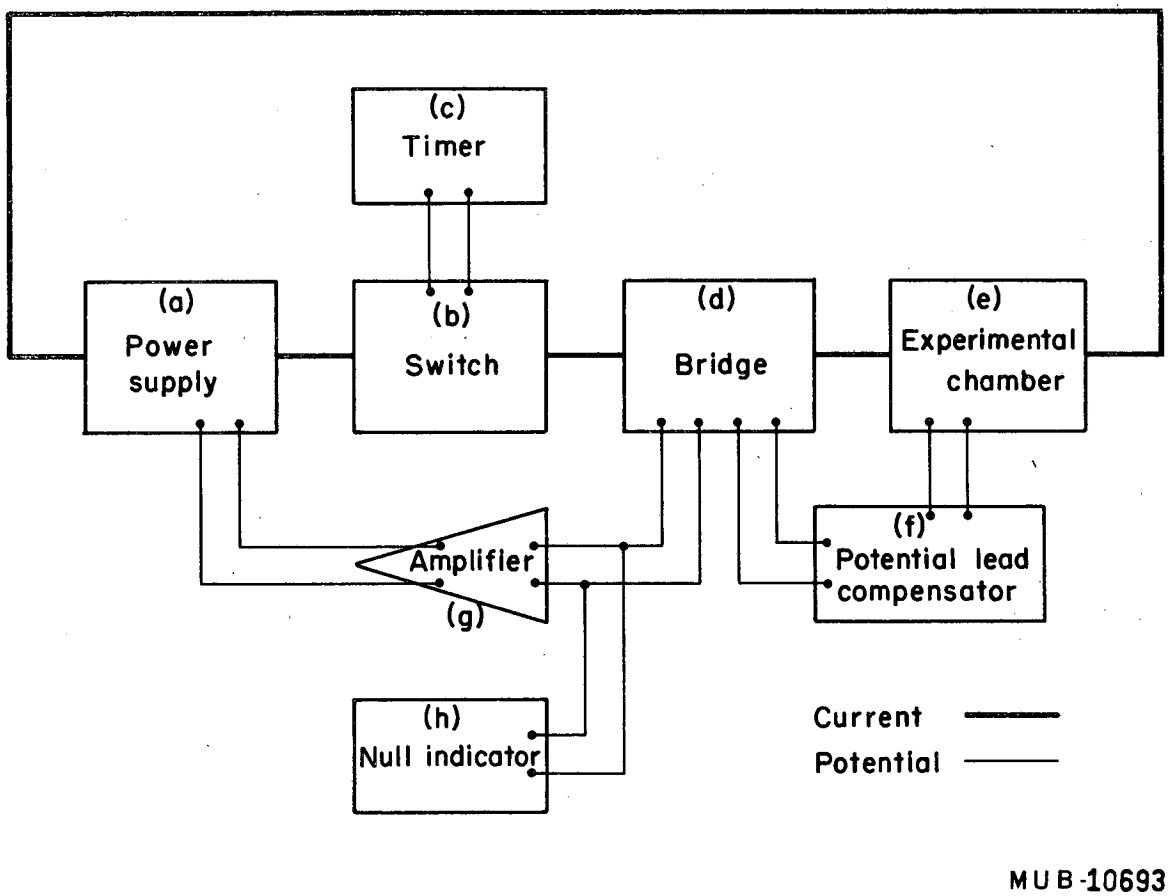

Fig. 10 Block diagram of components used in conducting an annealing cycle: a. direct current power supply; b. silicon controlled rectifier switching unit; c. pre-set timer (Beckman Instrument, Inc., Model 5423); d. portable Kelvin double bridge (Honeywell Model 1622); e. experimental chamber; f. potential lead compensator; g. differential d.c. amplifier (Dynamics Model 6450); h. electronic null indicator (Brown, Model 104W1-G).

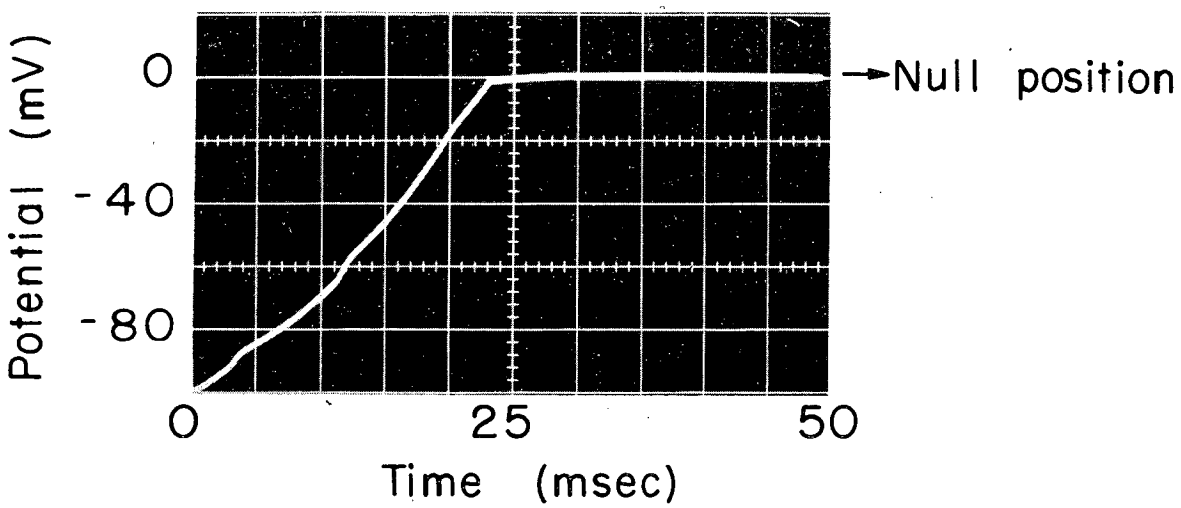

ZN-5623

Fig. 11 Oscillographic trace of the bridge error signal for a pulse from 4.2° to 273°K.

concluded that the average temperature of the specimen, as determined from its resistance, could be controlled to within ±0.1°C in the temperature range -100° to +100°C. Outside of this range the temperature regulation was ≈ ±0.5°C.

The annealing time was controlled by a Beckman pre-set digital counter (Model 5423). This unit was electronically coupled with a silicon controlled rectifier switching circuit which was placed in series with the d.c. power supply (see Fig. 10). The timer was actuated coincidental with the closing of the current loop. At the completion of a preset time interval a pulse from the timer activated the open circuitry controlling the SCR. Time intervals could be controlled to within ±0.1%.

The details of this circuitry will be published in the future along with information regarding advantages as well as limitations of the technique.[80]

B. Electron Microscopy Experiments

Copper single crystals of the desired orientations were grown under vacuum in graphite molds by a modified Bridgman technique. Crystals were cut by spark erosion, chemically thinned to the appropriate thickness, pre-annealed in the quenching chamber under a dynamic vacuum, and gas quenched in a directed spray of helium gas. Cooling profiles were recorded oscillographically. Quenched and isothermally annealed specimens were electropolished for examination in the electron microscope. High resolution dark-field electron microscopy techniques were used in the detection and identification of defect aggregates formed after vacancy precipitation. Throughout all of the above procedures, precautions were

taken to avoid gaseous and metallic contamination, deformation, defect damage resulting from polishing, and ion damage in the microscope.

1. Material and Specimen Preparation

Single crystals of copper were prepared from 99.999+% pure copper, grade A-58, supplied by the American Smelting and Refining Company in the form of ≈ 1.88 cm diam. rod. Sections of the as-received copper rod were cold rolled into 0.05 cm thick strips without any intermediate annealing. These strips were sheared to size (1.88 cm × 25.4 cm), etched in dilute HNO_3 to remove surface contamination, rinsed in distilled water and ethyl alcohol. This material was then used as the charge for growing single crystals with ⟨111⟩ and ⟨110⟩ foil normals. Polycrystalline strips were inserted into a previously outgassed, split, graphite crucible (National Carbon Company AUC grade) along with a seed crystal of the desired orientation. Crystals were grown in a dynamic vacuum of about 1×10^{-6} torr at a rate of 5 cm/hr. Induction heating was employed. Seed crystals were prepared in a similar manner from suitably orientated, spherical single crystals. Orientations were determined by the standard Laue back reflection technique and found to be within a few degrees of the desired orientations.

Single crystals were cut into 1 cm lengths using a servomet spark cutter and then chemically thinned to ≈ 0.005 cm thickness in a solution of 50% nitric acid, 25% glacial acetic acid, and 25% phosphoric acid.

2. Pre-quench Annealing, Quenching, and Isothermal Annealing Techniques

Following chemical thinning, specimens ≈ 0.005 cm × 1.0 cm × 1.88 cm were placed in a fused quartz support (see Fig. 12a) which was designed to minimize contact with the foil and to accommodate dimensional changes accompanying heating and cooling. Samples were then annealed in the

quenching chamber (see Fig. 12b) under a dynamic vacuum ($\approx 8\times10^{-7}$ torr) for one hour at 800°C. Induction heating was employed. The temperature was then raised to the desired T_q. In early experiments the quenching temperature was taken as the point where local melting ($T_q \approx 1050$°C as shown by thermocouples spot welded to control specimens) was induced. Later T_q was determined from platinum-platinum 10% rhodium thermocouple wires (0.005 cm diam) which were spot welded to the edge of the crystal.

The experimental chamber was isolated from the vacuum system and specimens quenched in a directed spray of purified helium gas which was precooled to 77°K. For this purpose the helium was admitted through a vacuum solenoid valve and the induction power cut to zero simultaneously by electronic coupling (see Fig. 13). Because the efficiency with which the solenoid valve opened was quite sensitive to the pressure differential, a capacitor discharge circuit (see Fig. 14) was incorporated into the switching operation thereby eliminating this pressure dependence. The helium gas passed through two frits (Kimax Fritted Glass Ware - extra coarse No. 28280) which were 30 mm in diameter and separated by a distance of about 2 cm. The flow was directed perpendicular to the foil surface. The specimen assumed a stable position between the two frits.

Platinum-platinum 10% rhodium thermocouple wires (0.005 cm diam) were spot welded to control foils of the same dimensions as the single crystals previously discussed. The thermal emf from the couple was then monitored oscillographically during the quench. Temperature decay curves were photographed using a Polaroid camera. Because the induction heater RF ($\approx$ 350 kc) saturated the oscilloscope amplifier, it was necessary to introduce a low-pass filter into the potential circuit in order to eliminate these frequencies but selected so as not to cause distortion

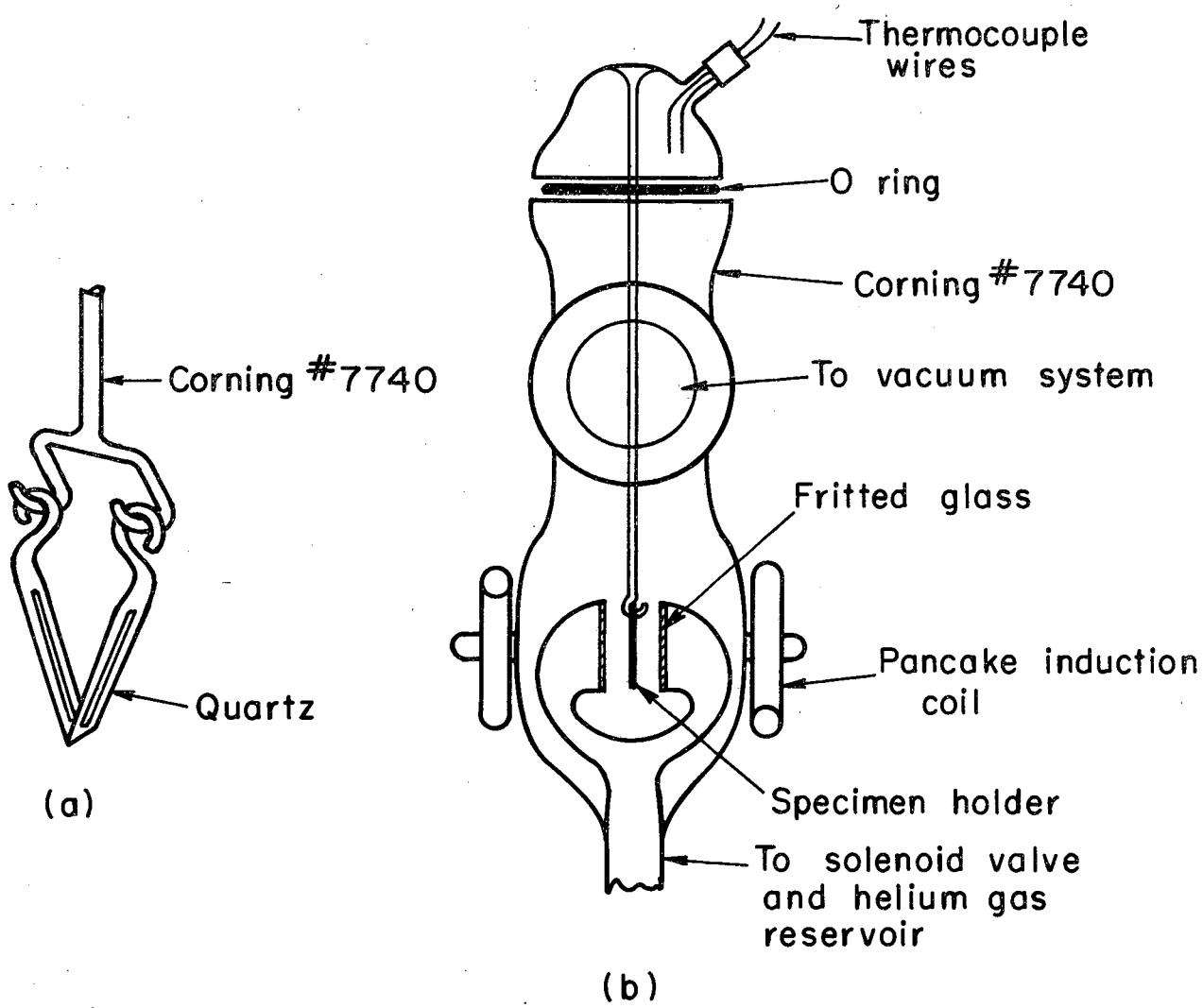

Fig. 12 Foil quenching apparatus: a. specimen holder; b. quenching chamber.

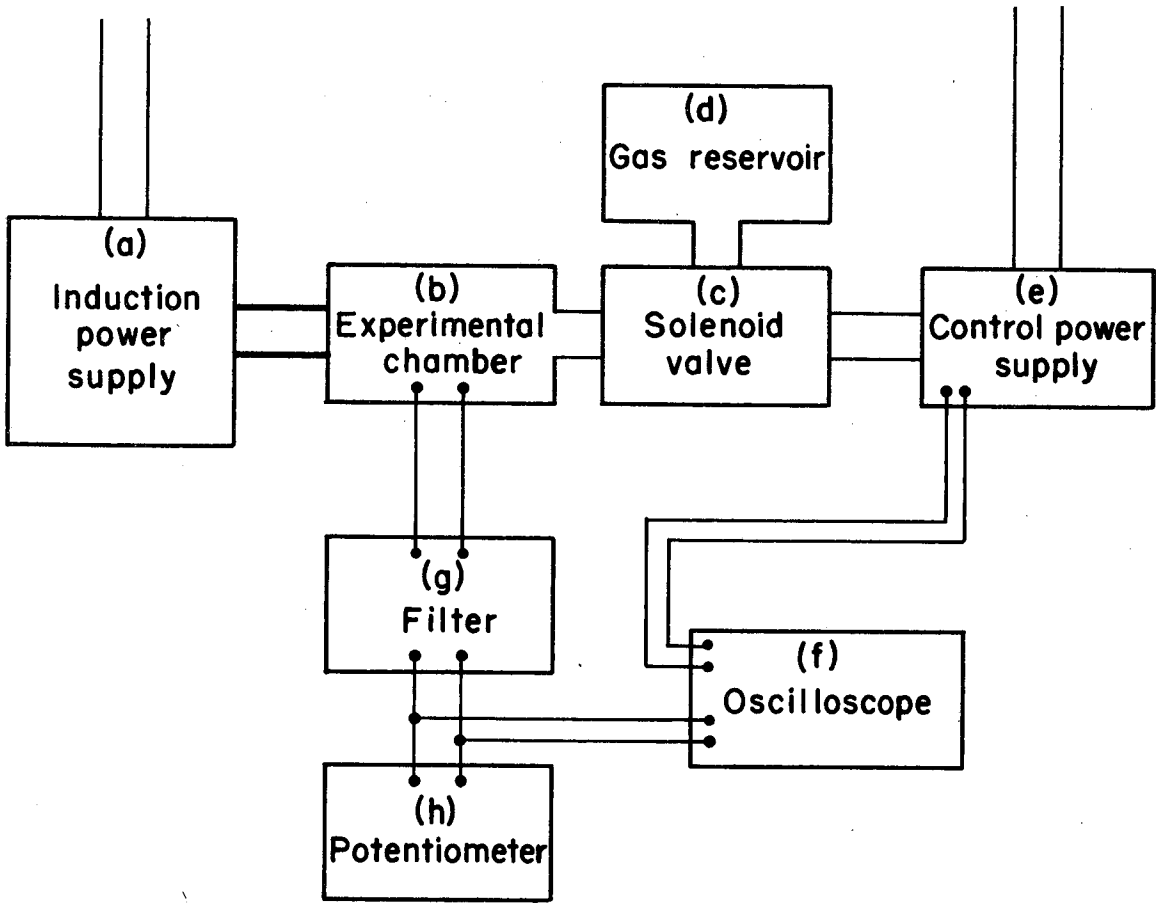

MUB-10694

Fig. 13 Block diagram of components used in carrying out foil quenching cycle: a. 30 kW induction power supply (Radio Frequency Co., Model 30000B); b. experimental chamber; c. vacuum solenoid valve (Veeco, Model SV62); d. helium gas reservoir; e. control power supply (i.e. induction power off, trigger oscilloscope and open solenoid valve); f. oscilloscope (Tektronix dual-beam scope, Type 502); g. low pass filter; h. potentiometer (Leeds and Northrup, Model 8691).

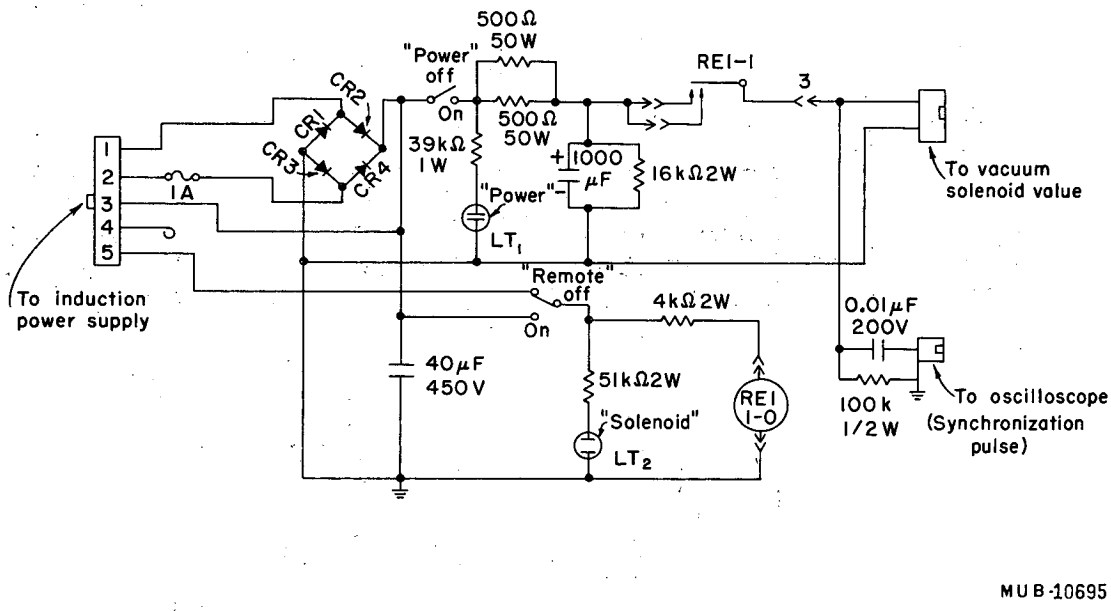

Fig. 14 Circuit diagram of foil quenching control power supply.

of the desired decay curve.

It was found that, for a given quenching temperature, fixed specimen size, and initial pressure of helium gas in the reservoir, quenching profiles were quite reproducible. A temperature-time profile characteristic of the quenching conditions generally employed in this work is shown in Fig. 15. The average quenching rate for the first 500°C is about 5000°C/sec.

Quenched specimens were annealed isothermally at 0°C or ≈ 25°C for various periods of time (i.e., ≈ 20 sec to 2 weeks) then heated to 100°C and isothermally annealed at this temperature for either 1, 2, or 3 hours. A constant temperature bath (i.e., ±2°C) containing silicon oil (Dow Corning 704) was used for the 100°C annealing treatments.

3. Preparation of Thin Foils

Quenched and annealed specimens were electropolished at room temperature in a 50% distilled water, 25% phosphoric acid, and 25% ethyl alcohol electrolyte (≤ 2 volts) to a thickness just slightly greater than that necessary for good transmission of electrons. Final thinning was done in a 67% methyl alcohol and 33% nitric acid solution maintained at about -60°C (≤ 8 volts). A special specimen holder was used throughout so as to minimize foil bending which normally accompanies the thinning of very small foils.

4. Observation and Identification of Defect Aggregates

As was previously reported,[78] defect aggregates in quenched and annealed copper are generally less than 200Å in diameter. Because of this, normal bright field diffraction contrast imaging gives very little information about their shape (i.e., planar or spherical), their sense (i.e., vacancy or interstitial), or their crystallography (i.e., lattice

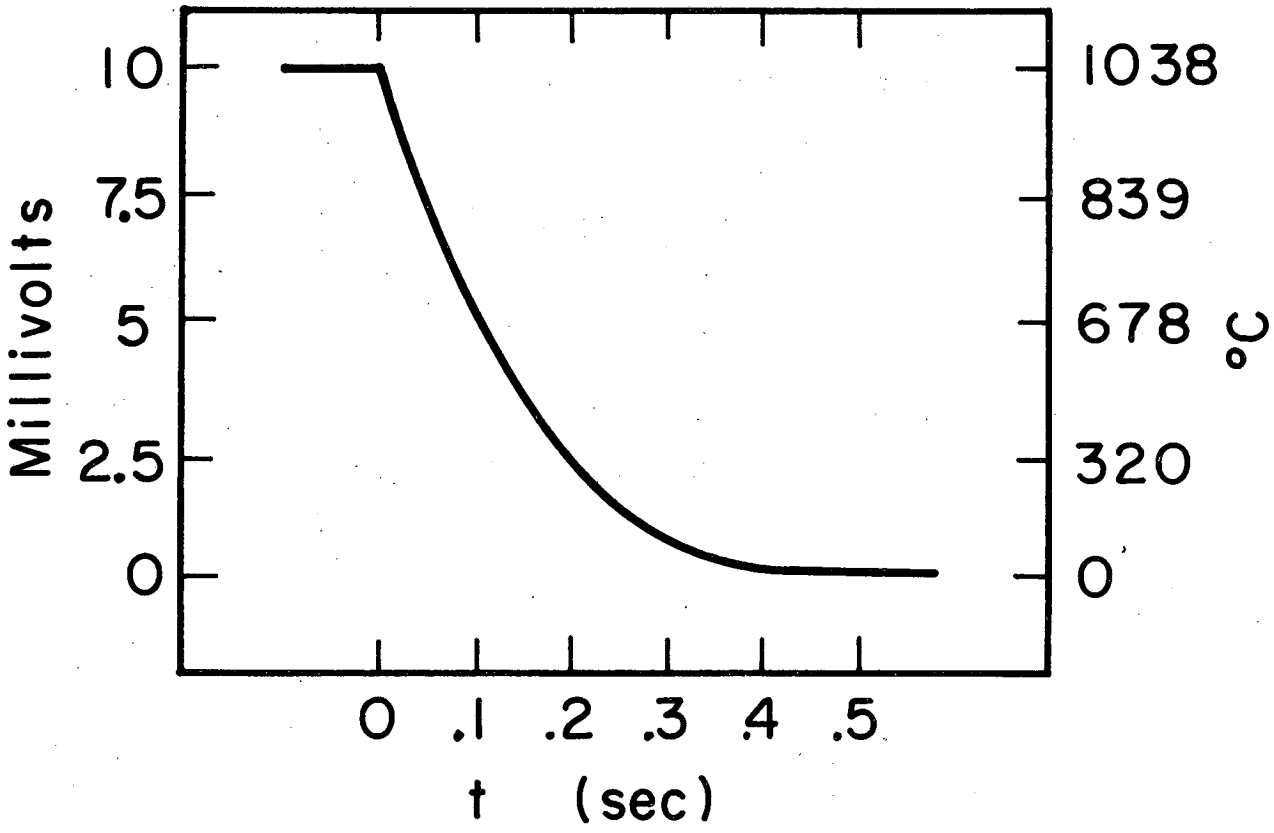

MUB-3764

Fig. 15 Change in foil temperature as a function of time corresponding to an initial helium reservoir pressure of 20 psi.

displacement vector and habit plane). This is understandable in view of the fact that diffraction contrast images of dislocations are ≈ 100Å wide, and therefore the sides of a dislocation loop are not resolvable when the loop is less than a few hundred angstroms in diameter. Furthermore, when the loop is small, its strain field is altered (actually diminished), as a result of interactions between various segments of dislocation line surrounding the loop.

Because of the foregoing it is necessary to observe and identify small defect aggregates by strain contrast imaging. Such images are obtained from defects when the crystal is near the ideal Bragg condition ($s \approx 0$, where s is the deviation from the ideal Bragg condition in reciprocal space*) and appear as black-white "lobes" against the background. The parameter $\bar{g} \cdot \bar{b}$ (where $\bar{g}$ is the reciprocal lattice vector corresponding to the set of crystal planes responsible for diffraction and $\bar{b}$ is the lattice displacement vector of the defect and is usually referred to as the Burgers vector) responsible for phase changes in both the transmitted and diffracted beam by locally modifying s, is important in strain contrast imaging just as it is in the case of diffraction contrast. If $\bar{g} \cdot \bar{b}$ is zero, weak or no contrast is observed. Small localized strain fields which may not give rise to significant diffraction contrast can be detected by this mechanism.[63,78,81,82]

Foils were examined in a Siemans Elmiskop 1 microscope equipped with a double-tilting specimen stage. Dark field observations were made by gun tilting.[78] The use of two beam dark field imaging techniques

---

* s is the distance of the reciprocal lattice point from the reflecting sphere and is taken to be positive if the real point lies inside the sphere.

is of particular importance in the present investigation for two reasons. (1) One desires to work at or near the ideal Bragg condition. The dark field image is symmetrical about $s = 0$ and therefore maximum diffracted intensity occurs at the center of the contour corresponding to the reflection being imaged. Under this condition all defects giving rise to strain contrast can usually be observed (except of course if $\bar{g} \cdot \bar{b} = 0$). (2) Dark field images, obtained by tilting the gun in such a way that the diffracted beam passes down the center of the microscope column, have enhanced resolution with respect to the same bright field image because of the lower level of inelastically scattered electrons (i.e., background). There are two additional experimental features* related to this work which are worth noting. (1) The best condition for "seeing" black-white contrast is, as expected, against a gray background (i.e., at thicknesses of $nt_o/4$, where n is an odd integer and t_o is the extinction distance). (2) In resolving plate-like defects (e.g., prismatic loops) the habit plane of the defect should be nearly parallel, (or within about 15°) to the incident beam.

The theory of strain contrast as formulated by Ashby and Brown[83,84] predicts that, for a spherically symmetric inclusion and a planar defect whose displacement vector is normal to its habit plane, the image will consist of dark and light lobes separated by a line of no contrast perpendicular to the displacement vector of the defect. A spherically

---

* The application of and numerous difficulties associated with strain contrast imaging have recently been reviewed and discussed by Thomas and Bell.[81] The reader is referred to this publication for additional information.

symmetric defect effectively has a displacement vector, $\bar{b}$, normal to all diametric planes and therefore a corresponding line of no contrast which is always perpendicular to the operating reflection, $\bar{g}$. On the other hand, a plate has its line of no contrast perpendicular to a unique $\bar{b}$ which is normal to the habit plane of the defect and therefore independent of $\bar{g}$. The shape of the image, i.e., the direction of streaking of the black-white image, should be symmetrical about the line of no contrast. Figure 16a shows a schematic of this situation for the case of the planar defect. The theory does not account for the shape of the image when the displacement vector of a planar defect is not normal to its habit plane. Since such a defect is quite commonly observed in quenched f.c.c. metals (i.e., the perfect prismatic loop, a/2 ⟨110⟩ {111}) and anticipating the results, a schematic is presented in Fig. 16b in which the direction of streaking is not symmetrical about the line of no contrast but is skewed.

In addition, the theory predicts that in dark field the normal to the line of no contrast and direction of the operating reflection, $\bar{g}$, are related by an acute angle on the <u>white</u> side of the black-white image for a vacancy-type inclusion (as in Fig. 16a) and by an acute angle on the <u>black</u> side of the black-white image for an interstitial-type inclusion (as in Fig. 16b).

These predictions were originally expected to be valid at or near the ideal Bragg condition ($s \approx 0$) and within half an extinction distance of either surface of the foil.[84] However, recent work[85] has shown that strain contrast images from defects should be observed at all foil depths under $s \approx 0$ condition and not just near the two surfaces as predicted by Ashby and Brown.[84]

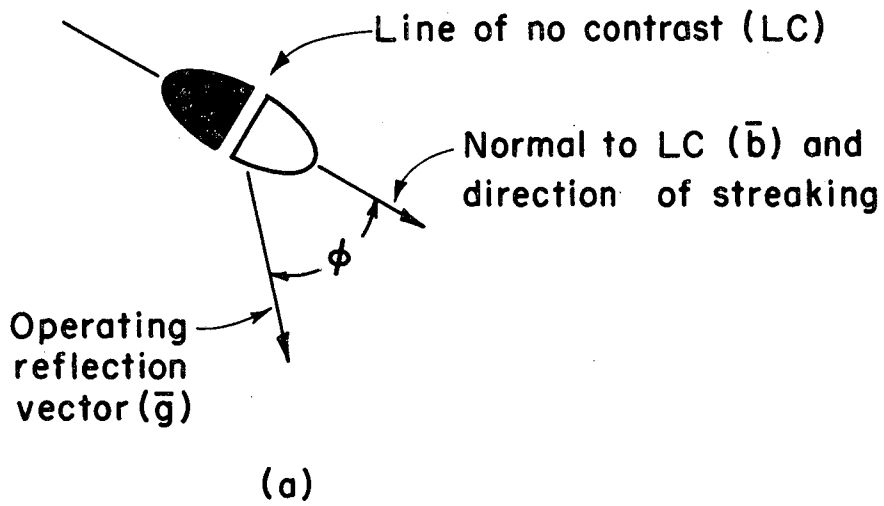

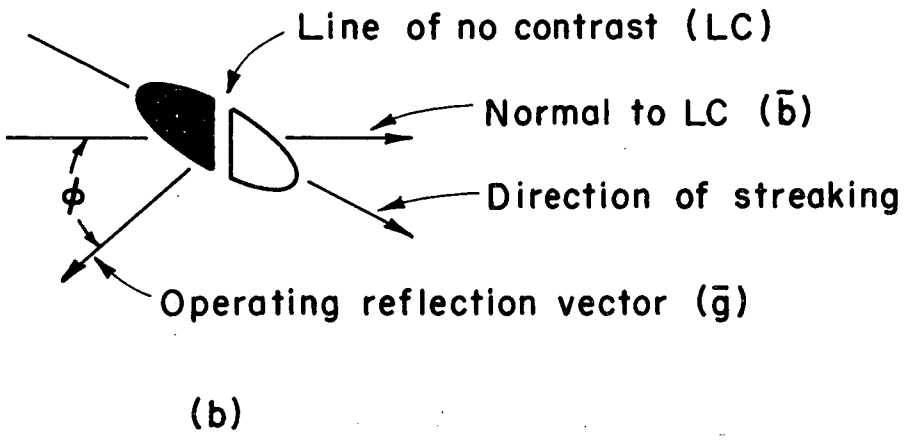

MUB-10696

Fig. 16 Schematic of dark field strain contrast images expected from planar loops: a. imperfect prismatic loop: the lattice displacement vector or its projection, $\bar{b}$, is normal to LC; b. perfect prismatic loop: the lattice displacement vector or its projection, $\bar{b}$, is normal to LC and the direction of streaking is parallel to the habit plane normal (or its projection).

Identification of defect aggregates (i.e., shape, sense, and lattice displacement vector) can be accomplished therefore by investigating the following features. A planar loop can be distinguished from a spherically symmetric defect,* for example, since in the former case the line of no contrast would make various angles with different reflecting vectors whereas in the lattice case the line of no contrast would be perpendicular to the operating reflection regardless of which vector was operative. The sense of the lattice displacement due to the aggregate can be determined from the angular relationship between the normal to the line of no contrast and $\bar{g}$. The actual lattice displacement vector of the aggregate can be determined by comparing the direction of the normal to the line of no contrast to the projections of all possible displacement vectors onto the plane of the foil, e.g., an imperfect prismatic loop would have a line of no contrast perpendicular to a ⟨111⟩ direction lying in or projected onto the plane of the foil when observed under strain contrast conditions. It is of course important to select crystal orientations which avoid ambiguities in the analysis.**

These criteria will be utilized in Sec. III.D of the results.

* The distinction between, say, loops and voids is more complicated than the spherical inclusion. To observe voids one makes use of so-called mass thickness contrast (i.e., at a void $t_o^{eff} \rightarrow \infty$, where t_o is the extinction distance) and therefore observations must be made in very thin regions of the foil.

** As an example, in the [001] cubic orientation both [111] and [110] projected vectors lie along the same direction so it is not possible to distinguish between these displacement vectors.

III. EXPERIMENTAL RESULTS

Upon quenching copper wires from temperatures in the range 460° to 670°C, an increase in resistivity was observed which could be best described by the following relationship:

$$\Delta\rho(T_q) = [(1.7\pm0.2)\times10^{-4} \text{ ohm-cm}] \exp(1.09\pm0.04 \text{ eV}/kT_q). \qquad (16)$$

The quench induced resistivity for temperatures above 670°C fell below the values predicted by this relationship.

The isochronal recovery of specimens quenched from ~700°C exhibited three annealing stages. Maximum annealing rates were observed at about -40°, +200°, and +400°C. Pulsing a quenched specimen to -10°C for 20 sec curtailed the low temperature recovery activity but annealing peaks still occurred at about the same temperatures.

When copper single crystals were quenched from ≈ 1040°C and subsequently annealed for 15 min at 0°C and then 1 hr at 100°C, randomly orientated, planar, vacancy aggregates were observed by transmission electron microscopy. Both perfect and imperfect loops were identified. The maximum size of the imperfect loop rarely exceeded 125Å, whereas the perfect loops ranged in size from 100 to 200Å. Annealing conditions are reported which resulted in no apparent resolvable loops by electron microscopy.

A. Formation Enthalpy Data

The temperature dependence of quench induced resistance was determined between 460°C and 800°C. The incremental resistance associated with a particular quenching temperature, denoted by $\Delta R(T_q)$, was determined from the difference between the resistance of a specimen quenched from T_q and the resistance of the same specimen in the

well annealed state just prior to the quench. Therefore

$$\Delta R(T_q) = [R(T_q) - R_o]_{4.2°K} \tag{17}$$

The corresponding changes in resistivity have been calculated from the relationship

$$\Delta\rho(T_q) = \frac{\rho(0°C)\ \Delta R(T_q)}{R(0°C)} \tag{18}$$

where $\rho(0°C)$ was taken as equal to $1.57 \pm 0.05 \mu\Omega$-cm, which is consistent with values determined during the present work and with the best values reported in the literature for copper.[86-88] $R(0°C)$ was measured prior to the initiation of a quench series. The constancy of $R(0°C)$ was checked periodically during the series.

The resistance increment quenched into four different specimens is plotted on a logarithmic scale as a function of the inverse quench temperature in Figs. 17 through 20. The apparent vacancy formation enthalpy, deduced from the best straight line through the data (i.e., for $T_q \leq 670°C$) by a least squares fit, is also shown. As can be seen in Fig. 17, the absolute value of $d[\log \Delta R(T_q)]/d(1/T)$ decreases with increasing quenching temperature above $\approx 670°C$. The fact that this is so, is clearly shown in Fig. 21, where a portion of the same data is plotted on an expanded scale in terms of resistivity increments.

These results are compared in Fig. 22. For this purpose the logarithm of the resistivity changes was plotted against the reciprocal of the quench temperature. In the limiting case, the quenched-in increments are described by

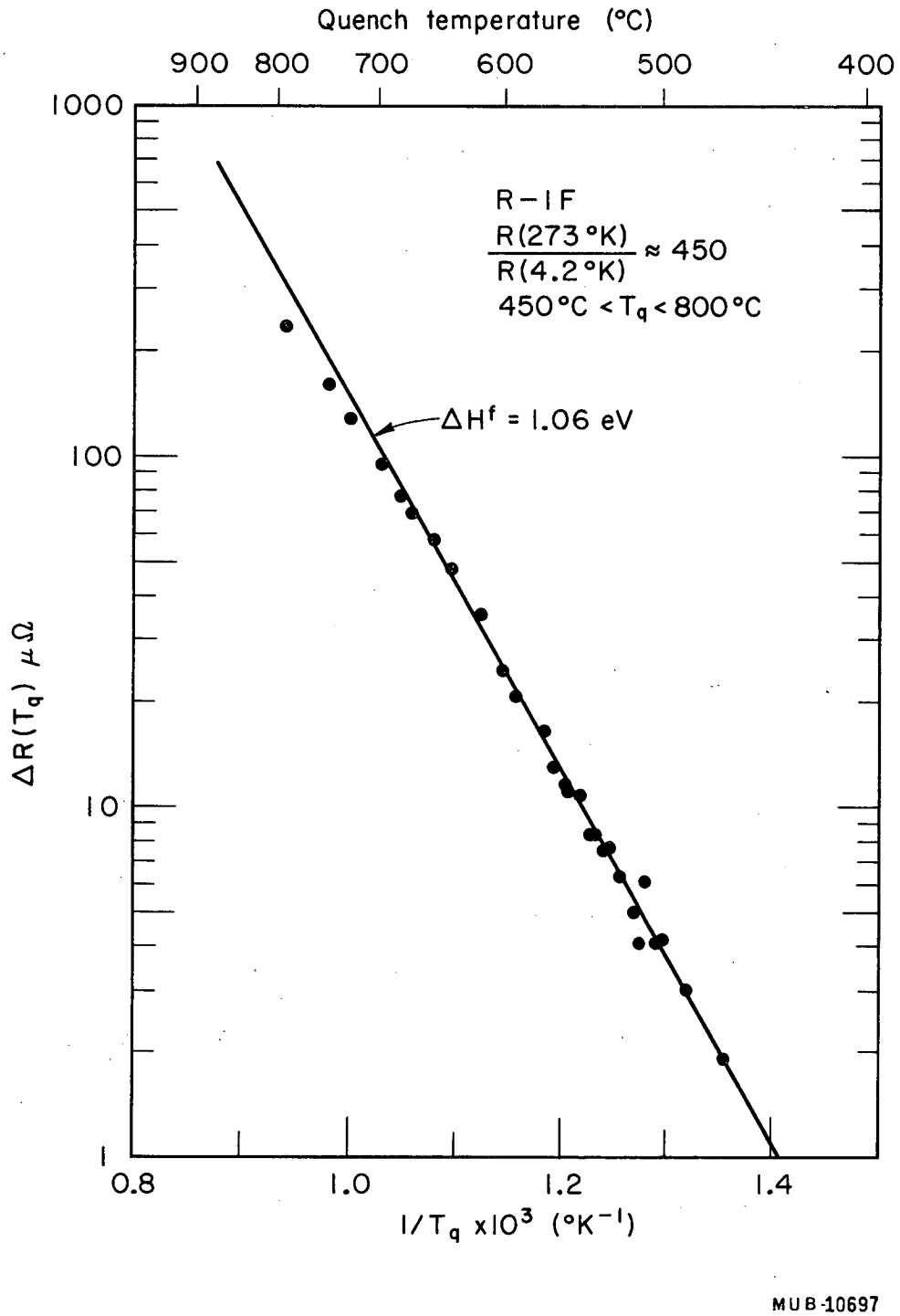

Fig. 17 The logarithm of the resistance increment quenched into a copper wire, R(273°K)/R(4.2°K) ≈ 450, plotted as a function of the inverse quench temperature (450°C < T_q < 800°C).

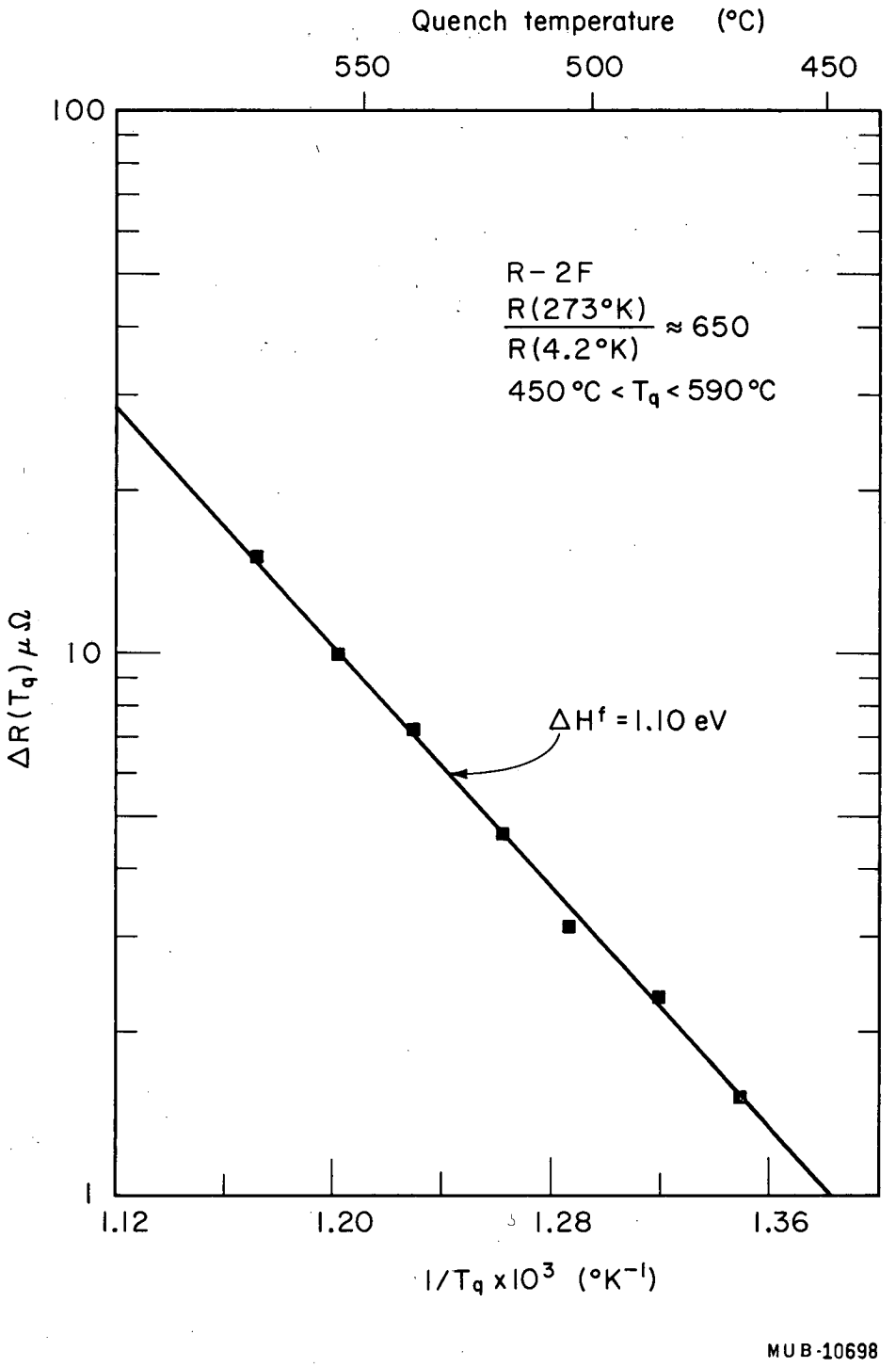

Fig. 18 The logarithm of the resistance increment quenched into a copper wire, R(273°K)/R(4.2°K) ≈ 650, plotted as a function of the inverse quench temperature (450°C < T_q < 590°C).

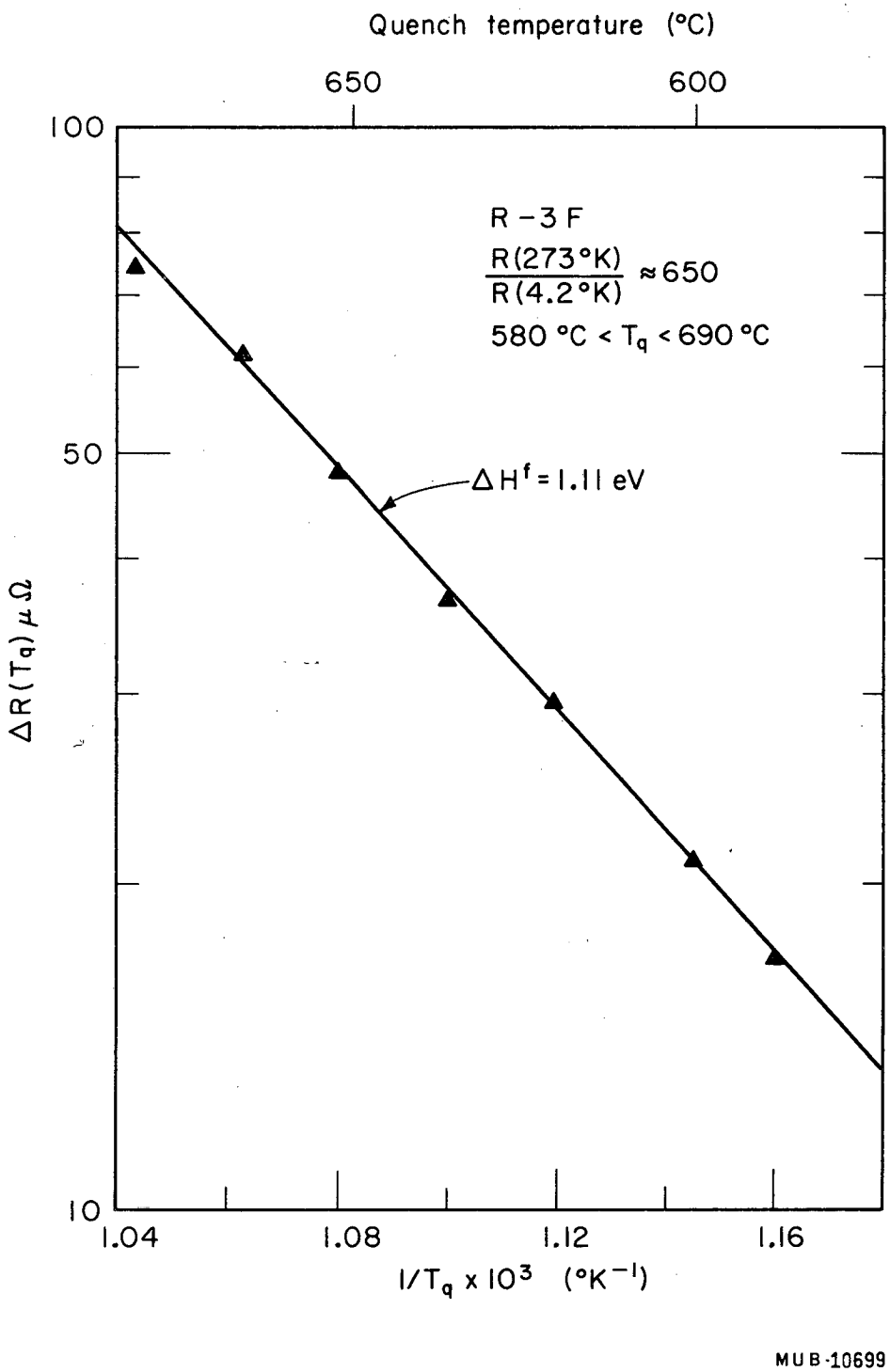

Fig. 19 The logarithm of the resistance increment quenched into a copper wire, R(273°K)/R(4.2°K) ≈ 650, plotted as a function of the inverse quench temperature (450°C < T_q < 690°C).

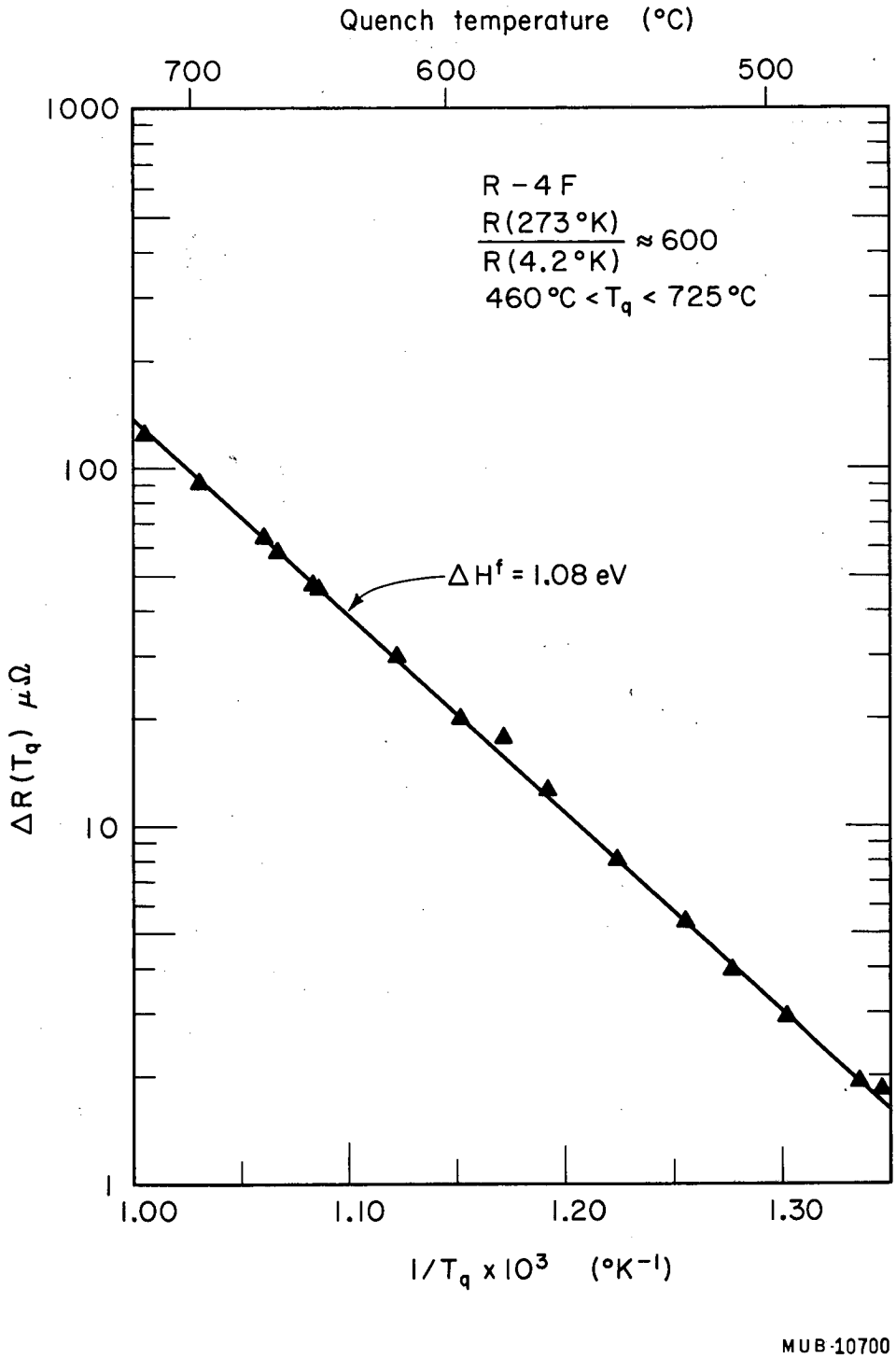

Fig. 20 The logarithm of the resistance increment quenched into a copper wire, R(273°K)/R(4.2°K) ≈ 600, plotted as a function of the inverse quench temperature (450°C < T_q < 725°C).

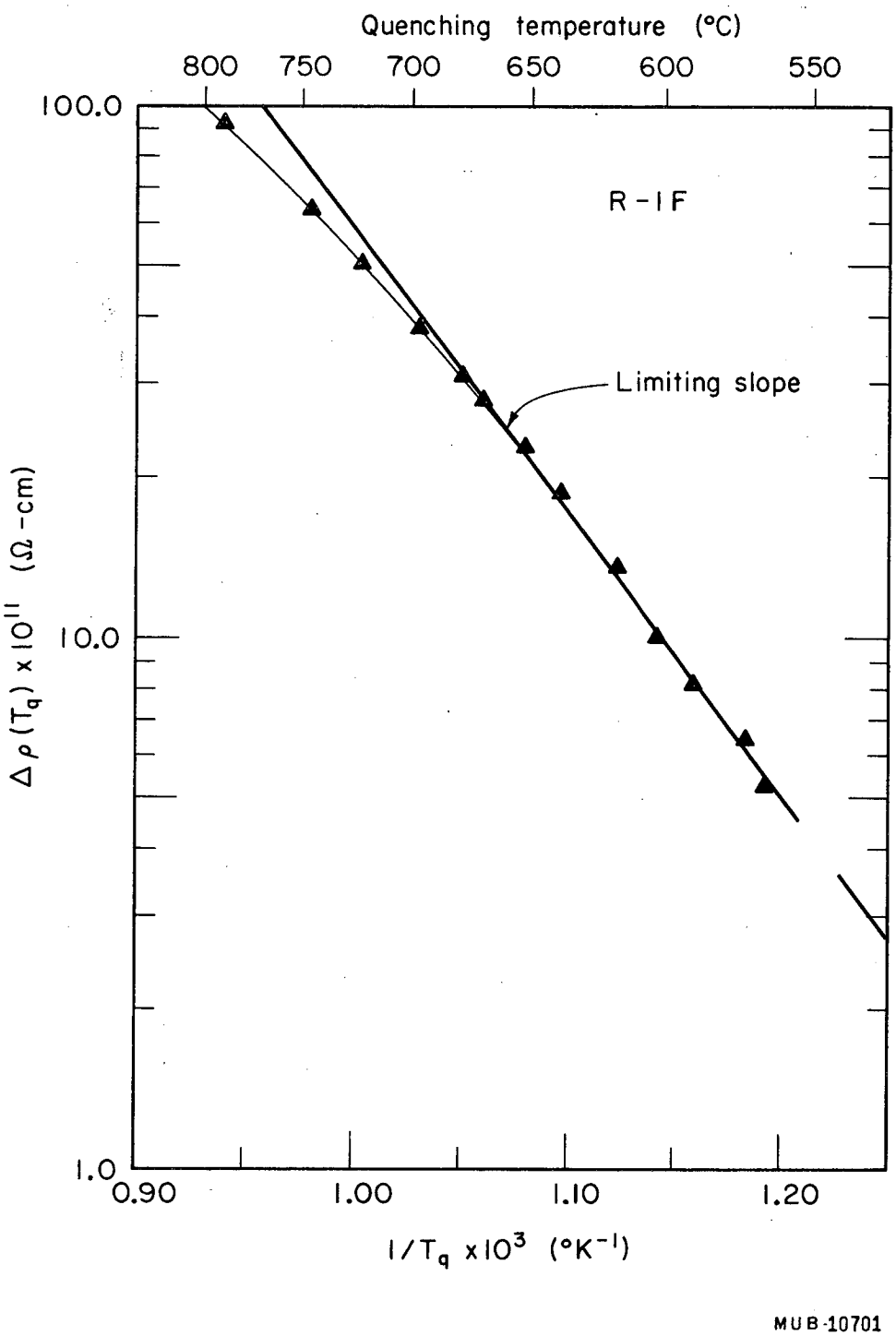

Fig. 21 Expanded plot of data shown previously in Fig. 17 illustrating that the absolute value of $d[\log \Delta\rho(T_q)]/d(1/T)$ decreases with increasing quench temperature above $T_q \approx 670°C$.

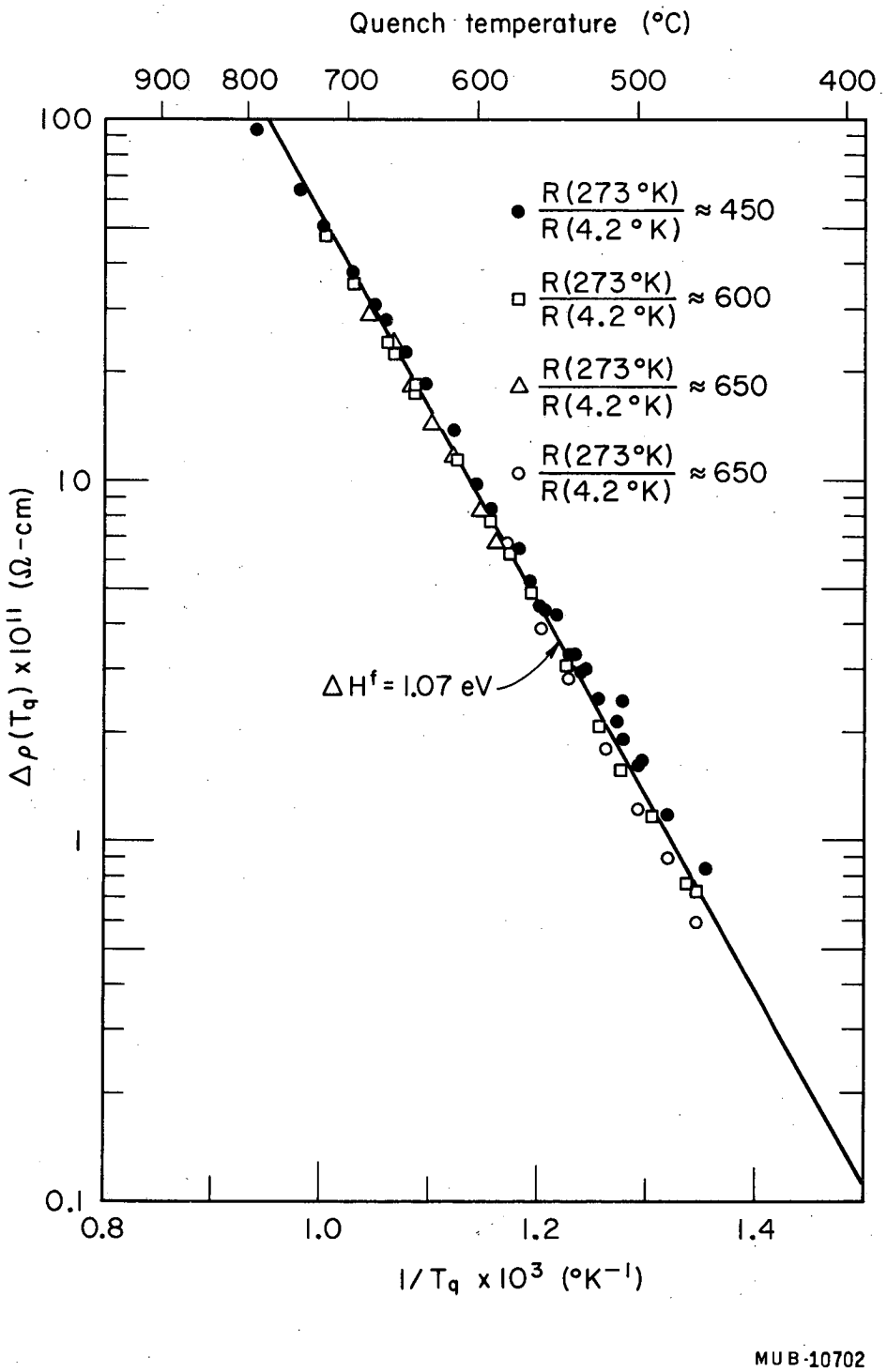

Fig. 22 Comparison of resistivity increments quenched into copper wire specimens.

$$\Delta\rho(T_q) = [(1.4\pm0.3)\times10^{-4}\ \text{ohm-cm}]\ \exp\ (1.07\pm0.05\ \text{eV}/kT_q) \qquad (19)$$

The stated error in the pre-exponential term, i.e., $\Delta\rho(T \to \infty)$, includes the estimated uncertainty in: a) $\rho(0°C)$ of $\approx 2\%$, b) $\Delta R(T \to \infty)$ which was taken as the maximum observed deviation in the predicted values of $\Delta R(T_q)$ in accordance with the least squares calculation (i.e., $\approx 20\%$), and c) $R(0°C)$ of $\approx 0.05\%$ simply added together. The uncertainty in the activation enthalpy includes the estimated error in $\Delta\rho(T \to \infty)$ (i.e., $\approx 22\%$), the average error in $\Delta\rho(T_q)$ over the temperature range of interest which includes both the average uncertainty in the least squares computed values (i.e., $\approx 12\%$) and an average measuring error of $\approx 7\%$, and the average estimated uncertainty in the temperature of $\approx 10°C$. In arriving at the stated uncertainty, the values were treated as independent random errors.

The data for the case $R(273°K)/R(4.2°K) \approx 450$ favor slightly larger quench induced resistivity increments and therefore a correspondingly lower effective formation enthalpy. This is apparent when the changes in resistivity for a specimen having a resistance ratio $R(273°K)/R(4.2°K)$ of ≈ 450 are compared to the increments quenched into specimens having resistance ratios of ≈ 650, as seen in Fig. 23. Since $R(273°K)/R(4.2°K)$ is considered a measure of specimen purity, the inference is that this effect could be attributed to differences in the concentration or distribution of impurities or possibly only a certain impurity (relative to specimens with higher resistance ratios).

Data obtained from wires having resistance ratios ≈ 600 and ≈ 650 are compared in Fig. 24. In the temperature range where the three sets of data overlap, there appears to be good agreement. For $T_q \leq 670°C$

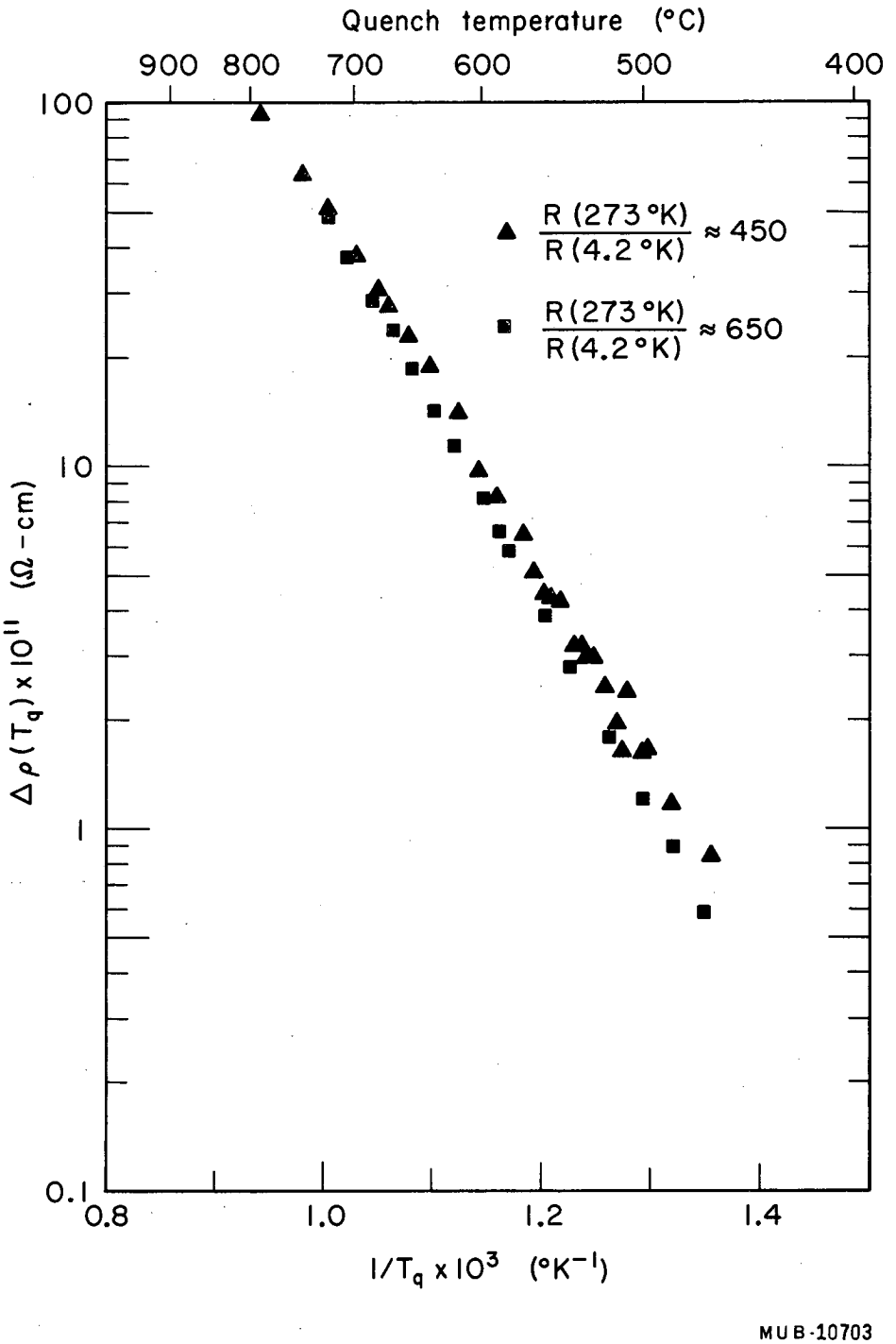

Fig. 23 Comparison of resistivity increments quenched into a specimen having a resistance ratio R(273°K)/R(4.2°K) of ≈ 450 to those increments quenched into specimens having resistance ratios of ≈650.

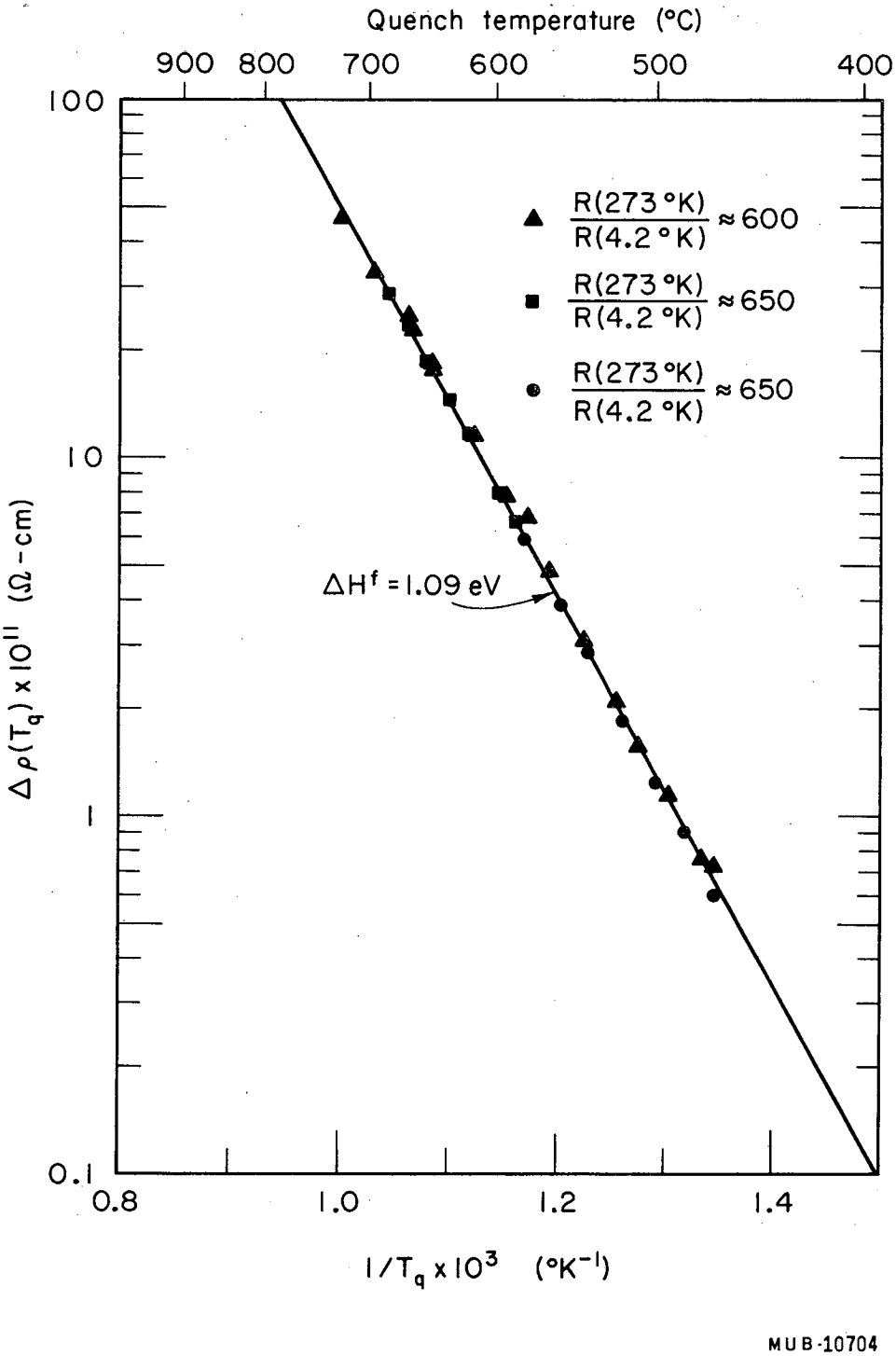

Fig. 24 Comparison of quench-induced resistivity increments for copper specimens whose resistance ratios were ≈ 600 and ≈ 650.

the quenched-in increments are described by

$$\Delta\rho(T_q) = [(1.7\pm0.2)\times10^{-4}\text{ohm-cm}]\ \exp\ (1.09\pm0.04\ \text{eV}/kT_q). \qquad (16)$$

The stated errors were obtained in the same way as was indicated above for Eq. (19). The differences in the magnitude arise from lower maximum and average uncertainties in the least squares computed values of $\Delta\rho(T_q)$, i.e., ≈ 10% and ≈ 5%, respectively.

B. Isochronal Annealing Data

The isochronal recovery spectrum (-220° to 500°C) was investigated by annealing quenched specimens at a constant rate of 4°C per minute. This was accomplished by annealing for fixed periods of time at successively higher temperatures according to the following schedule:

a) $-200°C \leq T_a \leq 260°C$; $\Delta t = 5$ min, $\Delta T = 20°C$,

b) $260°C < T_a \leq 500°C$; $\Delta t = 10$ min, $\Delta T = 40°C$,

where T_a is the annealing temperature. The recovery progress was followed by measuring the change in residual electrical resistance of the specimen at 4.2°K.

The isochronal annealing of copper quenched from temperatures around 700°C shows a rapid annealing process in the temperature range from -100° to 0°C. Above 0°C the recovery proceeds quite slowly. Approximately 60 to 70% of the quenched in resistance anneals out by 100°C. The onset of more rapid annealing occurs above 100°C with an apparent completion at ≈500°C. Typical behavior is illustrated in Fig. 25. This specimen was quenched from ≈720°C; the resistivity increment quenched in was $\Delta\rho(720°C) \approx 4.5\times10^{-10}\Omega$-cm. The data show the percentage of the resistance increase, $\Delta R(T_q)$, that remained after each cycle.

To illustrate this behavior in detail, the numerical derivatives of the curve displayed in Fig. 25 were calculated and are shown as a function of the mean temperature in Fig. 26. Three peaks, indicating maximum annealing rates, occur at ≈ 40°, ≈ 200°, and ≈ 400°C.

In order to investigate the effect of quenching to a temperature around 0°C (a base temperature most commonly used in quenching experiments, see Table III) on the isochronal recovery, a specimen was pulsed to -10°C from 4.2°K for 20 seconds subsequent to a quench from 695°C. The resistivity increment quenched-in was $\Delta\rho(695°C) \approx 3.7\times10^{-10}$ ohm-cm. The recovery curve and derivatives of this curve are shown in Figs. 27 and 28. The lower temperatures annealing behavior which was previously evident has been markedly curtailed, although the annealing maxima occur at about the same temperatures as those in specimens which were not pulsed. During the pulse ≈ 17% of the quenched-in resistance recovered.

C. Experimental Accuracy

When the quenched-in resistivities are compared, as in Fig. 22, the data can be contained within two error lines separated by ±15°C from the best straight line fitted to the entire set of points. The average deviation was estimated to be ≈ 6°C.

It appears as if not all of the scatter can be attributed to the uncertainty in the quench temperature. The accuracy in the measurement of the specimen resistance at T_q and variations in the specimen resistance at 0°C lead to a random error in the quench temperature of about ±6°C. Temperature inhomogeneities present along the specimen gauge length certainly are contributing to the scatter, although it is difficult to estimate the extent of their contribution. In general, they have been

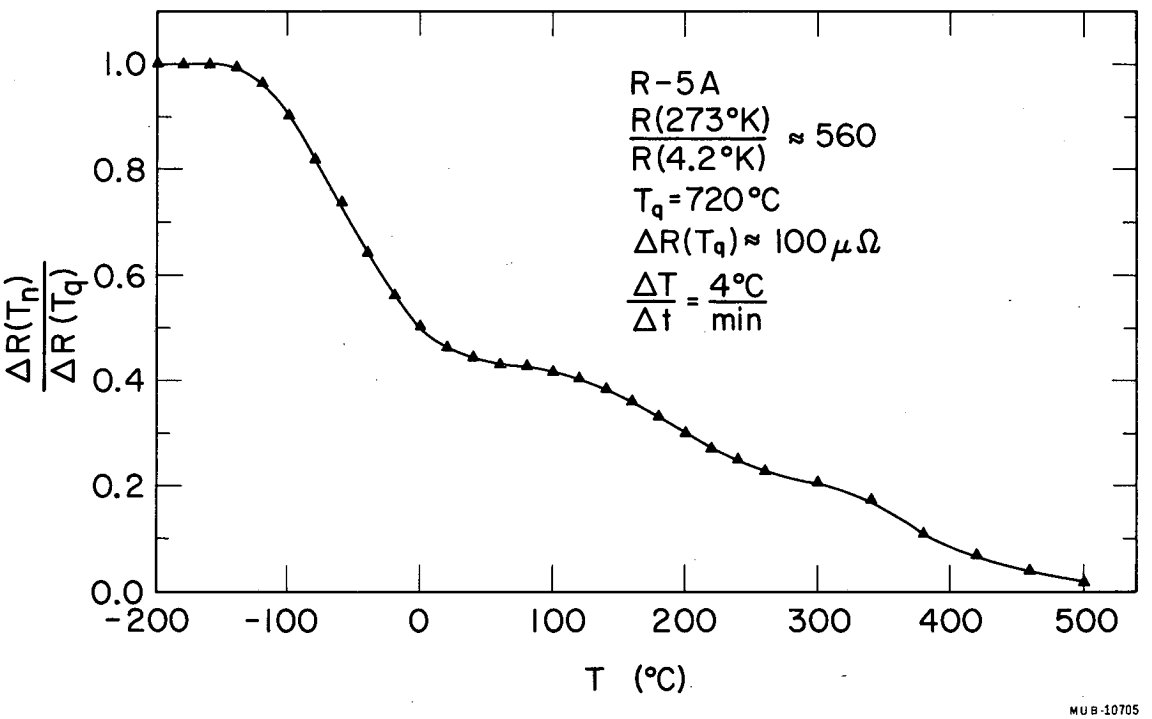

Fig. 25 Typical isochronal recovery curve for a copper specimen quenched from about 700°C to -196°C. Heating rate was 4°C per minute.

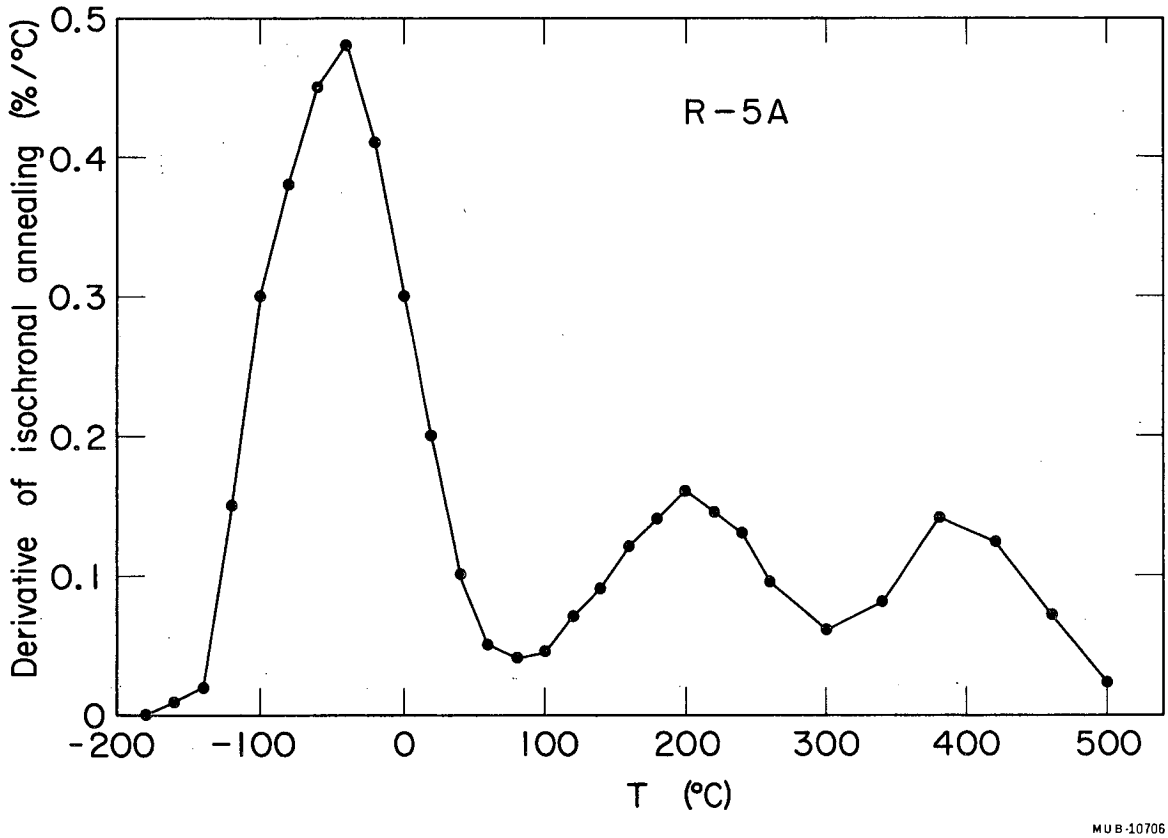

Fig. 26 Negative of the numerical derivative of the isochronal recovery curve shown in Fig. 25 versus mean annealing temperature in °C. Derivative computed from:

$$\frac{\Delta R(T_n)/\Delta R(T_q) - \Delta R(T_{n+1})/\Delta R(T_q)}{(T_n - T_{n+1})} \cong \frac{d[\Delta R(T)/\Delta R(T_q)]}{dt} .$$

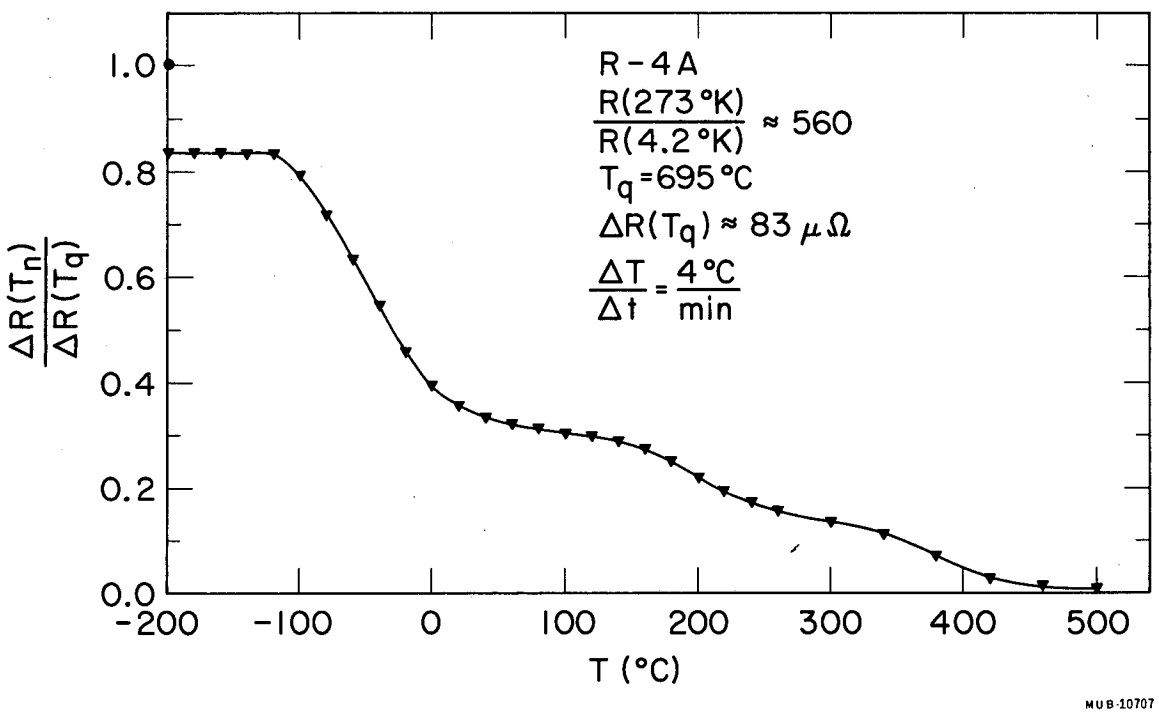

Fig. 27 Isochronal recovery curve for a copper specimen quenched from 695°C to -196°C, pulsed to -10°C for 20°sec and subsequently heated at a rate of 4°C per minute.

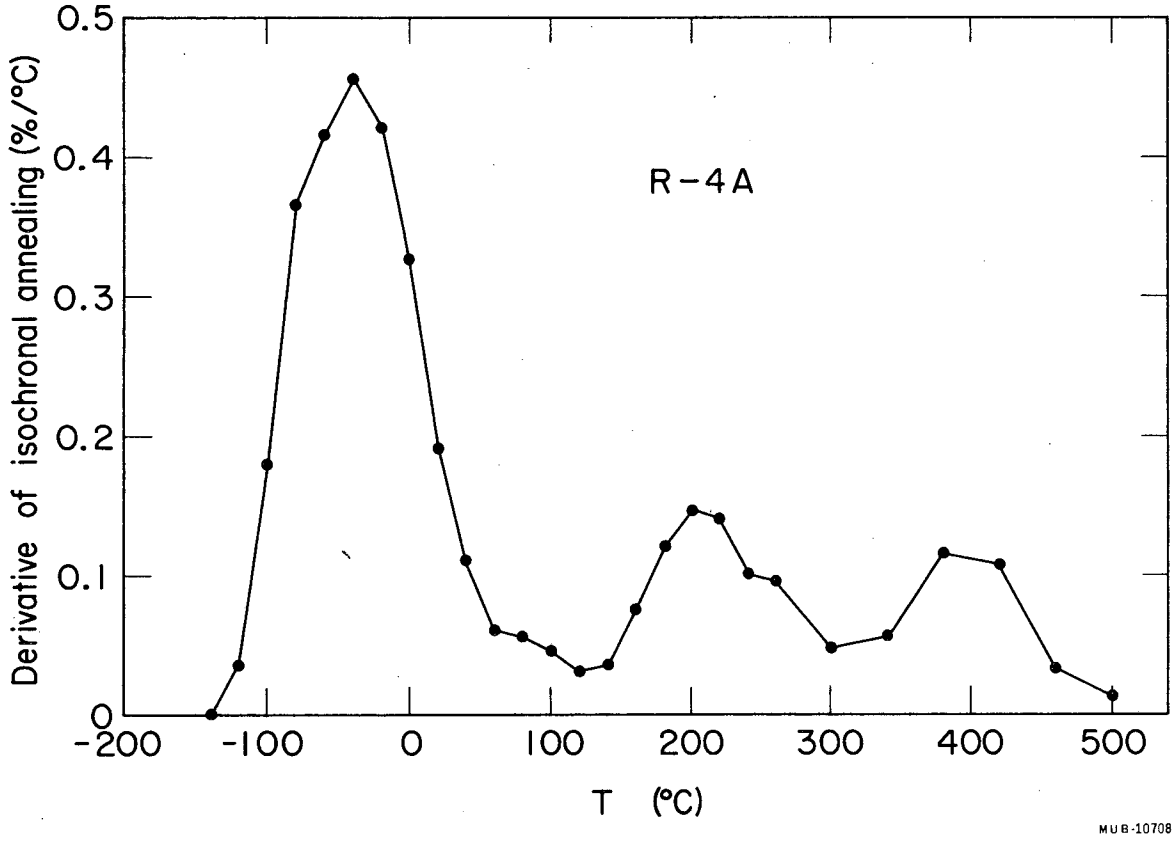

Fig. 28 Negative of the numerical derivative of the isochronal recovery curve shown in Fig. 27 vs the mean annealing temperature in °C.

considered as second order effects when employing the average temperature as a measure of the true specimen temperature.[10] It is concluded that the average temperature, in the present case, is well-defined but the temperature at any particular point along the gauge length is probably rather ill defined. This appears to be one of the largest weaknesses of the self-heating technique under experimental conditions which are compatible with very rapid specimen cooling.

Some of the observed scatter is undoubtedly due to differences in specimen substructure (i.e., in the vacancy sink density and impurity level and distribution) and variations in the temperature-time characteristics of the quenches. Attempts were made to minimize the contributions of these two factors by standardizing annealing cycles and routine monitoring of quenching profiles.

In the present case, where the quench induced increments were small $[\Delta R(T_q)/R_o]_{max} \approx 26\%$, non-reproducibility of the base resistance, R_o, can result in very significant uncertainties in $\Delta R(T_q)$. When the prequench annealing routine, as characterized in Sec. II.A4, was used, the base resistance was reproducible to within an error of 0.1% (i.e., about $\pm$ 1μΩ) and a corresponding standard deviation of $\sim 3\times10^{-12}$ ohm-cm. When this uncertainty is compared to the increments retained for the lowest quenching temperatures employed, the error in these values can be as large as 50%. It is worth noting, however, that the average error in the least squares computed values of $\Delta\rho(T_q)$ presented in Figs. 22 and 24 are 12% and 5%, respectively. It is concluded that the observed scatter appears to be reasonably compatible with the known sources of experimental uncertainty.

Systematic errors may enter into the results because a) the

temperature versus resistance ratios for copper, determined from the literature, were in error, b) gaseous contamination of wire specimens occurred during heating in helium prior to the quench, and c) quenching strains perturbed the retained vacancy concentration characteristic of T_q. Controlled heating and cooling experiments in helium gas demonstrated that the resistance of wire specimens remained constant during a cycle within the measurement error of the circuitry. In addition isochronal recovery processes (up to $T \approx 500°C$) were conducted with the specimen in 500μ Hg of helium gas and no irregularities during annealing runs nor during control runs were observed that could be attributed to contamination from residual impurity gases or by the helium gas itself. Systematic investigations of strains in quenched metals[41,42] have demonstrated that their effects are expected to be negligible for the present experimental conditions (i.e., type of material, specimen size, and quenching mode).

D. Defect Aggregates

The electron micrographs which are presented pertain to copper single crystals quenched from ≈ 1040°C to 0°C; annealed at the latter temperature for 15 minutes; rapidly heated to 100°C; and isothermally annealed at 100°C for 60 minutes. The electron microscopy observations pertaining to this annealing schedule have been previously reported[78] and a critical evaluation of the contrast has been made.[63,78,81] The results are presented at this time along with unpublished observations for clarification purposes and in order to integrate them more fully into the recovery picture of quenched copper.

It is important to note that no evidence of resolvable defect aggregates was found for the following conditions:

1. When specimens were quenched from ≈ 1040°C and

   a. annealed at ≈ 25°C for periods as long as two weeks,

   b. immediately (i.e., ≈ 20 sec) heated to 100°C and given isothermal anneals of various duration at 100°C,

   c. annealed 1 to 2 min at 0°C and then isothermally annealed at 100°C for 60 min,

   d. annealed at ≈ 25°C for about 2 weeks and then isothermally annealed at 100°C for 60 min.

2. When specimens were quenched from temperatures below about 950°C, regardless of the post-quench annealing cycle.

Dark field micrographs obtained from specimens annealed 15 min at 0°C and 60 min at 100°C are shown in Figs. 29 through 33. The results will be presented in light of the criteria established for observation and identification of defect aggregates in Sec. II.B4.

The fact that the line of no contrast makes various angles (excluding 180°) with operating reflection vectors (they are normal only for ⟨220⟩ and ⟨111⟩ reflections) indicates that the defect aggregates are not spherically symmetrical. A spherically symmetric defect will always exhibit a line of no contrast perpendicular to the operating reflection vector regardless of which vector is operative. End-on dislocation line images are also of the black-white "lobe" type, but the line of no contrast is always parallel to the operating reflection vector.[89] Planar defects would be invisible or exhibit residual contrast under this condition since then $\bar{g} \cdot \bar{b} = 0$. The fact that this condition is satisfied in the present case is demonstrated in Fig. 29 where the operating reflection in Fig. 29a is parallel to the line of no contrast of the majority of images which are visible in Fig. 29b and

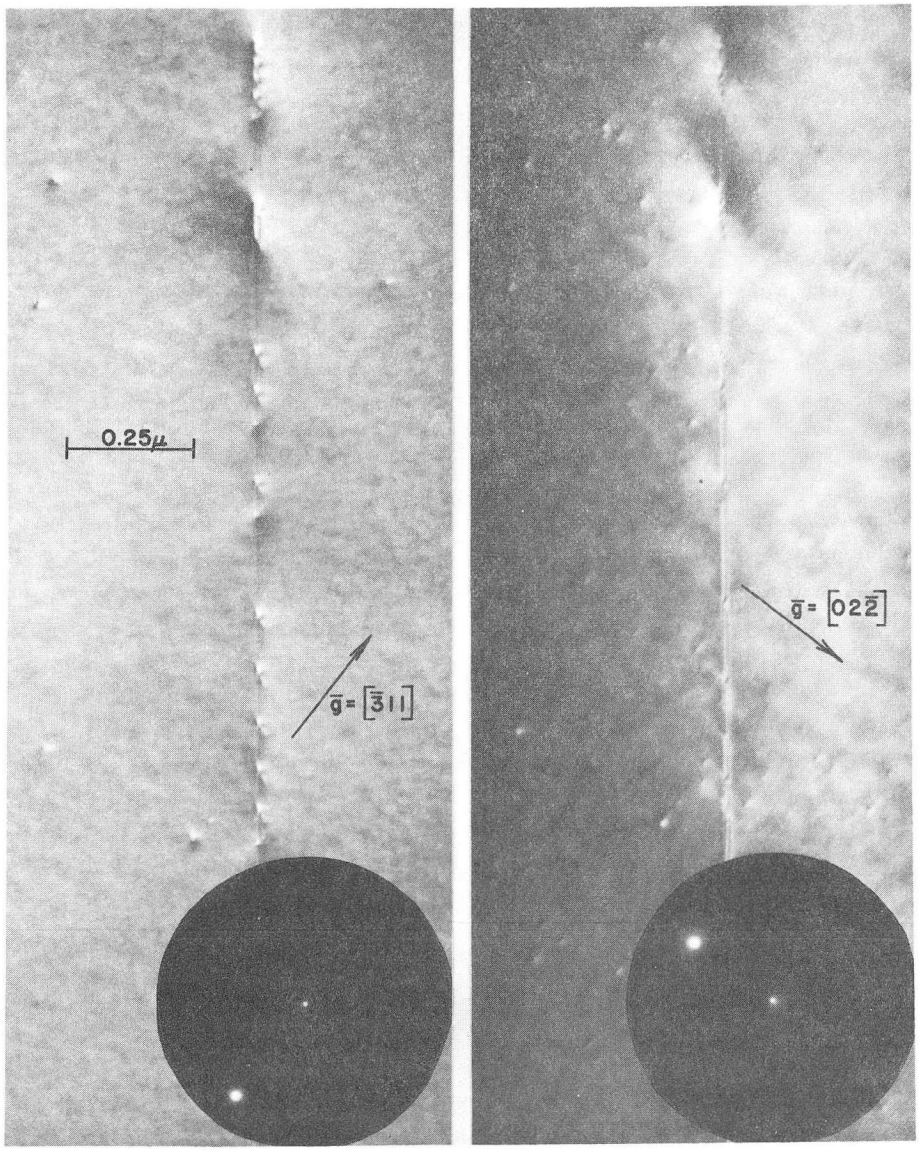

(a) (b)

ZN-4389

Fig. 29 Dark field micrograph which illustrates that the observed aggregates are invisible or exhibit only residual contrast under $\bar{g} \cdot \bar{b} = 0$. a. the operating reflection is normal to the lattice displacement vector of the majority of defects visible in 29b, hence $\bar{g} \cdot \bar{b} = 0$ and no defects are observed; b. the operating reflection is parallel to the displacement vector $\bar{b} = a/2\ [01\bar{1}]$, and the corresponding set of defects is visible.

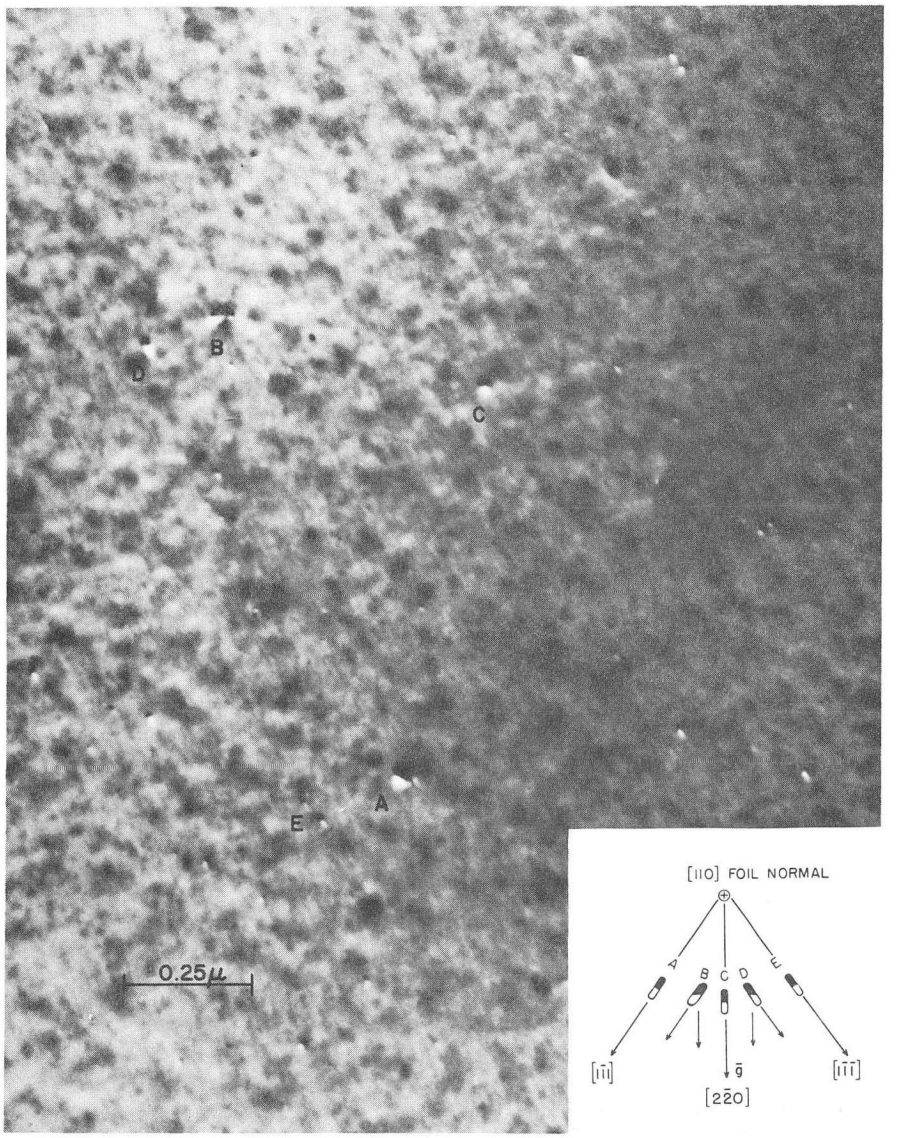

ZN-4393

Fig. 30a The dark field strain contrast images of imperfect prismatic loops, A and E, are symmetrical about their line of no contrast, whereas the images of perfect prismatic loops, B and D, are clearly streaked in a direction normal to their habit plane. The defect at A may be a perfect loop which has rotated into near edge orientation, i.e., a/2 [1̄10], (1̄10).

Fig. 30b Schematic of the five identifiable defect systems.

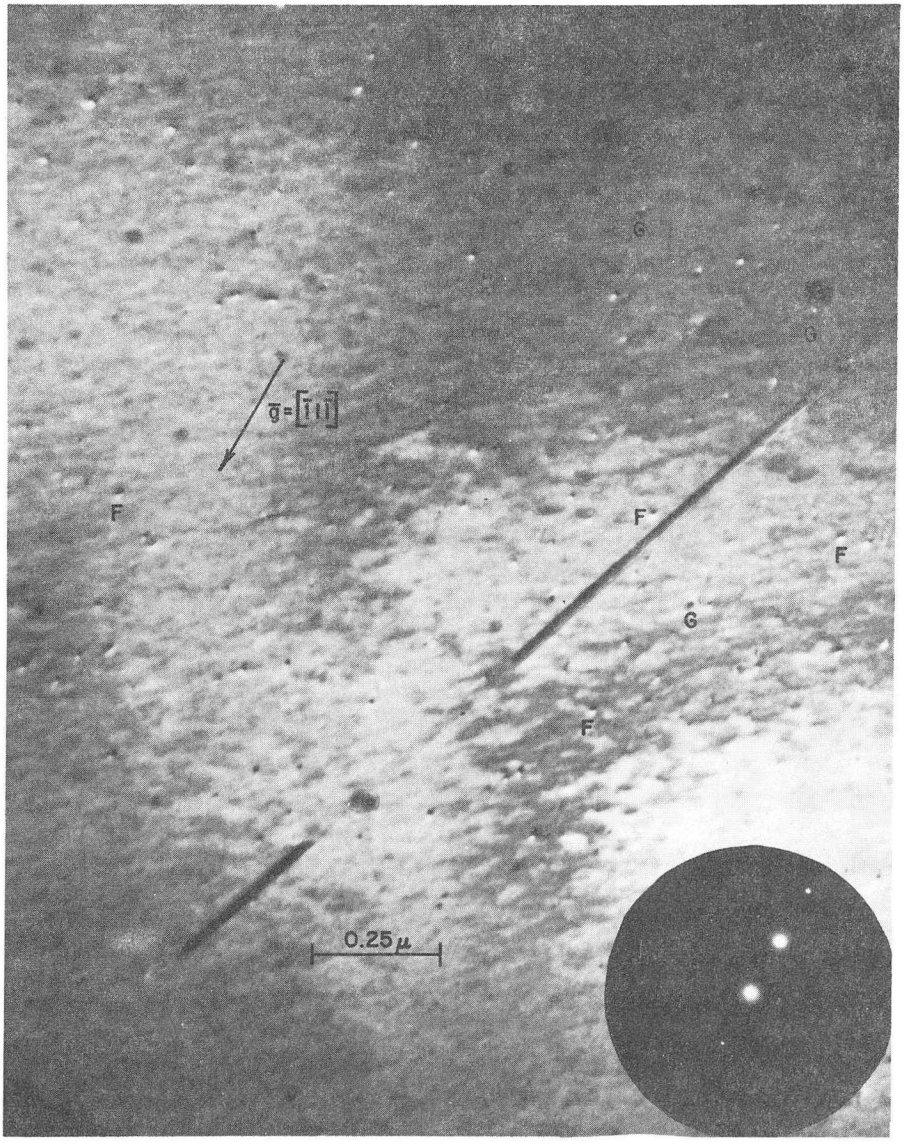

ZN-4391

Fig. 31 Dark field micrograph showing strain contrast when a ⟨220⟩ beam is used. The primary defects appearing are perfect prismatic loops whose displacement vectors are parallel to the operating reflection.

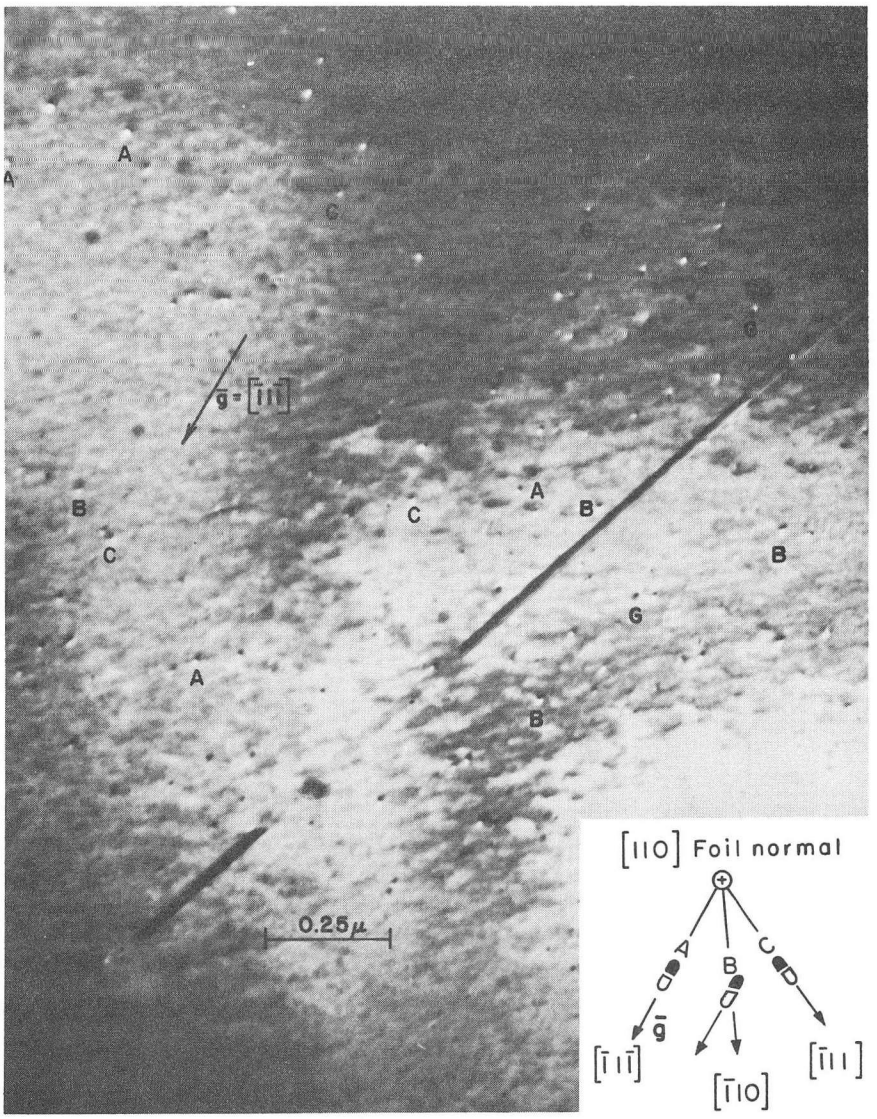

(a) (b)

ZN-4390

Fig. 32a Dark field micrograph showing strain contrast images when the [$\bar{1}$1$\bar{1}$] beam is operative in a [110] foil. The set of imperfect loops, A, and perfect loops, B, are in good contrast (i.e., $\bar{g} \cdot \bar{b} = 1$). An additional set of imperfect loops, C, is also visible. The defects at G exhibit strain contrast that would be expected from an interstitial inclusion: b. Schematic of the three identifiable vacancy-type defect systems.

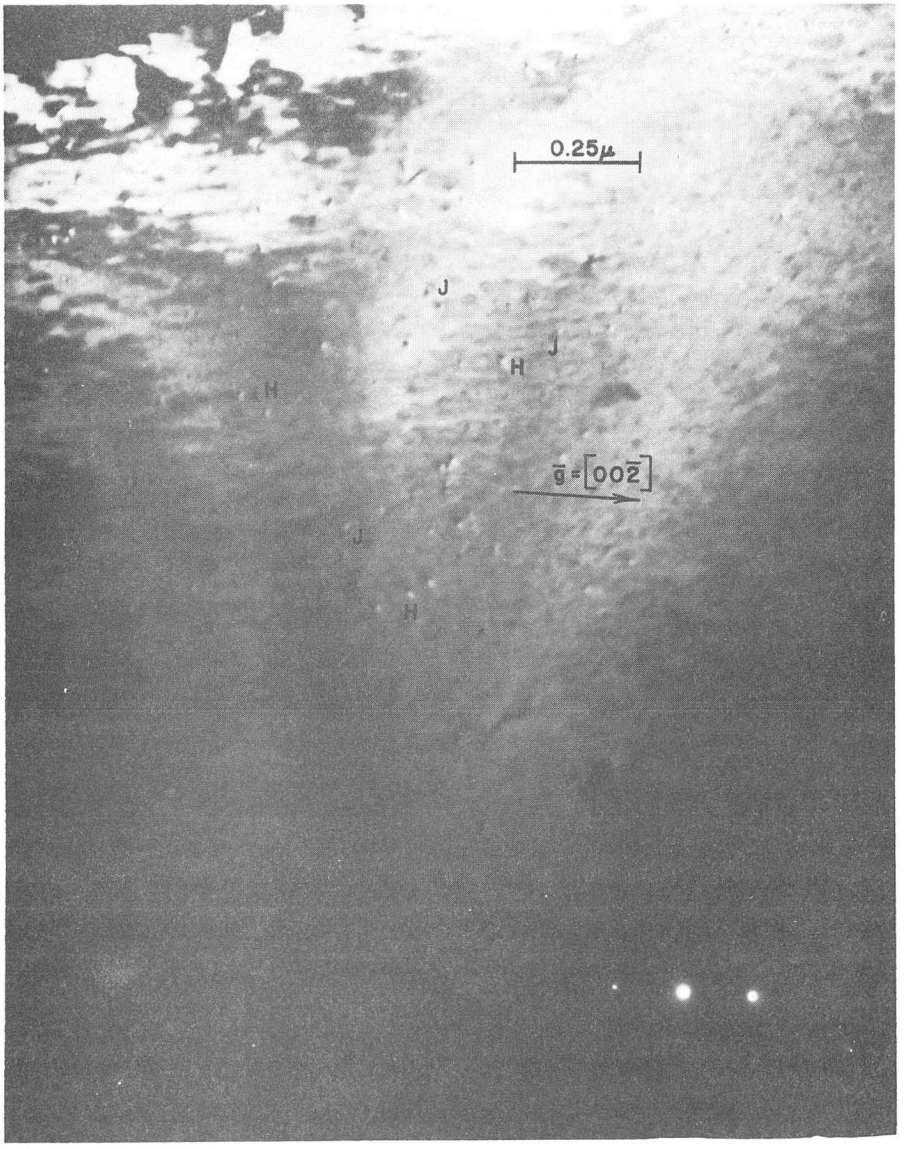

ZN-4392

Fig. 33 Dark field micrograph showing strain contrast images when the $[00\bar{2}]$ beam is operative in a [110] foil. Relatively weak contrast (i.e., $\bar{g} \cdot \bar{b} = 2/3$) is exhibited by two systems of imperfect loops, H and J, lying on the two ⟨111⟩ planes which are normal to the plane of the foil.

therefore normal to the displacement vector of those defects. Hence $\bar{g} \cdot \bar{b} = 0$, and no or very weak strain contrast is observed in Fig. 29a. Strain contrast images from small stacking fault tetrahedra are considerably more complicated[81] than the images observed to date in quenched copper, and can therefore be ruled out in the present case. It is thus concluded that the aggregates are planar.

Since the operating reflection vector, $\bar{g}$, is related to the normal to the line of no contrast through an acute angle on the white side of the image in better than 99% of the cases observed, for all foil orientations, and for all operating reflections, the aggregates are vacancy-type defects as expected.

The fact that the lines of no contrast are in all cases perpendicular to ⟨110⟩ or ⟨111⟩ directions in or projected onto the plane of the foil (e.g., see Fig. 30) indicates that the displacement vectors of the defects are of two types (a/2) ⟨110⟩ and (a/3) ⟨111⟩ and thus the aggregates are unresolvable prismatic loops of the perfect and imperfect type.

In the following it is demonstrated that the necessary and sufficient conditions for the visibility of perfect and imperfect prismatic vacancy loops are: (a) that the normal to the habit plane of the defect must be nearly parallel to the foil surface, (b) that the lattice displacement vector, $\bar{b}$, of the defect must also lie in the plane of the foil,* and (c) that $|\bar{g} \cdot \bar{b}| > 0$ (of course, $|\bar{g} \cdot \bar{b}|_{max}$ results in strongest contrast). Three examples are now considered.

If a ⟨220⟩ reflection is used in a {111} foil, the defects showing

---

* This criterion is a necessary addition because the normal to the defect plane and the lattice displacement vector, of course, are not the same for perfect loops.

strongest contrast will be those whose displacement vector is parallel to the operating reflection vector as in Fig. 31, that is (a/2) ⟨110⟩ type.* On the other hand, if a ⟨111⟩ reflection is employed in a {110} foil, as in Fig. 32, the defects showing good contrast will be those whose displacement vector is of the (a/3) ⟨111⟩ type parallel to the operating reflection vector and designated as the A system in Fig. 32b. Two additional systems are also observed, i.e., systems B and C having displacement vectors (a/2) $[\bar{1}10]$ and (a/3) $[\bar{1}1\bar{1}]$, respectively. Both of these systems satisfy conditions (a) and (b) for visibility. Since $\bar{g} \cdot \bar{b}_B = 1$, as was the case for system A, B-type defects are in equally good contrast. However for system C, $\bar{g} \cdot \bar{b}_C = 1/3$, and therefore these defects give rise to very weak contrast. If a reflection such as ⟨200⟩ in a {110} foil is used, then two (a/3) ⟨111⟩ systems are resolved and no strong (a/2) ⟨110⟩ systems (see Fig. 33). This is expected, since the only perfect loops which strictly satisfy conditions (a) and (b) for visibility, e.g., (a/2)$[\bar{1}10](\bar{1}1\bar{1})$, would show at most only residual contrast because $\bar{g} \cdot \bar{b} = 0$ for this case.

An important feature of the black-white strain contrast image of a planar, vacancy precipitate is the direction of streaking; that is the major axis of the elliptically shaped image pointing from black to white as previously illustrated schematically in Fig. 16. The angular relationship between the direction of streaking and the characteristic line of no contrast depends upon whether the loop is of edge or mixed character and possibly upon the angular relationship between the displacement vector of the defect and the foil surface. This dependency is illustrated in

---

* The images are, in general, poorly defined. This is probably because the angle between the normal to the habit plane and the foil surface could be as large as 20° in this case.

the following observations.

In Fig. 30a there are three well defined directions of streaking, four lines of no contrast, and a total of five defect systems (as shown schematically in Fig. 30b). Two systems, A and E, are streaked in ⟨111⟩ directions with (a/3) ⟨111⟩ displacements vectors; systems B and D are also streaked in ⟨111⟩ directions but have a $(a/2)[1\bar{1}0]$ displacement vector; lastly, C is streaked in the $[1\bar{1}0]$ direction and has a corresponding $(a/2)[1\bar{1}0]$ displacement vector.

It appears that if both the displacement vector of a perfect prismatic loop and the normal to the defect plane lie in the plane of the foil (i.e., conditions (a) and (b) for visibility are very nearly satisfied), the direction of streaking can clearly be interpreted as being normal to the habit plane of the defect and the strain image is correspondingly skewed about the line of no contrast. This is expected, since the strain field of the perfect loop is not maximized around $\bar{b}$ but about the displacements around the habit plane. When the lattice displacement vector, $\bar{b}$, is perpendicular to the habit plane (as for the (a/3)⟨111⟩ imperfect loop), the strain image is symmetrical about the line of no contrast as expected from theory.[84] The direction of streaking is therefore normal to the habit plane. The obvious implication of these observations is that the direction of streaking under certain conditions becomes a valuable tool in the determination of the habit plane of a small precipitate.

Case C which is illustrated in Fig. 30b, where the displacement vector is well defined from theory[84] but where the habit plane and therefore the character of the loop (i.e., edge or mixed) is in doubt, has been previously discussed in detail[78] and will not be considered here.

It should be noted that in certain instances, strain contrast images were observed which are the reverse of those expected for a vacancy-type defect. These images occur when a ⟨111⟩ reflection is operative (see Fig. 32) and were almost completely absent when higher order reflections, such as ⟨220⟩ and ⟨311⟩, were employed. This reversal of image could be associated with defects near the top and bottom of the foil. A region of the foil where the conditions necessary for the application of the two beam dynamical theory are believed not to be satisfied, especially for lower order beams. The implications of this effect are presently being investigated by Bell and Thomas.[90]

The imperfect vacancy loops appear to range in size from less than 60Å to a maximum of about 125Å in diameter, as determined from their strain contrast image. Perfect loops, in general, appear to be larger, ranging in size from 100Å to 200Å in diameter.

Punched loops of the type reported in previous transmission investigations on quenched copper[34,35,74,75] were not observed when high purity single crystals were employed. Although in some early work, where polycrystals of lower nominal purity were used, some instances of so-called prismatic punching were found.

Control experiments carried out on unquenched, well annealed, single crystals produced the following important results concerning the techniques employed and defect aggregates observed:

1. When the voltage conditions, as previously characterized (see Sec. II.B3), were adhered to, no polishing damage of the type reported by Essmann and Wilkens[91] was observed.

2. The possibility that the strain contrast images observed were the result of so-called Pashley-Presland[92] ion damage in the microscope

was excluded since similar images were not present when well annealed single crystal foils were examined under the same microscope conditions (i.e., vacuum, beam current,and time) as quenched foils. In addition, the density and size of defects observed in quenched foils were independent of the viewing time.

IV. DISCUSSION

The vacancy formation enthalpy is obtained from the temperature dependence of quenched-in resistivity. In arriving at this estimate it has been assumed that the loss of vacancies during the quench is approximately constant for $T_q \leq 670°C$ and that the resistivity per atomic percent vacancies is, to the first approximation, independent of the state of aggregation for low order clusters (i.e., $j \leq 3$). The loss of vacancies during an exponential quench is considered and the assumption regarding this point is shown to be reasonable.

The resistivity per atomic percent vacancies and the monovacancy formation entropy are estimated. Under the assumption that self-diffusion in copper occurs principally by the motion of monovacancies, an estimate of the migration enthalpy is also obtained. These results are compared with theory.

The isochronal annealing behavior of retained vacancies is qualitatively considered both with reference to previous experimental work reported in the literature and electron microscopy results obtained in the present investigation. Brief consideration is given to the problem of divacancy formation during a so-called exponential quench. It is shown that an appreciable fraction of the quenched-in vacancy population is in the form of divacancies for the case $B_{2v} = 0.4$ eV. Numerous processes are suggested to explain the observed recovery spectrum. The many possibilities serve to demonstrate the complexities associated with a more detailed investigation of the kinetics.

A. Monovacancy Formation Enthalpy

The retained vacancy concentration and distribution of the various defect clusters subsequent to a quench are very sensitive functions of the quench temperature, quenching rate, temperature to which the specimen is cooled, sink density and vacancy cluster binding energies.

When a specimen is rapidly cooled from high temperatures, sufficient time elapses during the quench so as to allow some fraction, $f(T_q)$, of the initial equilibrium vacancy concentration to migrate to sinks. Furthermore, during the early stages of the quench, the formation and break-up of certain small vacancy clusters occur so rapidly that, for example, divacancies are maintained at their equilibrium value appropriate for the instantaneous temperature.[48] Association of vacancies is therefore expected to occur during the quench, in addition to vacancy losses to fixed sinks. The extent to which vacancy aggregation affects the quenched-in resistivity depends on how appreciable the electron scattering cross section per vacant lattice site in the cluster is altered relative to an isolated vacancy. Such redistribution is not expected to have serious effects on the determination of the formation enthalpy from the temperature dependence of the quench induced resistivity, since the linear approximation, $\Delta\rho_{jv} \approx j\Delta\rho_{1v}$ is expected to be valid to within about 10% for low order clusters.[53,54] This is within the total uncertainty in $\Delta\rho(T_q)$ in the present experiments. The change in defect distribution during the quench can, however, markedly influence the low temperature annealing behavior and therefore the ease by which large vacancy aggregates (e.g., voids, loops, etc.) are nucleated and grow. A more detailed discussion of the formation of vacancy clusters during

the quench will be deferred at present.

It was observed that for quenching temperatures above ≈ 670°C, the resistivity increase is less than that predicted from an extrapolation of the low temperature values (see Fig. 21). In the present experiment the loss of vacancies during a quench must involve the diffusion of defects to various sinks, i.e., free surfaces, grain boundaries, subgrain boundaries, and free dislocations. Experiments in which the quenching rate is deliberately varied provide information about the migration of vacancies to this complicated sink structure at high temperatures where, under certain conditions, the difficulties arising from the clustering of vacancies should be minimized relative to the low temperature annealing situation. Mori et al.[44] and Flynn, Bass, and Lazarus[45] conducted studies of this type on gold which demonstrated quite clearly that the fractional loss of vacancies increased as the linear quenching rate was reduced. Flynn and coworkers[45] concluded that the most probable sinks at high temperatures were either free dislocations or subgrain boundary walls. It was not possible to distinguish between the two cases because of a lack of knowledge of the specimen substructure. More recently, Balluffi and Seidman[46] calculated the maximum expected monovacancy loss to a measured dislocation density in quenched gold employing a diffusion limited climb model. The time-temperature conditions were approximated as linear. The calculated maximum fractional loss was ≈ 36% for T_q = 878°C and was ≈ 6% for a quench from 658°C. Relatively good agreement was found between the experimentally observed losses and those which were calculated.

In an attempt to account for the observed losses in the present experiment, the maximum expected monovacancy loss to an assumed dislocation density was calculated on the basis of the diffusion limited climb model

first proposed by Seidman and Balluffi.[46,93] Quenching temperatures in the range 575° to 750°C were considered and the experimentally measured exponential time-temperature cooling behavior employed.

In the usual way, the problem is simplified by replacing the three dimensional dislocation network by a regular array of straight parallel dislocations. Each dislocation was represented by an infinite absorbing circular cylinder of radius r_d. The problem can thus be reduced to diffusion between concentric circular cylinders with the outer cylinder being a perfect reflector of radius R_d, where πR_d^2 equals the dislocation density, N_d. The climb motion of the dislocation which accompanies the absorption of vacancies was neglected as it has been shown[94] that this motion does not cause any significant complication. In addition it was assumed that:

1. The dominate defect at the quench temperature was the monovacancy and therefore the loss of defects can best be described in terms of the appropriate monovacancy properties. As can be seen in Table IV this condition is reasonably satisfied even for the high binding energy model in copper.

2. The concentration of monovacancies is altered only by the annihilation of vacancies at dislocations of effectively fixed size and position in the lattice and therefore it is implicitly assumed that there are no significant interactions between vacancies during the quench.

3. The monovacancy diffusion coefficient is independent of position in the lattice. This condition which is expected to be satisfied if the specimen has a small diameter and high thermal conductivity[41] so that thermal gradients are minimized.

The general diffusion equation under consideration is

$$\frac{\partial C_{1v}}{\partial t} = \nabla \cdot (D_{1v} \nabla C_{1v}) \qquad (20)$$

Table IV. Estimated Equilibrium Concentration of Mono-, Di-, and Trivacancies in Copper for Low and High Binding Energy Models*

T(°C)	C_{1v}	B_{2v}=0.2(eV) C_{2v}	B_{3v}=0.6(eV) C_{3v}	$C_{1v}/\frac{\Delta N}{N}$	B_{2v}=0.4(eV) C_{2v}	B_{3v}=1.2(eV) C_{3v}	$C_{1v}/\frac{\Delta N}{N}$
700	5.248×10^{-6}	0.005×10^{-6}	0.000	≈ 0.998	0.052×10^{-6}	0.010×10^{-6}	≈ 0.975
800	1.862×10^{-5}	0.005×10^{-5}	0.000	≈ 0.994	0.044×10^{-5}	0.012×10^{-5}	≈ 0.940

Pertinent relationships and assumptions:

a. $(\Delta N/N)_T = C_{1v}(T) + 2C_{2v}(T) + 3C_{3v}(T)$.

b. $C_{1v}(T) = \exp(\Delta S^f_{1v}/k)\ \exp(-\Delta H^f_{1v}/kT)$; $\Delta S^f_{1v} \cong 1k$, $\Delta H^f_{1v} \cong 1.1$ eV.

c. $C_{2v}(T) = 6[C_{1v}(T)]^2\ \exp(-\Delta S^b_{2v}/k)\ \exp(B_{2v}/kT)$; $\Delta S^b_{2v} = 2\Delta S^f_{1v} - \Delta S^f_{2v} \cong -1k$.

d. $C_{3v}(T) = 2[C_{1v}(T)]^3\ \exp(-\Delta S^b_{3v}/k)\ \exp(B_{3v}/kT)$; $\Delta S^b_{3v} = 3\Delta S^f_{1v} - \Delta S^f_{1v} \cong -3k$.

* The divacancy binding energies are assumed values. It was also assumed that $\Delta G^b_{3v} \cong 3\Delta G^b_{2v}$ and that the concentration of monovacancies is independent of the concentration of clustered vacancies. The fractional concentration of vacancy aggregates larger than j=3 was found to be negligible for reasonable estimates of ΔG^b_{jv}. Most theoretical estimates of B_{2v} in face-centered cubic metals fall in the range 0.1 to 0.4 eV, while estimates of B_{3v} are less certain (see Table VII).

where $D_{1v} = D_{1v}(t)$, so that Eq. (20) becomes

$$\frac{\partial C_{1v}}{\partial t} = D_{1v}(t)\ \nabla^2\ C_{1v}. \tag{21}$$

The time-dependent monovacancy diffusion coefficient, $D_{1v}(t)$ is given by

$$D_{1v}(t) = a_o^2\ \nu_{1v}\ \exp(\Delta S^m_{1v}/k)\ \exp[-\Delta H^m_{1v}/kT(t)] \tag{22}$$

Here a_o is the lattice parameter, ν_{1v} is the vibrational frequency of those atoms which are nearest neighbors to a vacancy, ΔS^m_{1v} is the monovacancy migration entropy and ΔH^m_{1v} is the monovacancy migration enthalpy. $T(t)$ was taken as the experimentally observed exponential time law

$$T(t) = T_o + \Delta T\ \exp(-\alpha t) \tag{15}$$

where $T_o = 77°K$, $\Delta T = T_q - T_o$, and α is the rate constant (sec^{-1}).

The boundary conditions, including a time-dependent equilibrium boundary condition at the dislocation core, r_d, are:

$$\begin{aligned} C_{1v}(t) &= \exp(\Delta S^f_{1v}/k)\ \exp[-\Delta H^f_{1v}/kT(t)] && t > 0 \quad r = r_d \\ [\partial C_{1v}/\partial r] &= 0 && \text{all } t \quad r = R_d \\ C_{1v} &= C_{1v}(T_q) && t = 0 \quad r_d \leq r \leq R_d \end{aligned} \tag{23}$$

where ΔS^f_{1v} and ΔH^f_{1v} are the monovacancy formation entropy and enthalpy, respectively. It is possible to obtain a solution to this problem by a general method previously reported by Seidman et al.[46,93] The concentration profile is accordingly given by

$$C_{1v}(r,t') = C_{1v}(T_q) - \pi \sum_{n=1}^{\infty} \left[\int_o^{t'} F(\tau)\ \exp(\alpha_n^2 \tau)d\tau\right]$$

$$\times \left[\frac{J_1^2 (R_d\alpha_n)\, J_o(r_d\alpha_n)\, Y_o(r\,\alpha_n) - J_o(r\,\alpha_n)\, Y_o\,(r_d\alpha_n)}{J_o^2(r_d\alpha_n) - J_1^2(R_d\alpha_n)} \right] \times \exp(-t'\alpha_n^2) \tag{24}$$

and by integration the mean concentration is

$$\overline{C}_{1v}(t') = C_{1v}(T_q) - \frac{2\pi}{R_d^2 - r_d^2} \sum_{n=1}^{\infty} \int_o^{t'} F(\tau)\exp(\alpha_n^2\tau)d\tau \left[\frac{\exp(-t'\alpha_n^2) J_1^2(R_d\alpha_n)}{J_o^2(r_d\alpha_n) - J_1^2(R_d\alpha_n)} \right] \tag{25}$$

where

$$t' = \int_o^t D_{1v}(t)\, dt \tag{26}$$

and $J_n(x)$ and $Y_n(x)$ are Bessel Functions of the first and second kind of order n. The α_n are the zeros of

$$Y_o(r_d\alpha_n) J_1(R_d\alpha_n) - J_o(r_d\alpha_n)\, Y_1\,(R_d\alpha_n) = 0 \tag{27}$$

and F(t) is given by

$$F(t) = C_{1v}(T_q) - \exp\,(\Delta S_{1v}^f/k)\ \exp\left[-\Delta H_{1v}^f/kT(t)\right]. \tag{28}$$

Equations (24) and (25) were evaluated on the IBM 6600 computor. The fractional loss of vacancies for various quenching temperatures was calculated and the results are summarized in Table V. The indication is that most of the vacancies are retained (i.e., > 90%) for quenches from below 675°C but that a substantial loss of defects accompanies higher quench temperatures.

These calculations are interpreted as indicating that the fractional loss of vacancies during a quench was approximately constant (i.e., $f(T_q) \cong$ constant) for $T_q < 650°C$. The estimated total equilibrium vacancy

Table V. Calculated Fractional Loss of Vacancies to a Regular Array of Dislocations During an Exponential Quench

Quench Temperature (°C)	Fractional Loss $C_{1v}(T_q) - \overline{C}_{1v}/C_{1v}(T_q)$*
750	0.1213
700	0.1062
675	0.0891
650	0.0822
625	0.0702
600	0.0620
575	0.0547

* Here $C_{1v}(T_q)$ is the equilibrium monovacancy concentration at the quench temperature, T_q, and $\overline{C}_{1v}$ is the calculated average concentration retained after the quench.

Pertinent Data:

$\alpha = 28\ \text{sec}^{-1}$

$T_o = 77°K$

$a_o^2 \nu_{1v} = \exp(\Delta S^m_{1v}/k) = D_o^{SD}/f_{1v} \exp(\Delta S^f_{1v}/k) = 0.2036$

$\Delta H^m_{1v} = 1.0\text{eV}$

$\Delta S^f_{1v} = 0.8k$

$\Delta H^f_{1v} = 1.09\text{eV}$

$N_d = 1\times10^8\ \text{cm-cm}^3$

$r_d = 3\times10^{-8}\ \text{cm}$

$R_d = (\pi N_d)^{-1/2} = 5.64\times10^{-5}\ \text{cm}$

$\overline{C}_{1v}(\text{tmax}) = \overline{C_{1v}(100°C)}$

concentrations, which were calculated for assumed values of ΔG^b_{2v} and ΔG^b_{3v} (see Table IV), indicate that in the temperature range of interest the monovacancy is the dominate defect, i.e., $(\Delta N/N)T_q \cong C_{1v}(T_q)$. Further, assuming that the resistivity per atomic percent vacancies is, to a first approximation, independent of the state of aggregation, it is concluded that the temperature dependence of the quenched-in resistivity can be represented by*

$$[\Delta\rho(T_q)]_{4.2°K} \cong A' \exp[-H^f_{1v}/kT_q] \qquad (29)$$

where $A' = (1.7\pm0.2) \times 10^{-4}$ ohm-cm** and $H^f_{1v} = 1.09\pm0.04$ eV, consistent with the values predicted by specimens with $R(273°K)/R(4.2°K) \geq 600$. The uncertainty in ΔH^f_{1v} encompasses all estimated values. If the data for the case $R(273°K/R(4.2°K) \approx 450$ are included, the result is $\Delta H^f_{1v} = 1.07\ 0.05$ eV. As was previously demonstrated (see Fig. 23), these data are clearly biased toward higher quenched-in increments. While the origin of this difference is not clear, it is tempting to attribute it to an impurity effect. Nevertheless the data are far too limited to persue the point further. Finally it is worth noting that similar behavior has been reported in the case of quenched gold for $R(273°K)/R(4.2°K) \approx 300$[56] and platinum for $R(273°K)/R(4.2°K) \approx 475$.[42]

It is of interest to compare the present estimate of the monovacancy formation enthalpy to that determined from equilibrium measurements. Assuming S^f_{1v} (1.5 0.5)k, Simmons and Balluffi[11] obtained $\Delta H^f_{1v} = 1.17\pm0.11$ eV.

---

* See Eqs. (9) - (13) in Sec. I-D.

** $A' \cong 100 \cdot f \cdot \Delta\rho_{1v} \cdot \exp(\Delta S^f_{1v}/k)$.

With an assignment of $\Delta S^f_{1v} = 0.8$ k, their result is brought into better agreement with the present nonequilibrium estimate. This alternate selection of the entropy term is not inconsistent with theoretical calculations for the copper lattice (see Table VII).

B. Monovacancy Resistivity and Formation Entropy

Conclusions from the previous discussion permit an evaluation to be made of the monovacancy resistivity, $\Delta\rho_{1v}$. For $T_q = 1075°C$, an extrapolation of the measured temperature dependence of the quenched-in resistivity predicts $\Delta\rho(1075°C) = (1.4\pm0.2)\times10^{-8}$ ohm-cm. This increment can be expressed as

$$[\Delta\rho(1075°C)]_{4.2°K} = 100[\Delta\rho_{1v}C_{1v}(T^*) + \Delta\rho_{2v}C_{2v}(T^*) + \ldots], \quad (9')$$

(see Eq. (9)). The constants $\Delta\rho_{jv}$ may be slightly temperature dependent.[56] If it is assumed that $f(T_q) \simeq 1$ and therefore that this resistivity increment is truly representative of the high temperature equilibrium concentration of vacancies, and again that $\Delta\rho_{jv}$ varies linearly with j, then

$$[\Delta\rho(1075°C)]_{4.2°K} \simeq 100\ \Delta\rho_{1v}[C_{1v}(T^*) + 2C_{2v}(T^*) + \ldots]$$
$$= 100\Delta\rho_{1v}\ [(\Delta N/N)_{1075°C}]. \quad (30)$$

Employing the experimentally determined value of $(\Delta N/N)_{1075°C} = (1.9\pm0.5)\times10^{-4}$ obtained from equilibrium measurements,[11] it follows that the vacancy resistivity at 4.2°K is

$$\Delta\rho_{1v} = (0.75\pm0.35)\mu\text{ohm-cm/at.\% vacancies}. \quad (31)$$

The uncertainty is based on the error asising from the assumption that $\Delta\rho \approx j\Delta\rho_{1v}$, i.e., 10% on the stated errors in $\Delta\rho(1075°C)$ of 12% and $(\Delta N/N)_{1075°C}$ of 26%.

It is also possible to estimate the monovacancy formation entropy from the experimentally determined value of A' and the estimated value of $\Delta\rho_{1v}$. The result is

$$\Delta S^f_{1v} = (0.8 \pm 0.5)k. \qquad (32)$$

The uncertainty is significantly large because of the correspondingly large errors in A' and $\Delta\rho_{1v}$.

C. Monovacancy Migration Enthalpy

Provided that self-diffusion occurs principally by the motion of monovacancies, an estimate of the migration enthalpy, ΔH^m_{1v}, can be obtained from the present data and the relationship

$$Q^{sd} = \Delta H^f_{1v} + \Delta H^m_{1v} . \qquad (33)$$

As an indication of the relative contribution to high temperature self-diffusion that might be expected from monovacancies and divacancies, the ratio D^{sd}_{1v}/D^{sd}_{2v} is considered. The tracer self-diffusion coefficient due to monovacancies is given by

$$D^{sd}_{1v} = a_o^2 \, f_{1v}\nu_{1v} \exp(-\Delta S^m_{1v}/k) \exp(-\Delta H^m_{1v}/kT) \cdot C_{1v}(T) \qquad (34)$$

where a_o is the lattice parameter, f_{1v} is the correlation factor, ν_{1v} is the vibrational frequency of those atoms which are nearest neighbors to a vacancy, and ΔS^m_{1v} is the migration entropy. The corresponding diffusion coefficient due to divacancies is

$$D^{sd}_{2v} = \left(\frac{2}{3}\right) a_o^2 \, f_{2v}\nu_{2v} \exp(\Delta S^m_{2v}/k) \exp(-\Delta H^m_{2v}/kT) \cdot C_{2v}(T) \qquad (35)$$

where it is assumed that the only atoms which exchange with the defect are

nearest neighbors to both divacancy sites. Here ν_{2v} is the vibrational frequency of the four atoms which are nearest neighbors to both vacancies in a divacancy. If it is assumed that $\nu_{1v} \approx 2\nu_{2v}$ and $\Delta S^m_{1v} \approx 2\Delta S^m_{2v} = 2k$,* and since $f_{1v} \approx 0.78$[95] and $f_{2v} \approx 0.48$,[96] the desired ratio is given approximately by

$$D^{sd}_{1v}/D^{sd}_{2v} \approx [C_{1v}(T)/C_{2v}(T)] \quad \exp[\Delta H^m_{2v} - \Delta H^m_{1v})/kT] \cdot 14 \ . \qquad (36)$$

At the melting point of copper, the ratio of the diffusivities, D^{sd}_{1v}/D^{sd}_{2v}, is ≈42 and ≈7 for a low and high binding energy model, respectively. These estimates, along with the pertinent data and assumptions, are summarized in Table VI. The existing experimental determinations of B_{2v} favor the low binding energy model for copper (i.e., $0.1 < B_{2v} < 0.2$).[12] These results are tentatively interpreted as indicating that high temperature self-diffusion in copper occurs primarily by means of monovacancy migration. Therefore taking $Q^{sd} = (2.10 \pm 0.02)$ eV[8] (also see Sec. I-C), it is concluded that $\Delta H^m_{1v} = (1.01 \pm 0.06)$ eV. The error was again obtained by summation.

It is also possible to evaluate the contribution of divacancies to high temperature self-diffusion under the condition that the diffusion coefficient is given explicitly by[11,12]

$$D^{sd} = D^{sd}_{1v} + D^{sd}_{2v} = D_o \exp\,(Q^{sd}/kT). \qquad (37)$$

If reasonable assumptions are again made about divacancy properties in copper, the quantity $\Delta H^f_{1v} + \Delta H^m_{1v}$ was found to be lowered slightly, but the alteration

---

* Since the nearest neighbor relaxation is expected to be greater around a divacancy than a monovacancy, and because there is less straining of the lattice when an atom jumps into a divacancy than a monovacancy, these approximations are qualitatively reasonable.[4]

Table VI. Estimation of the Ratio of the Diffusivities D^{sd}_{1v}/D^{sd}_{2v} at the Melting Point of Copper (1083°C) for Low and High Binding Energy Models.

B_{2v}(eV)	$C_{1v}\ 10^4$	$C_{2v}\ 10^4$	C_{1v}/C_{2v}	D^{sd}_{1v}/D^{sd}_{2v}
0.2	1.93	≈ 0.03	≈ 64	≈ 42
0.4	1.70	≈ 0.15	≈ 11	≈ 7

Pertinent relationships and assumptions:

a. $(\Delta N/N)_T = C_{1v}(T) + 2C_{2v}(T)$; $(\Delta N/N)_{1083°C} = (2.0 \pm 0.5)\ 10^{-4}$.[11]

b. $C_{2v}(T) = 6C^2_{1v} \exp(\Delta G^b_{2v}/kT)$.

c. $$C_{1v}(T) = \frac{-1 + \sqrt{1 + 48\,(\Delta N/N)_T \exp(\Delta G^b_{2v}/kT)}}{24 \exp(\Delta G^b_{2v}/kT)}.$$

d. $\Delta G^b_{2v} = B_{2v} - T\Delta S^b_{2v}$; $\Delta S^b_{2v} = 2\Delta S^{\cdot\cdot}_{1v} - \Delta S^f_{2v} \approx -1k$.

e. $\left(D^{sd}_{1v}/D^{sd}_{2v}\right)_T \approx 0.65 \left[C_{1v}(T)/C_{2v}(T)\right]_{B_{2v}}$ for $\Delta H^m_{1v} \approx 1$ eV,

and $\Delta H^m_{2v} \approx 0.65$ eV.

is not appreciable and within the experimental uncertainty in Q^{sd}.[12,13] Therefore the contribution of divacancies to D^{sd} for this model does not alter the present result.

D. Comparison with Theory

Numerous theoretical calculations have been made of the formation enthalpy, migration enthalpy and various other properties of monovacancies as well as of vacancy pairs and larger aggregates. In general, copper has been employed as the prototype. All but the most recent of these investigations have been summarized and discussed by Damask and Dienes.[1] Many of the theoretical values derived for copper are collected in Table VII. These results have, in many instances, been quite helpful in indicating the many possibilities which migh exist and, as such, have been a valuable guide in the interpretation of experimental results. Nevertheless in view of the range of possible values in some cases, the acceptance and use of numerical results (especially for clusters) must be done with caution. In quoting previously from theory, these considerations were implicitly assumed and it is in this same spirit that the present results have been evaluated and are now compared to theory.

The reported estimates of the monovacancy formation and migration enthalpies fall in the middle range of the theoretical predictions (see Table VII). On the other hand, the resistivity per atomic percent vacancies is about a factor of two smaller than the generally accepted theoretical estimate for copper of 1.7 μohm-cm/at.% vacancies.[11,12] This disagreement is not considered to be serious in view of the large uncertainties associated with the individual quantities involved and of the many assumptions required to obtain the desired experimental result. The estimated

Table VII. Theoretical Estimates of Some Vacancy Properties in Copper

Defect	Formation Enthalpy ΔH^f_{1v} (eV)	Formation Entropy $\Delta S^f_{jv}/k$	Migration Enthalpy ΔH^m_{jv} (eV)	Binding Energy B_{jv} (eV)	Resistivity $\Delta\rho$ ($\mu\Omega$-cm/at.%)
Monovacancy	1 to 1.2[a]	1.5[g]	1[i]		0.4[l]
	0.9[b]	0.5[h]	0.6[b]		1.3[m]
	0.8[c]		0.97[j]		1.3[n]
	1.0[d]		1.3[k]		1.5[o]
	0.97±0.25[e]		1.06[a]		1.5[p]
	1.0[f]				1.7[c]
					0.6[q]
Divacancy		2.8[h]	0.35[j]	0.3[j]	0 to 10% less[v]
			0.2[k]	0.64[s]	than $2\Delta\rho_{1v}$
			0.2 to 1.0[r]	0.1 to 0.2[t]	
			0.6[e]	0.36[u]	
Trivacancy			1.9[k]	0.5 to 2.9[x]	
			0.5 to 1.0[w]	1.1 to 2.1[u]	
Tetravacancy			≈1.9[k]	1 to 3[u]	

a. see reference 103
b. see reference 104
c. see reference 105 and 106
d. see reference 107
e. see reference 108
f. see reference 109
g. see reference 110
h. see reference 23
i. see reference 103 and 111
j. see reference 112
k. see reference 16
l. see reference 113
m. see reference 114
n. see reference 115
o. see reference 116
p. see reference 117
q. see reference 118
r. see reference 119
s. see reference 120
t. see reference 121
u. see reference 122
v. see reference 53, 54, and 123
w. see reference 124
x. see reference 16 and 125

value of the formation entropy is consistent with theory, although the present value is somewhat lower than that favored by Simmons and Balluffi[11] and is closer to the recent estimate of Schottky et al.[23] However, the calculation is not very accurate and the result must therefore be interpreted as only suggestive.

E. Isochronal Annealing and Vacancy Aggregation

In general, the quenched-in defect structure and the manner in which it responds to thermal energy are quite complicated. The fractional concentration of the numerous possible defect clusters (i.e., vacancy-vacancy clusters, as well as vacancy-impurity clusters) after the quench is uncertain. For the most part, this is the result of our ignorance about the various properties of such clusters (e.g., their characteristic binding energies). Recent machine calculations for a "typical" noble metal[75] have illustrated many of the important features of both homogeneous and heterogeneous nucleation of clusters during the quench. The results indicated quite clearly that such alterations in the distribution of aggregates must be taken into account when detailed studies of defect mobilities and vacancy clustering phenomena are carried out. Little is known about the spatial distribution of the defects although it is generally implicitly assumed that the distribution is random. Specific defects may anneal out in different temperature ranges. In addition, two or more annealing processes may occur simultaneously and to a variety of sinks which may be effectively fixed, (e.g., subgrain boundaries) as well as variable (e.g., stable vacancy aggregates) in character. These various sinks are, in many instances, competing for the excess vacancy concentration. The effectiveness of a particular sink may depend strongly on its spatial distribution and possibly on

the annealing temperature. The fact that when the annealing temperature is sufficiently low, vacancies cluster and the resulting aggregates constitute the major sinks supports this viewpoint. The importance of certain impurities in promoting heterogeneous nucleation of vacancy aggregates was suggested as a result of electron microscopy investigations by Cotterill and Segall[60,97] for the case of quenched gold. This conclusion was quantitatively substantiated recently by Ytterhus et al.[57,58] These authors showed that small concentrations of specific impurities (i.e., $< \approx 4\times10^{-3}$ at.%) played a dominant role in determining the effective vacancy aggregate sink density in gold and similar behavior is expected in other noble metals.

Therefore, descriptively, the recovery of quench induced vacancies, as inferred from a) theoretical considerations, b) measurements of the change in the residual resistivity and c) direct observation of precipitated aggregates by electron microscopy, is expected to involve the annihilation of certain mobile vacancy clusters at a relatively complicated sink structure. Mobile defects may combine with one another and depending on their character, dissociate into lower order defects. There will be a general tendency for large clusters to be established through a series of additive events. When an aggregate reaches a "critical" size it becomes a stable, immobile vacancy sink which then grows by the inward diffusion of mobile defects.[59] In light of our present knowledge, the "stable cluster" is by necessity poorly defined. For instance, it could be a) one of the numerous possible trivacancy or tetravacancy complexes,[99] b) merely a region in the lattice where locally the concentration of vacancies is very high, i.e., a region of very low density, and c) an actual discrete void of the type suggested from small-angle scattering experiments[24,64] and larger versions of which have been observed directly in quenched aluminum by transmission electron microscopy.[62,98] Fixed and variable

sinks compete for vacancies. Impurities are expected to play an important role in promoting heterogeneous nucleation of stable clusters. As a consequence of this picture, the corresponding form of any particular annealing curve, and therefore the migration processes, initial stages of vacancy clustering, final form of vacancy aggregates, and the processes associated with their elimination, is expected to be quite structure and impurity sensitive. In addition, as was pointed out by Balluffi and Siegel,[59] the actual shape of the annealing curve may not, in fact, be related uniquely to the vacancy migration processes which occur. It is therefore evident that a comparison of data obtained from different laboratories usually involves a number of difficulties and may be of limited significance in many cases if sufficient information is not reported. The discussion which follows is presented in a spirit consistent with this description. Several likely possibilities are presented to explain the observed annealing behavior. The data are far too limited to arrive at any definite conclusions.

The isochronal recovery behavior pertains to specimens quenched from about 700°C with a corresponding fractional retained vacancy concentration of $(\Delta N/N)_{700°C} \approx 5\ 10^{-6}$. Three annealing stages were observed with maximum annealing rates occurring at about -40°, +200° and +400°C. For the convenience of discussion these stages will be referred to as Stage III_q, Stage IV_q and Stage V_q which is consistent with accepted terminology.

Stage III_q annealing can be qualitatively considered in terms of the relative motion expected from monovacancies, the dominant defect at the quench temperature, and for the sake of discussion divacancies. The monovacancy diffusion coefficient is given by

$$D_{1v} = \frac{a_o^2}{12}\ \Gamma_{1v} = a_o^2\ \nu_{1v}\ \exp(\Delta S_{1v}^m/k)\ \exp(-\Delta H_{1v}^m/kT) \tag{38}$$

where Γ_{1v} is the average number of jumps a monovacancy makes per second. The corresponding expression for divacancies is

$$D_{2v} = \frac{a_o^2}{24}\ \Gamma_{2v} = \frac{a_o^2}{6}\ \nu_{2v}\ \exp(\Delta S_{2v}^m/k)\ \exp(-\Delta H_{2v}^m/kT). \tag{39}$$

Here Γ_{2v} is the average number of nondissociative jumps a vacancy in a divacancy configuration makes per second. If one assumes as before that $\nu_{1v} = 2\nu_{2v}$ and $\Delta S_{1v}^m \approx 2\Delta S_{2v}^m = 2k$, then the ratio of the diffusion coefficient of a divacancy to that of a monovacancy at a temperature T_a is

$$D_{2v}/D_{1v} \approx 0.03\ \exp[\Delta H_{1v}^m - \Delta H_{2v}^m/kT_a]. \tag{40}$$

Taking $\Delta H_{1v}^m \approx 1.0$ eV, $\Delta H_{2v}^m \approx 0.65$ eV* and $T_a = 233°K$ (i.e., -40°C), one obtains $D_{2v}/D_{1v} \sim 1.2\times10^6$. Therefore for any realistic ratio of C_{1v}/C_{2v}, annealing would be completely dominated by divacancy motion in this situation.

An equivalent way of looking at the problem is to consider the average number of jumps, n_{jv},** a particular defect would make during a given isoannealing step. The average number of jumps made by a monovacancy, n_{1v}, during a 5 min. anneal at -40°C was estimated to be $\approx 1\times10^{-3}$, whereas a divacancy (assuming $\Delta H_{2v}^m \approx 0.65$ eV) would be expected to take $\approx 3\times10^2$

---

* Existing experimental results have been interpreted as indicating that $0.6 < \Delta H_{2v}^m < 0.7$ for copper.[13,24]

** Since the average number of jumps made by a defect in time τ is $n_{jv}=\Gamma_{jv}\tau$,[95] it follows from Eqs. (38) and (39) that

jumps on the average during the same interval of time. Therefore the dominant defect migrating during Stage III_q is not expected to be the monovacancy but some higher order cluster.

In view of the qualitative evidence against the monovacancy contributing significantly to Stage III_q annealing, the formation of vacancy clusters during an exponential quench was considered. The simple case of divacancy formation was investigated. The details are presented in Appendix III. The general model considered was first suggested by Koehler et al.[47] and subsequently employed in the analysis of results on quenched gold.[48-50] The following describes the main points of the model and presents the pertinent results of its application to this investigation.

For quenching rates which are experimentally attainable in the laboratory and compatible with the aims of, say, the present investigation, vacancies no doubt make a large number of jumps during the initial part of the quench. The number of vacancy-vacancy collisions is sufficiently high so that the thermal equilibrium concentration of divacancies is attained (as indicated by the kinetic equations which are used to approximately describe the physical situation)[48,49] even during the short time that the specimen is at a particular temperature. As the temperature decreases, a point is reached where the reactions of interest proceed too slowly to satisfy the equilibrium demands. The actual concentration of defects therefore deviates from the equilibrium values. The temperature at which this deviation occurs is defined as T^*.[48] Any change in the vacancy distribution which occurs below T^* is small. An estimate of T^* and the corresponding fractional concentration of the various vacancy cluster characteristic of T^* is of interest.

If it is assumed that the defects are distributed randomly and that the loss of vacancies to fixed sinks during the quench is negligible, (i.e. $\Delta N/N \approx C_{1v} + 2C_{2v}$ = constant for all t and characteristic of T_q) then the kinetic equation describing the time dependence of the monovacancy concentration, C_{1v}, is given by[1]

$$\frac{dC_{1v}}{dt} = -2C_{1v}^{2}K_1 + 2C_{2v}K_2. \tag{41}$$

Here K_1 and K_2 are so-called rate constants and written as follows:

$$K_1 = 84\nu_{1v} \exp(\Delta S^m_{1v}/k) \exp(-\Delta H^m_{1v}/kT) \tag{42}$$

$$K_2 = 14\ \nu_{2v} \exp[(\Delta S^m_{1v} + \Delta S^b_{2v})/k] \exp[-(\Delta H^m_{1v} + B_{2v})/kT] \tag{43}$$

where 84 and 14 are the appropriate combinatory numbers for the association of monovacancies and dissociation of divacancies, respectively.

The associative rate of change of the monovacancy concentration required to maintain the instantaneous equilibrium concentration of divacancies is obtained by differentiating the equilibrium expression

$$C_{2v} = 6\ C_{1v}^{2} \exp(\Delta G^b_{2v}/kT) \tag{44}$$

with respect to time and using the fact that $\frac{dC_{1v}}{dt} = -2\ \frac{dC_{2v}}{dt}$. The equilibrium requirement can formally be written

$$\left(\frac{dC_{1v}}{dt}\right)_{eq} = \frac{12C_{1v}^{2}\ \frac{B_{2v}}{kT(t)^2}\ \frac{dT}{dt}\ \exp\left[\Delta G^b_{2v}/kT(t)\right]}{\left[1 + 48\ (\Delta N/N)T_q\ \exp\ \{\Delta G^b_{2v}/T(t)\}\right]^{1/2}} \tag{45}$$

The temperature T^* is reached when the associative rate required by equilibrium just equal the associative term in Eq. (41) Thus, it can be shown that T^* is defined by the following equality for a so-called exponential

quench having a time constant α sec^{-1}:

$$\alpha(T^* - T_o) = \frac{14 D_{1v}(T^*) k T^{*2} \left[1 + 48(\Delta N/N)_{T_q} \exp(\Delta G^b_{2v}/kT^*)\right]^{1/2}}{a_o^2 B_{2v} \exp(\Delta G^b_{2v}/kT^*)} \quad (^\circ K/sec). \tag{46}$$

Values of T^* were determined for $T_q = 700^\circ C$ and assumed divacancy binding energies. The ratios of the divacancy concentration to the monovacancy concentration characteristic of T^* and total defect population were calculated and are summarized in Table VIII. In the case where the binding energy is high $0.3 \leq B_{2v} \leq 0.4$ an appreciable fraction of the retained vacancies are in the form of divacancies. For the purpose of comparison, the relative fraction of vacancies which are in the form of divacancies when the reaction under consideration is allowed to go to completion at $-40^\circ C$ was also computed and tabulated.

Stage III_q recovery is consistent with the general conclusions drawn from the literature in Sec. I-D (i.e., $-80^\circ C < T_{III_q} < +100^\circ C$). The fact that in some instances very little recovery was reported for annealing temperatures lower than $0^\circ C$ can be attributed in part to the choice of T_o (i.e., the temperature to which the specimen is quenched). As was illustrated clearly by the present pulsing experiment (see Fig. 27), a significant amount of recovery occurs at temperatures around $0^\circ C$ even when the time spent there is short. Care must therefore be taken in any quantitative interpretation of quenched-in increments when quenching to, say $0^\circ C$. The time spent at T_o is usually quoted as being much less than the 20 sec employed in the present pulsing experiment, nevertheless it serves to demonstrate the point. Similar but more marked behavior has been observed for aluminum where time spent at temperatures as low as $-100^\circ C$ appears to be critical.[62]

Table VIII Calculated Values of the Critical Temperature, T^*, and the Relative Contribution of Divacancies to the Defect Population*

Calculated Quantities	Divacancy Binding Energy (eV)			
	0.1	0.2	0.3	0.4
$(\Delta N/N)_{T_q} \times 10^6$	5.02	5.03	5.05	5.27
T^* (°C)	150	197	239	274
$\frac{C_{2v}(T^*)}{C_{1v}(T^*)} \times 10^2$	0.17	1.1	6.5	27.2
$\frac{2C_{2v}(T^*)}{(\Delta N/N)_{T_q}} \times 10^2$	0.34	2.2	11.6	35.2
$\frac{2[C_{2v}(-40°C)]_{eq}}{(\Delta N/N)_{T_q}} \times 10^2$	2.37	59.4	95.8	99.6

* See Appendix III, Table X for pertinent parameters used in the calculation.

Stage III_q annealing of quenched copper can be contrasted to quenched silver where a low temperature recovery stage has also been reported.[28,29] Doyama and Koehler[28] have tentatively identified the defect which migrates at temperatures below 0°C as the divacancy and estimated that its binding energy is between 0.3 and 0.4 eV. Detailed kinetic studies have not been carried out on copper in this temperature region but the present annealing results indicate that such an investigation would be desirable.

Stage IV_q (centered at ≈ 200°C) and Stage V_q (centered at ≈ 400°C) will be briefly discussed in light of the following experimental observations:

1. Ramsteiner et al.[13] have observed an annealing stage in quenched copper in the temperature range from 100° to 200°C (see Table II). The kinetics have been interpreted as indicating that the migrating defect is the monovacancy. The activation enthalpy for the process was found to be 1.0 to 1.1 eV. Similar observations and conclusions were reported by these authors[100] as a result of an investigation of the recovery processes in copper subsequent to cold work.

2. Small angle-x-ray scattering experiments[24,64] made on copper quenched from close to the melting point and annealed at, or slightly above, room temperature have been interpreted as indicating the existence of three dimensional vacancy aggregates (maximum dimension ~30Å). Clusters were first detected after about 30 min. annealing at 25°C.[64] Recovery of the observed low temperature scattering phenomenon occurred at an annealing temperature of about 190°C. This recovery was attributed to either the dissociation of vacancy agglomerates and annealing out of the products, or to the reordering of the agglomerates (i.e., their collapse into prismatic loops).[24] It must be kept in mind that the analysis of these x-ray data

is made difficult because three dimensional voids cannot easily be distinguished from small loops; nevertheless the presence of scattering centers which are initially about 10Å in diameter is an experimental reality.[64]

3. The present results show that when copper single crystals are quenched from $T_q \approx 1040°C$ and subsequently annealed for 15 min. at 0°C and then for 1 hr at 100°C, randomly oriented, planar, vacancy aggregates are directly observed by electron microscopy. When these annealing conditions are combined with those outlined in Sec. III-D which resulted in no evidence of resolvable aggregates, it seems quite clear that the presence of loops which are large enough to be detected by electron microscopy is apparently controlled by the so-called "pre-aging" treatment (i.e., in the present experiments the time at 0°C). Therefore, as expected, the final structure is a sensitive function of the nucleation processes (i.e., annealing at 0°C) and the availability of mobile defects in a sufficiently high concentration to support growth processes at higher temperatures (i.e., annealing at 100°C). The fact that voids have not been observed cannot be used as an argument against their existence. The detection of voids is dependent on "mass thickness" contrast (i.e., at a void the extinction distance, t_o, effectively approaches infinity). It has been estimated that voids can be detected by this mechanism only when the defect is greater than about 10% of the foil thickness.[101] Considerable difficulty in detecting voids has been encountered by a number of authors,[102] but recently their existence was proven in quenched aluminum.[98] It is possible that such defects may represent a necessary stage of vacancy aggregation prior to loop formation, as has been suggested for some time.[102] The exact relationship between the void and the prismatic loop in quenched aluminum is still not completely clear, however.[62]

Recognizing the fact that the thermal history of wire specimens used in the present isochronal annealing studies differs significantly from those employed in the above mentioned investigations, the following possibilities are suggested as processes which might be contributing to Stage IV_q and Stage V_q recovery phenomena.

Stage IV_q:

1. Diffusion of monovacancies to prismatic loops and/or stable three dimensional vacancy aggregates,

2. Dissociation of relatively small immobile clusters and the diffusion of the products to prismatic loops, and/or stable three dimensional vacancy aggregates and fixed sinks,

3. Annealing out of three dimensional vacancy aggregates with products contributing to the growth of prismatic loops,

4. Collapse of three dimensional vacancy aggregates into prismatic loops.

Stage V_q:

1. Growth of large prismatic loops at the expense of smaller ones and the eventual annealing out of the loops altogether,

2. Annealing out of three dimensional vacancy aggregates.

The effects of impurity atoms are implicitly considered in terms of (a) monovacancy migration occurring as a consequence of the defect having been "stabilized" to higher temperatures by interactions with impurities, (b) immobile "clusters" where clusters are of the vacancy-vacancy type and vacancy-impurity type and (c) the existence of prismatic loops some of which could have originated as a result of prismatic punching.

There are certainly other possibilities but these seem to be the most likely in terms of what is already known about recovery in this range of temperatures. The many possibilities serve to demonstrate the complexity of the problem.

V. CONCLUSIONS

1. The temperature dependence of quench induced resistivity indicates that the monovacancy formation enthalpy in nominally 99.999% pure copper is (1.09±0.04) eV.

2. If the activation enthalpy for self-diffusion is taken as (2.10±0.02) eV, then the monovacancy migration enthalpy is (1.01±0.06) eV.

3. When the present resistivity data are combined with equilibrium measurements of $(\Delta N/N)_T$, the resistivity per atomic percent vacancies, $\Delta\rho_{1v}$, is (0.75±0.4) μohm-cm and the monovacancy formation entropy, ΔS^f_{1v}, is estimated as (0.8±0.5)k.

4. Isochronal recovery of copper quenched from ≈700°C to -196°C exhibits three principal annealing stages. Maximum annealing rates occur at about -40°, +200°, and +400°C. The dominant defect contributing to Stage III_q (-40°C) recovery is not expected to be the monovacancy but some higher order cluster. Stage V_q (+400°C) is attributed to the annealing out of prismatic loops and possibly three dimensional vacancy aggregates. Numerous possibilities have been suggested to account for Stage IV_q (+200°C). Detailed kinetic studies under carefully controlled conditions are necessary to clarify Stage III_q and Stage IV_q as observed in the present investigation.

5. When copper single crystals are quenched from $T_q \approx 1040°C$ and subsequently annealed under quite restrictive conditions, planar vacancy aggregates are observed by transmission electron microscopy. The aggregates are identified as both perfect and imperfect dislocation loops. The presence of vacancy loops which are large enough to be directly observed has been shown to be a sensitive function of the nucleation processes

and the availability of mobile defects in a sufficiently high concentration to support growth processes at higher temperatures.

6. It is felt that the reported results are representative of vacancy behavior in nominally 99.999% pure copper and that the difficulties from the numerous possible complicating features have, for the most part, been minimized.

ACKNOWLEDGMENTS

The author would like to express his appreciation to his advisor, Prof. G. Thomas, for his encouragement and advice throughout this investigation. He would also like to thank J. L. Strudel for many helpful suggestions concerning experimental techniques and for the numerous interesting and informative discussions. Thanks are also extended to Prof. D. N. Seidman of Cornell University for making his computor program (i.e., the fractional loss of vacancies during a downquench based on a diffusion limited dislocation climb model) available.

This work was carried out under the auspices of the United States Atomic Energy Commission through the Inorganic Materials Research Division of the Lawrence Radiation Laboratory.

Appendix I - Purification of Helium Gas

Because of the importance of minimizing complications which arise from gaseous contamination (e.g., O_2, N_2, and H_2), considerable care was taken in the preparation of the helium gas used in this study. High purity titanium sponge at elevated temperatures and silica gel at liquid nitrogen temperature were used as purification materials. The basic design and operational parameters were deduced from an evaluation of the purification of helium gas conducted by Malgiolio, et al.[126] In line gas chromatrographic techniques with a sensitivity of 1 to 2 parts per million by volume were employed by these authors in order to analyze the effluent helium gas for contaminants. The parameters selected for the present purification train are consistent with conditions under which no gaseous impurities were detected.[126]

A schematic of the purification system used in this investigation is illustrated in Fig. 34.* Water pumped tank helium with an initial impurity level of 300 to 400 ppm by volume was dried by passing the gas through a high pressure dehydrafilter containing a Molecular Sieve** cartridge. The gas was then passed over hot titanium sponge. For this purpose two columns of metal sponge were employed. The columns were located in separate tube furnaces. The temperature of the two furnaces was selected as optimum for the removal of oxygen (i.e., 750°C), and

---

* Many of the features of this purification train were first suggested and successfully employed by Guinan and Himmel.[127]

** Trade mark, Linde Company, Union Carbide Corporation

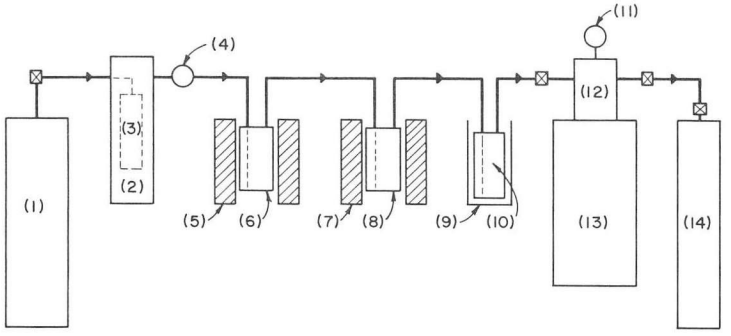

(a)

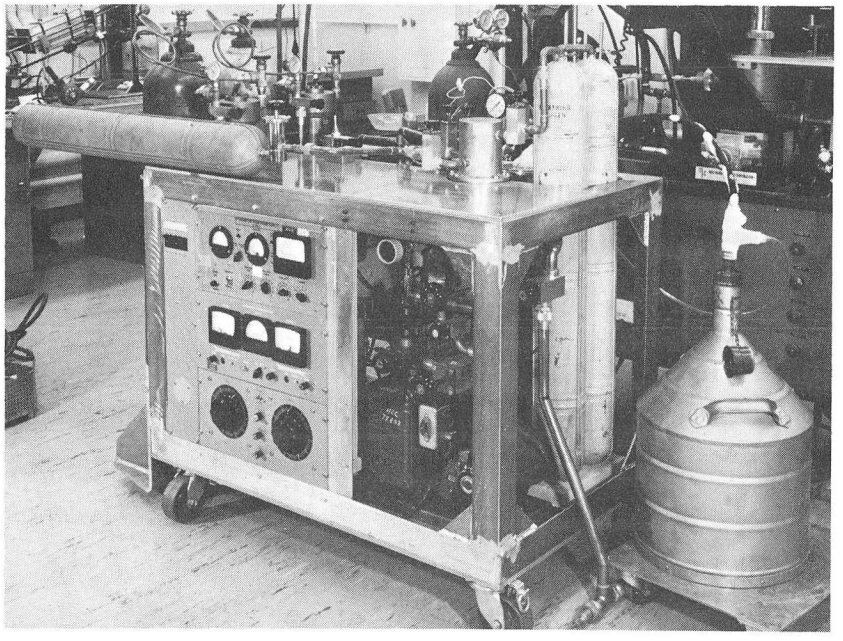

(b)

ZN-5624

Fig. 34 Helium gas purification system: a. Schematic of purification system; 1. tank of helium gas; 2. dehydrofilter (Hankison Corp.); 3. molecular sieve cartridge; 4. micro-metering regulator (Millaflow); 5. furnace (Marshall Products Co.); 6. column of titanium sponge (750°C); 7. furnace (Marshall Products Co.); 8. column of titanium sponge (900°C); 9. liquid nitrogen dewar; 10. column of silica gel; 11. compound gauge (30"-0-100); 12. vacuum manifold; 13. high vacuum system (Veeco 400" series); 14. stainless steel gas storage tank. b. photo of front view.

hydrogen and nitrogen (i.e., 900°C).* Upon exiting from the 900°C furnace, the gas was quenched to liquid nitrogen temperature and passed through a column of silica gel at this temperature. Prior to each purification run the silica gel was baked under vacuum for ≈ 12 hours at about 150°C. The exit helium gas was stored at about 60 psi in stainless steel tanks whose inner walls had been chemically polished. The storage tanks were always baked at about 350°C while under vacuum for 24 hours prior to being filled. A constant flow rate of 5 cubic feet per hour was maintained by a calibrated micro-metering regulator. The entire system was evacuated to about 1×10^{-7} torr before and after each purification run.

Attempts were made to have the purified helium gas analyzed, but the very high sensitivity requirement precluded the establishment of any reasonable estimate of the impurity level. Mass spectrometer analysis showed that oxygen, hydrogen, nitrogen, carbon monoxide, and water vapor were present in quantities less than 5 ppm, as expected.

---

* The titanium sponge was initially and periodically activated by passing purified hydrogen gas through the columns at a temperature of about 950°C for ≈4 hours.

Appendix II - Temperature Dependence of the Resistance

In the present investigation copper specimens were d.c. resistance heated. The temperature of a test wire was determined from the known temperature dependence of the resistance. The data of Meechan and Eggleston,[17] i.e., R(163°C)-R(950°C), and Leeds and Northrup,[79] i.e., R(-200°C)-R(200°C), were used as standards. In the former investigation[17] the precision of the temperature determination was ±0.5°C. Leeds and Northrup[79] quote values of the resistance in steps of one degree and place an uncertainty in the temperature of ±0.05°C. The nominal purity of the copper used in both of these cases was identical to that employed in the present work.

The two sets of data were internally consistent if one put R(0°C) = 0.08989 Ω in the Meechan and Eggleston case. With this assignment the resistance ratios, R(T°C)/R(0°C), for the temperature range 163° to 810°C were fitted to an expression of the form

$$R(T^\circ K)/R(273^\circ K) = a+bT^1+ cT^2 \qquad (46)$$

using a least squares criterion. In this equation T is the temperature in degrees Kelvin and the coefficients a, b, and c are 9.9820×10^{-2}, $3.2667\times10^{-3}(^\circ K^{-1})$ and $9.0538\times10^{-7}(^\circ K^{-2})$, respectively. The average error in the computed ratios was ≈0.07% which corresponds to an uncertainty in the temperature of ≈0.5°C and is therefore equivalent to the quoted experimental error.[17] In view of this, the calculated temperature dependence of the resistance was considered as a very good representation of the experimental data. Therefore from the measured resistance of a test specimen at a particular temperature and from the ratio of this resistance to that measured at 0°C, the desired average specimen

temperature T(°K) , was readily calculated from the relationship

$$T(^{\circ}K) = \frac{-a+[b^2 - 4a'c]^{1/2}}{2a'} \qquad (47)$$

where $a' = a - [R(T^{\circ}K)/R(273^{\circ}K)]$.

The experimental and calculated resistance ratios are tabulated in Table IX and the temperature dependence of the resistance ratio, $R(T^{\circ}C)/R(0^{\circ}C)$, over the range of quench temperatures employed in this work is shown in Fig. 35.

Table IX Resistance Ratios, R(T°C)/R(0°C), for High Purity Copper

T (°C)	$R(T)^{a}_{meas}$ (ohms)	$[R(T°C)/R(0°C)]^{b}_{meas}$	$[R(T°C)/R(0°C)]^{c}_{calc}$
163.9	0.15275	1.6993	1.7005
179.4	0.15852	1.7635	1.7636
205.7	0.16802	1.8692	1.8717
239.2	0.18064	2.0096	2.0112
269.8	0.19249	2.1414	2.1404
334.6	0.21770	2.4218	2.4195
370.6	0.23210	2.5820	2.5779
413.5	0.24933	2.7737	2.7698
450.2	0.26402	2.9371	2.9365
497.2	0.28350	3.1539	3.1536
549.7	0.30555	3.3992	3.4008
600.3	0.32716	3.6396	3.6438
651.9	0.34998	3.8934	3.8964
699.9	0.37159	4.1358	3.1357
739.9	0.38979	4.3363	4.3385
770.6	0.40420	4.4966	4.4960
810.1	0.42307	4.7064	4.7011

[a] Meechan and Eggleston[17]

[b] R(0°C) = 0.08989Ω

[c] $[R(T°K)/R(273°K)]_{calc} = a + bT + cT^2$

where $a = 9.9820\times10^{-2}$

$b = 3.2667\times10^{-3}$ ($°K^{-1}$)

$c = 9.0538\times10^{-7}$ ($°K^{-2}$)

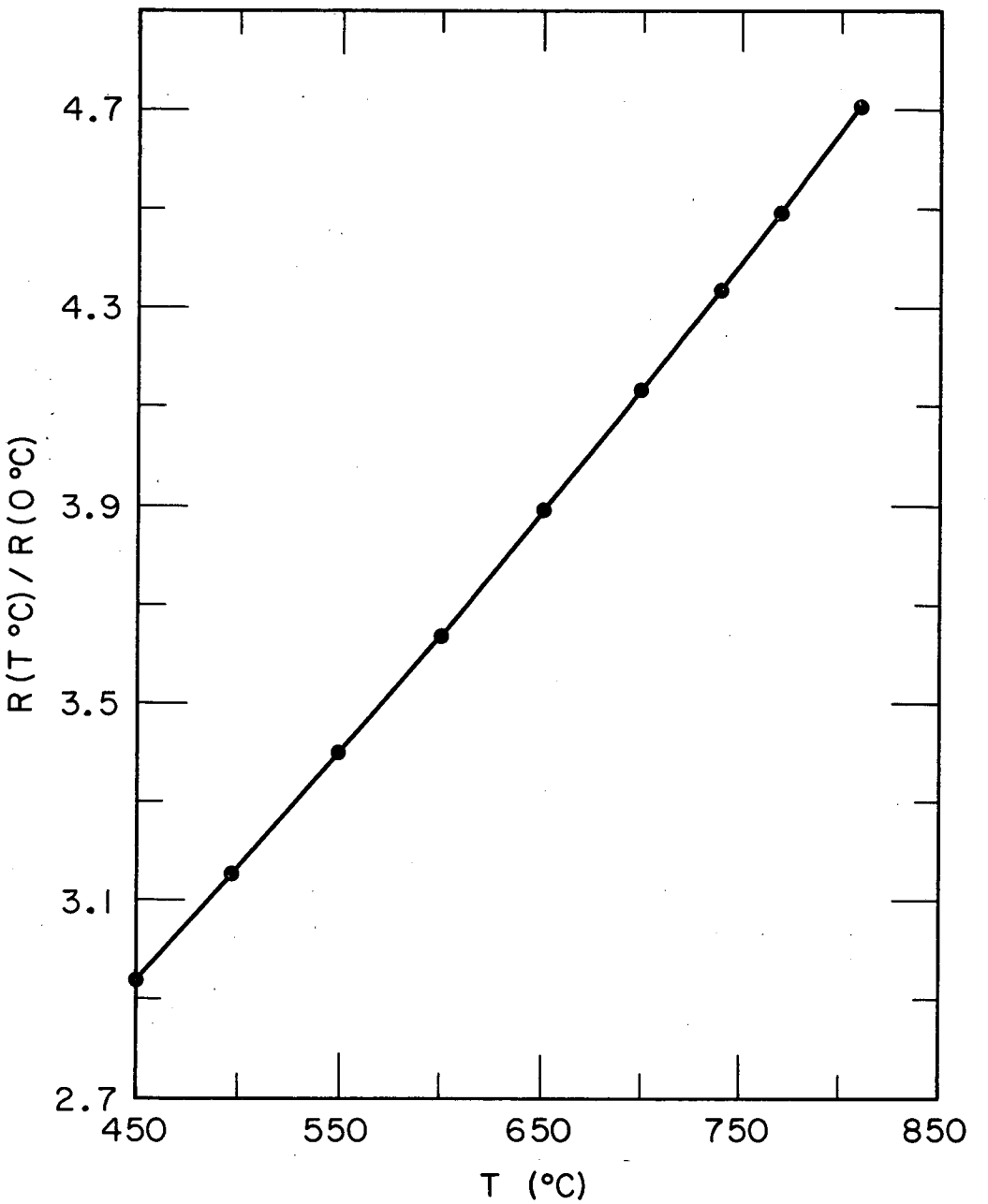

MUB-10709

Fig. 35 Ratio of the resistance of copper at temperature T, to that at 0°C plotted as a function of temperature.

Appendix III - Formation of Divacancies During an Exponential Quench

For quenching rates which are experimentally attainable in the laboratory and compatible with the aims of the present investigation, vacancies make a large number of jumps during the initial portion of the quench. The number of vacancy-vacancy and vacancy-cluster* collisions is sufficiently high so that the thermal equilibrium concentration of a number of the lower order defect clusters is attained (as indicated by the kinetic equations which are used to approximately describe the physical situation)[48,49,87] even during the short time that the specimen is at a particular temperature. As the temperature decreases, a point is reached where the reactions of interest proceed too slowly to satisfy the equilibrium demands. The actual concentration of the numerous defects therefore deviates from their equilibrium values. The temperature at which this deviation occurs is defined as T^*.[48] The temperature, T^*, is a function of the order and nature of the cluster,[97] as expected.

In the following, the simple case of divacancy formation (i.e., $C_{1v} + C_{1v} \underset{K_2}{\overset{K_1}{\rightleftharpoons}} C_{2v}$) during a so-called exponential quench is considered. The experimental time-temperature relationship for a quench from 700°C was used. An estimate of T^* and the corresponding

---

* Here a cluster is defined by example:

divacancy	vacancy-impurity
trivacancy	divacancy-impurity
.	.
.	.
.	.

fractional concentration of divacancies characteristic of T^* were determined for various assumed values of the divacancy binding energy in copper (i.e., B_{2v} = 0.1, 0.2, 0.3, and 0.4 eV). The general model considered was first suggested by Koehler et al.[47] and was subsequently employed in the analysis of experimental results on quenched gold.[48-50]

If it is assumed that the distribution of monovacancies and divacancies is random and that the loss of vacancies to fixed sinks during the quench is negligible (i.e., $\Delta N/N \cong C_{1v} + 2C_{2v}$ = constant for all t and characteristic of T_q), then the kinetic equation describing the time dependence of the monovacancy concentration, C_{1v}, is given by[1]

$$\frac{dC_{1v}}{dt} = -2C_{1v}^{2}K_1 + 2C_{2v}K_2 \quad . \tag{47}$$

Here K_1 and K_2 are so-called rate constants and written as follows:

$$K_1 = 84\nu_{1v} \exp(\Delta S^m_{1v}/k) \exp(-\Delta H^m_{1v}/kT) \tag{48}$$

$$K_2 = 14\nu_{2v} \exp\left[(\Delta S^m_{1v} + \Delta S^b_{2v})/k\right] \exp\left[-(\Delta H^m_{1v} + B_{2v})/kT\right] \tag{49}$$

where 84 and 14 are the appropriate combinatory numbers for the association of monovacancies and dissociation of divacancies, respectively.

The associative rate of change of the monovacancy concentration required to maintain the instantaneous equilibrium concentration of divacancies is obtained by differentiating the equilibrium expression

$$C_{2v} = 6\, C_{1v}^{2} \exp(\Delta G^b_{2v}/kT) \quad . \tag{50}$$

with respect to time and using the fact that $\frac{dC_{1v}}{dt} = \frac{-2dC_{2v}}{dt}$. The equilibrium requirement is formally written as

$$\left(\frac{dC_{1v}}{dt}\right)_{eq} = \frac{12C_{1v}(t)^2\ B_{2v}\ \exp[\Delta G^b_{2v}/kT(t)]\ \cdot\ (dT/dt)}{kT(t)^2\ [1+48(\Delta N/N)T_q\ \exp\ \{\Delta G^b_{2v}/kT(t)\}]^{1/2}} \qquad (51)$$

The temperature T^* is reached when the associative rate required by equilibrium just equals the associative term in Eq. (47). Thus, T^* is defined by the following equality

$$-\frac{dT^*}{dt} = \frac{14\nu_{1v}\ kT^{*2}[1+48(\Delta N/N)_{T_q}\ \exp(\Delta G^b_{2v}/kT^*)]^{1/2}}{B_{2v}\ \exp[(\Delta G^m_{1v} + \Delta G^b_{2v})/kT^*]}\ (°K/sec). \qquad (52)$$

Since T(t) is taken as the experimentally observed exponential time law

$$T(t) = T_o + \Delta T\ \exp(-\alpha t) \qquad (15)$$

it follows that $dT/dt = -\alpha(T-T_o)$. Therefore the desired T^* is the root of

$$\alpha(T - T_o) - A(T) = 0 \qquad (53)$$

where the function A(T) is the right hand side of Eq. (52).

Equation (53) was evaluated on the IBM 6600 computer. Computed values of T^*, $C_{1v}(T^*)$, $C_{2v}(T^*)$ and $C_{2v}(T^*)/C_{1v}(T^*)$ for assumed divacancy binding energies and T_q = 700°C are summarized in Table X along with other pertinent parameters used in the calculation. In addition, the relative fraction of vacancies which are in the form of divacancies, is compared to that fraction which is expected if the reaction under consideration was allowed to go to completion at -40°C.

Table X. Summary of Calculated Results of the Critical Temperature, T^*, Divacancy Concentrations, Relative Contribution of Divacancies to the Defect Population, and Other Pertinent Data

Calculated Quantities	Divacancy Binding Energy (eV)			
	0.1	0.2	0.3	0.4
$(\Delta N/N)_{T_q} \times 10^6$	5.024	5.030	5.050	5.268
$T^*(°C)$	150	197	239	274
$C_{1v}(T^*)\times 10^6$	5.007	4.920	4.466	3.413
$C_{2v}(T^*)\times 10^6$	0.0085	0.055	0.292	0.928
$C_{2v}(T^*)/C_{1v}(T^*)$	0.0017	0.011	0.065	0.272
$2C_{2v}(T^*)/(\Delta N/N)_{T_q}$	0.0034	0.022	0.116	0.352
$[C_{2v}(-40°C)]_{eq} \times 10^6$	0.0595	1.495	2.419	2.625
$\dfrac{2[C_{2v}(-40°C)]_{eq}}{(\Delta N/N)_{T_q}}$	0.0237	0.594	0.958	0.996

Pertinent relationships and assumptions:

a. $\alpha = 28\ (\mathrm{sec}^{-1})$

b. $T_q = 973°K$

c. $T_o = 77°K$

d. $k = 8.616\times 10^{-5}$ eV/deg

e. $\nu_{1v} \exp(\Delta S^m_{1v}/k) \cong 1.55\times 10^{14}(\mathrm{sec}^{-1})$

f. $\Delta H^m_{1v} = 1$ eV

g. $\Delta N/N = C_{1v} + 2C_{2v}$

h. $\Delta H^f_{1v} = 1.09$ eV, $\Delta S^f_{1v} \cong 0.8k$

i. $\Delta S^b_{2v} = (2\Delta S^f_{1v} - \Delta S^f_{2v}) \cong -1k$

REFERENCES

1. For a unified treatment see A. C. Damask and G. J. Dienes, Point Defects in Metals (Gordon and Breach Science Publishers, Inc., New York, 1963).
2. R. O. Simmons, J. S. Koehler, and R. W. Balluffi, Radiation Damage in Solids (International Atomic Energy Agency, Vienna) 1, 155 (1962).
3. R. W. Balluffi, J. S. Koehler, and R. O. Simmons, Recovery and Recrystallization of Metals, edited by L. Himmel (Interscience Publishers, Inc., New York) p.1 (1963).
4. R. O. Simmons and R. W. Balluffi, Phys. Rev. 117, 52 (1960).
5. R. O. Simmons and R. W. Balluffi, Phys. Rev. 119, 600 (1960).
6. R. O. Simmons and R. W. Balluffi, Phys. Rev. 125, 862 (1962).
7. T. S. Lundy and J. F. Murdock, J. Appl. Phys. 33, 1671 (1962).
8. A. D. LeClaire, Phil. Mag. (a) 7, 141 (1962); (b) 10, 641 (1964).
9. Lattice Defects in Quenched Metals (Academic Press, Inc., New York, 1965).
10. C. P. Flynn, J. Bass, and D. Lazarus, Phil. Mag., 11, 521 (1965).
11. R. O. Simmons and R. W. Balluffi, Phys. Rev. 129, 1533 (1963).
12. A. Seeger and D. Schumacher, Lattice Defects in Quenched Metals (Academic Press, Inc., New York, 1965) p. 15.
13. F. Ramsteiner, G. Lampert, A. Seeger, and W. Schüle, Phys. Stat. Sol. 8, 863 (1965).
14. L. Slitkin, Lattice Defects in Quenched Metals (Academic Press, Inc., New York, 1965) see Discussion, p. 75.
15. A. V. Granato and T. G. Nilan, Phys. Rev. Letters 6, 171 (1961).
16. A. C. Damask, G. J. Dienes, and V. G. Weizer, Phys. Rev. 113, 781 (1959).
17. C. J. Meechan and R. R. Eggleston, Acta. Met. 2, 680 (1954).

18. S. D. Gertsriken and B. F. Slynsar, Phys. Metals Metallog. (USSR-English Trans.) 6, 103 (1958).

19. K. Misek and J. Polak, J. Phys. Soc. Japan 18, Suppl. II (Intern. Conference on Crystals Lattice Defects) 1963, p. 179.

20. J. F. Nicholas, Acta Met. 3, 411 (1955).

21. J. E. Eshelby, J. Appl. Phys. 25, 255 (1954).

22. R. W. Balluffi and R. O. Simmons, J. Appl. Phys. 31, 2284 (1960).

23. G. Schottky, A. Seeger, and G. Schmid, Phys. Stat. Sol. 4, 439 (1964).

24. A. Seeger, V. Gerold, and M. Rüle, Z. Metallk. 54, 493 (1963).

25. M. S. Maier and H. R. Nelson, Trans. AIME 147, 39 (1942).

26. W. L. Mercer, Thesis, University of Leeds (1955). Also see A. D. LeClaire, Phil. Mag. 7, 141 (1962).

27. A. Kuper, H. Letaw, Jr., L. Slifkin, E. Sonder, and C. T. Tomizuka, Phys. Rev. 96, 1224 (1954).

28. M. Doyama and J. S. Koehler, Phys. Rev., 119, 939 (1960); 127, 21 (1962).

29. L. J. Cuddy and E. S. Machlin, Phil. Mag. 7, 745 (1962).

30. Y. Quéré, Compt. Rend. Acad. Sci. 251, 367 (1960).

31. Y. Quéré, J. Phys. Soc. Japan 18, Suppl. III, 91 (1963).

32. C. Budin, F. Denayrou, A. Lucasson, and P. Lucasson, Compt. Rend. Acad. Sci. 256, 1518 (1963).

33. P. G. Lucasson, A. Lucasson, C. Budin, and F. Denayron, J. Phys. Radium 24, 508 (1963).

34. R. S. Barnes and D. J. Mazey, Acta Met., 11, 281 (1963).

35. L. M. Clarebrough, R. L. Segall, M. H. Loretto, and M. E. Hargraves, Phil. Mag. 9, 377 (1964).

36. R. L. Segall and L. M. Clarebrough, Phil. Mag. 9, 865 (1964).

37. H. G. Van Bueren, Imperfections in Crystals (North-Holland Publishing Co., Amsterdam) 1961, pp. 276-81.

38. J. Takamura, Acta Met. 9, 547 (1961).

39. J. Takamura, K. Furukawa, S. Miura, and P. H. Shingu, J. Phys. Soc. Japan 18, Suppl. III (1963).

40. J. Takamura, Lattice Defects in Quenched Metals (Academic Press, Inc., New York, 1965) p. 521.

41. J. J. Jackson, Acta Met., 11, 1245 (1963).

42. J. J. Jackson, Lattice Defects in Quenched Metals (Academic Press, Inc., New York, 1965) pp. 467 and 479.

43. W. M. Lomer, Progr. Met. Phys. 8, 255 (1959).

44. T. Mori, M. Meshii, and S. W. Kauffman, J. Appl. Phys. 33, 2776 (1962).

45. C. P. Flynn, J. Bass, and D. Lazarus, Phil. Mag. 11, 521 (1965).

46. D. N. Seidman and R. W. Balluffi, Bull. Am. Phys. Soc., 10, 697 (1965).

47. J. S. Koehler, F. Seitz and E. Bauerle, Phys. Rev. 107, 1499 (1957).

48. H. Fumiwara, Tech. Rept. Dept. of Physics, University of Illinois (1960).

49. J. S. Koehler, M. de Jong, and F. Seitz, J. Phys. Soc. Japan 18, Suppl. III, (1963) p. 1.

50. M. de Jong and J. S. Koehler, Phys. Rev. 129, 40, 49 (1963).

51. G. Schottky, Z. Physik 160, 16 (1960).

52. H. Kimura, R. Maclin, and D. Kuhlmann-Wilsdorf, Acta Met. 7, 145 (1959).

53. H. Bross and A. Seeger, J. Phys. Chem. Solids 6, 324 (1958).

54. C. P. Flynn, Phys. Rev. 126, 533 (1962).

55. T. Federighi, Lattice Defects in Quenched Metals (Academic Press, Inc., New York, 1965) p. 217.

56. J. Bass, Ph.D. Thesis, University of Illinois (1964).

57. J. A. Ytterhus, R. W. Siegel, and R. W. Balluffi, Lattice Defects in Quenched Metals (Academic Press, Inc., New York, 1965) p. 679.

58. J. A. Ytterhus, R. W. Balluffi, Phil. Mag. 11, 707 (1965).

59. R. W. Balluffi and R. W. Siegel, Lattice Defects in Quenched Metals, (Academic Press, Inc., New York, 1963) p. 693.

60. R. M. J. Cotterill and R. L. Segall, Phil. Mag. 8, 1105 (1963).

61. G. Thomas and J. Washburn, Rev. Mod. Phys. 35, 992 (1963).

62. J. L. Strudel and J. Washburn, private communication.

63. W. L. Bell, Master's Thesis, Lawrence Radiation Laboratory Report, UCRL-16024.

64. J. Galligan and J. Washburn, Phil. Mag. 8, 1455 (1963); see also Lawrence Radiation Laboratory Report, UCRL-10606.

65. Referenced in R. O. Simmons and R. W. Baluffi, Phys. Rev. 129, 1541 (1963).

66. G. Airoldi, G. L. Bachella, and E. Germagnoli, Phys. Rev. Letters, 2, 145 (1959).

67. A. Seeger, Z. Physik 144, 637 (1956).

68. D. G. Martin, Phil. Mag. 7, 803 (1962).

69. W. Schüle, A. Seeger, F. Ramsteiner, D. Schumacher, and K. King Z. Naturforsch 16a, 323 (1961).

70. K. Chik, A. Seeger, and M. Rüle, Proc. 5th. Intern. Congr. Electron Microscopy (Academic Press, Inc., New York, 1962) p. J-11.

71. A. Seeger, V. Gerold, K. P. Chik, and M. Rühle, Phys. Letters (Netherlands) 5, 107 (1963).

72. P. B. Hirsch and J. Silcox, Growth and Perfection of Crystals (John Wiley and Sons, New SYork, 1958) p. 262.

73. R. E. Smallman and K. H. Westmacott, J. Appl. Phys. 30, 603 (1959).

74. R. E. Smallman, K. H. Westmacott, and J. H. Coiley, J. Inst. Metals, 88, 127 (1959).

75. R.M. J. Cotterill, Lattice Defects in Quenched Metals (Academic Press, Inc., New SYork, 1965) p. 97.

76. D. A. Jones and J. W. Mitchell, Phil. Mag. 3, 1 (1958).

77. J. E. Verfurth and R. A. Rapp, Trans. AIME 230, 1310 (1964).

78. W. Bell, D. M. Maher, and G. Thomas, Lattice Defects in Quenched Metals (Academic Press, Inc., New York, 1965) p. 739.

79. Leeds and Northrup Company, Standard Conversion Tables STD. 1068 and STD. 77-21-0-4 ISSUE 3.

80. J. L. Strudel and D. M. Maher (to be published).

81. G. Thomas and W. L. Bell, Honolulu Conference on Lattice Defects, September 1965; also see Lawrence Radiation Laboratory Report, UCRL-16271.

82. U. Essmann and M. Wilkens, Phys. Stat. Sol. 4, K53 (1964).

83. M. F. Ashby and L. M. Brown, Phil. Mag., 8, 1083 (1963).

84. M. F. Ashby and L. M. Brown, Phil. Mag., 8, 1649 (1963).

85. W. L. Bell and G. Thomas, Phys. Stat. Sol. 12, 843 (1965).

86. A. N. Gerritson, Handbüch der Physik, XIX, 137 (1956).

87. A. Goldsmith, T. E. Waterman and H. J. Hischorn, Handbook of Thermophysical Properties of Solid Materials, Vol. 1 (MacMillan, New York, 1961).

88. American Institute of Physics Handbook (McGraw-Hill Book Co., Inc., 1963) pp. 9-42.

89. W. J. Tunstall, P. B. Hirsch, and J. Steeds, Phil. Mag. 9, 99 (1964).

90. W. L. Bell and G. Thomas, Research in Progress.

91. M. Rühle, U. Essmann and M. Wilkens, Phys. Stat. Sol., 11, 819 (1965).

92. D. W. Pashley and A. E. B. Presland, Phil. Mag. 6, 1003 (1961).

93. D. N. Siedman and R. W. Balluffi, Phys. Rev. 139, A1824 (1965).

94. R. W. Balluffi and D. N. Seidman, J. Appl. Phys. 36, 2807 (1965).

95. P. G. Shewmon, Diffusion in Solids (McGraw-Hill Book Company, Inc., 1963) p. 52.

96. G. Schottky, Phys. Letters (Netherlands) 12, 95 (1964).

97. R. M. J. Cotterill, Phil. Mag. 6, 1351 (1961).

98. S. Yoshida, M. Kiritani, and Y. Shimomura, Lattice Defects in Quenched Metals, (Academic Press, Inc., New York, 1965), p. 713.

99. M. Doyama, Lattice Defects in Quenched Metals, (Academic Press, Inc., New York, 1965) p. 167.

100. F. Ramsteiner, W. Schüle, and A. Seeger, Phys. Stat. Sol., 7, 937 (1964).

101. K. Kuhlmann-Wilsdorf, Lattice Defects in Quenched Metals (Academic Press, Inc., New York, 1965) p. 269.

102. I. G. Greenfield and H. G. F. Wilsdorf, J. Phys. Soc. Japan, 18, Suppl. III (1963) p. 20.

103. H. B. Huntington and F. Seitz, Phys. Rev. 61, 315 (1942) and later modified by H. Brooks, Impurities and Imperfections (American Society for Metals, Cleveland, 1955) p. 1.

104. F. G. Fumi, Phil. Mag. 46, 1007 (1955).

105. A. Seeger and H. Bross, Z. Physik, 145, 161 (1956).

106. A. Seeger, Z. Physik, 144, 637 (1956).

107. A. Seeger and E. Mann, J. Phys. Chem. Solids 12, 326 (1960).

108. G. Schottky, A. Seeger and G. Schmid, Phys. Stat. Sol., 4, 419 (1964).

109. C. P. Flynn, Phys. Rev. 881, 125 (1962).

110. H. B. Huntington, G. A. Shirn, and E. S. Wajda, Phys. Rev. 99, 1085 (1955).

111. H. B. Huntington, Phys. Rev. 61, 325 (1942).

112. J. M. Bartlett and G. J. Dienes, Phys. Rev. 89, 848 (1953).

113. D. L. Dexter, Phys. Rev. 87, 768 (1952).

114. P. Jongenburger, Phys. Rev. 90, 710 (1953); Appl. Sci. Res. B3, 237 (1953); Nature 175, 545 (1955).

115. F. Abeles, Compt. Rend. 237, 796 (1953).

116. F. J. Blatt, Phys. Rev. 99, 1708 (1955); 100, 666 (1955).

117. A. W. Overhauser and R. L. Gorman, Phys. Rev. 102, 676 (1956).

118. L. Roth, Thesis, Harvard University (1956).

119. W. M. Lomer, Progr. Metal Phys. 8, 255 (1959).

120. V. G. Weizer and L. A. Girifalco, Phys. Rev. 120, 837 (1960).

121. A. Seeger and H. Bross, J. Phys. Chem. Solids 16, 253 (1960).

122. R. M. J. Cotterill and M. Doyama, Lattice Defects in Quenched Metals (Academic Press, Inc., New York, 1965) p. 653.

123. C. P. Flynn, J. de Phys. et Radium 23, 654 (1962).

124. G. Schottky, Z. Phys. 159, 584 (1960).

125. J. B. Gibson, A. N. Goland, M. Milgram, and G. H. Vineyard, Phys. Rev. 120, 1229 (1960).

126. J. Malgiolio, E. A. Limoncelli, and R. E. Cleary, AEC Research and Development Report PWAC 352 (1961).

127. M. Guinen, Ph.D. Thesis, Physics Department, University of California (1966).

128. R. L. Garwin, Rev. Sci. Instruments 29, 223 (1958).

This report was prepared as an account of Government sponsored work. Neither the United States, nor the Commission, nor any person acting on behalf of the Commission:

A. Makes any warranty or representation, expressed or implied, with respect to the accuracy, completeness, or usefulness of the information contained in this report, or that the use of any information, apparatus, method, or process disclosed in this report may not infringe privately owned rights; or

B. Assumes any liabilities with respect to the use of, or for damages resulting from the use of any information, apparatus, method, or process disclosed in this report.

As used in the above, "person acting on behalf of the Commission" includes any employee or contractor of the Commission, or employee of such contractor, to the extent that such employee or contractor of the Commission, or employee of such contractor prepares, disseminates, or provides access to, any information pursuant to his employment or contract with the Commission, or his employment with such contractor.